

Thèse

Pour obtenir le grade de
Docteur de l'Université Louis Pasteur de Strasbourg I

Discipline : Sciences du Vivant

Présentée par :

Lydia PRONGIDI FIX

Laboratoire de RMN et biophysique des membranes

CNRS UMR 7177

Structural and Thermodynamic Investigations of membrane associated polypeptides and peptide/DNA transfection complexes

Soutenue publiquement le 13 Décembre 2005 devant la commission d'examen

Pr.	Andrew GRIFFITHS	Rapporteur interne
Pr.	Joachim SEELIG	Rapporteur externe
Pr.	Robert TAMPE	Rapporteur externe
Pr.	Burkhard BECHINGER	Directeur de thèse
Dr.	Antoine KICHLER	Membre invité

Thèse

Pour obtenir le grade de
Docteur de l'Université Louis Pasteur de Strasbourg I

Discipline : Sciences du Vivant

Présentée par :

Lydia PRONGIDI FIX

Laboratoire de RMN et biophysique de membranes

CNRS UMR 7177

Structural and Thermodynamic Investigations of membrane associated polypeptides and peptide/DNA transfection complexes

Soutenue publiquement le 13 Décembre 2005 devant la commission d'examen

Pr.	Andrew GRIFFITHS	Rapporteur interne
Pr.	Joachim SEELIG	Rapporteur externe
Pr.	Robert TAMPE	Rapporteur externe
Pr.	Burkhard BECHINGER	Directeur de thèse
Dr.	Antoine KICHLER	Membre invité

A ma famille,

A mon mari,

Qui m'ont tellement soutenu
pendant mes années d'étude...

Remerciements

Ce travail a été effectué au sein du Laboratoire de RMN et biophysique de membranes (CNRS UMR 7177), sous la direction du Pr. Burkhard Bechinger.

Au **Pr. Burkhard Bechinger**,

Je tiens à vous remercier sincèrement de m'avoir accueilli dans votre laboratoire. Ces trois dernières années ont été très riches en expériences techniques et en connaissances. Un grand merci aussi pour la liberté de mouvements dont j'ai bénéficié et pour votre largesse d'esprit d'un point de vue scientifique.

Aux **Professeurs Andrew Griffiths, Joachim Seeling, Robert Tampé** qui ont accepté de juger ce mémoire de thèse ; Je suis consciente du travail que cela représente.

Au **Dr. Antoine Kichler** avec qui nous avons eu une collaboration très fructueuse sur le projet de la mucoviscidose.

Au **Dr. Barbara Winsor** qui m'a aidée maintes fois depuis ma licence autant au niveau matériel que par ces précieux conseils. Merci du fond du cœur.

Au **Dr. Philippe Bertani** qui m'a initiée à l'art de la RMN et qui m'a beaucoup aidée à la comprendre.

Au **Dr. Masae Sugawara** pour les expériences CD et pour sa bonne humeur.

Au **Dr. Phil Williamson** pour ses conseils précieux dans mon projet d'expression.

A **Jésus et Christopher** pour leur assistance au niveau technique.

A **James, Arnaud, Marie Catherine, Christophe**, ainsi que les autres membres de l'équipe pour la bonne ambiance du laboratoire.

A **Nadia**. Depuis qu'elle est dans le laboratoire les tâches administratives sont devenues beaucoup plus faciles.

A l'association **Vaincre la Mucoviscidose**, dont le soutien financier a permis la réalisation de ce travail.

A **mes parents** adorés. Leur amour m'a aidée à surmonter toute sorte d'épreuves et je sais qu'ils sont très fiers de moi.

A **mon cher mari** pour son amour et pour son soutien de tous les jours, surtout les week-ends quand il attendait que je termine mes expériences. Je t'aime.

A **mon grand-père** qui est parti trop tôt et à **ma grand-mère** pour son amour inconditionnel.

A **mon frère** qui est aujourd'hui là où j'ai commencé il y a 3 ans. « May the force be with you... » Petit frère je t'aime et je suis très fière de toi.

A mon ami **Mazen** avec qui j'ai partagé des moments géniaux pendant nos années d'études et nous avons vu ensemble le bout du tunnel. Strasbourg ne sera plus pareil sans toi, j'espère que tu nous reviendra très vite.

A **tous mes amis** que je n'ai pas mentionnés, de la Grèce et de la France.

INDEX

Chapter 1:	Introduction	p. 1
Chapter 2:	Theoretical Aspects	11
2.1	Introduction	11
2.2	Solid-State NMR	12
2.2.1	Oriented Samples	12
2.2.2	Non-Oriented Samples	17
2.2.3	Lipid Phase Transitions	21
2.2.4	Magic Angle Solid-State NMR	24
2.3	Isothermal Titration Calorimetry	27
2.3.1.	General Thermodynamic considerations	27
2.3.2	ITC	29
2.3.3	The association between Ligands and Macromolecules	32
2.4	Discussion	35
Chapter 3:	Membrane peptide helix alignments and dynamics	
	from non-oriented ^{15}N chemical shift spectra	36
3.1	Introduction	36
3.2	Materials and Methods	39
3.3	Results	41
3.4	Discussion	45

Chapter 4: Thermodynamic and structural study of a peptide transfection complex	50
4.1 Introduction	50
4.2 Thermodynamic Characterization of the LAH4/DNA complexes	55
4.2.1 Materials and Methods	55
4.2.2 Results	58
4.3 Structural characterization of the LAH4/DNA complexes	66
4.3.1 Sample preparation and proton-decoupled ¹³ C CP/MAS NMR NMR	66
4.3.2 Results	67
4.4 Discussion	70
Chapter 5: Expression of the LAH4 peptide in <i>E.coli</i>	79
5.1 Introduction	79
5.2 Constructs	82
5.3 Materials and Methods	86
5.4 Results	90
5.5 Discussion	97

Chapter 6: Solid state NMR studies on the diphtheria toxin domain T	99
6.1 Introduction	99
6.2 Material and Methods	105
6.3 Results	107
6.4 Discussion	113
Chapter 7: General Conclusions	118
References	124

Chapter 1

General Introduction

The correct functioning of a complex ensemble such as the cell relies on the accurate interaction between macromolecules. These interactions are, hence, the basis of life, and their comprehension is a challenge of utmost importance.

Biological macromolecules interact by non-covalent interactions, relatively weak in strength, but overall of supreme strength due to their large number. Non-covalent interactions are the hydrophobic forces, hydrogen bonds, electrostatic interactions and van der Waals dispersion forces. Their nature is electrostatic for all except the hydrophobic interactions (1).

Within the biomolecules, proteins, or more generally polypeptides, constitute the most multifunctional category, ensuring a wide variety and a large number of essential tasks. They also interact with all the other categories of macromolecules. Polypeptides are the major constituent of cells, representing 50 % of the cells dry weigh. Typical examples of specific interaction between proteins and other macromolecules are: the histones in the chromatine structure, ribosomes, or enzymes such as the ARN polymerase for the association with the DNA, the ABC transporters, or the G-Protein Coupled Receptors for their association with the membrane (2).

Membrane associated proteins and peptides constitute a privileged medical target. Some of them also present an important potential in therapeutics as they can be more potent and selective, less toxic and don't accumulate in tissues.

According to Frost & Sullivan (F&S) Drug Discovery Technology group, there are more than 40 marketed peptides worldwide, around 270 peptides in clinical phase testing, and about 400 in advanced preclinical phases. Natural peptides such as insulin, vancomycin, oxytocin, and cyclosporine and synthetically produced ones such as Fuzeon (enfuvirtide) and Integrilin (eptifibatide) are among the approved peptide-based drugs.

Membrane proteins and peptides adopt unique three-dimensional structures in their functional environment of i.e. the phospholipid bilayers. Nearly all of the residues in the polypeptide chains move anisotropically on time scales exceeding milliseconds; therefore the relevant dipolar couplings and chemical shift interactions in the backbone sites are not motionally averaged, and a wide variety of solid state NMR experiments are highly effective and can be used for structural determination (3, 4).

Two major constitutive elements take part in defining the structure of proteins, those are the α -helix and the β - sheets. Combinations of these two elements, with specific geometric arrangements form simple motifs that frequently associate to build up large structural and functional assemblies (1).

However, not all parts of a protein may be conveniently classified as α helix or β sheet.

Turns connect one α helix or β segment to another inside the polypeptide chains. β turns, the most compact type of turn are frequently observed in antiparallel β sheet structures.

They accomplish a complete reversal of the polypeptide chain within four residues.

Bends and turns in α helices frequently involve proline residues and often occur at the surface of proteins. Loops and termini are irregularly structured regions, referred to,

sometimes, as “random coil” regions. Each such region has its own particular folding which is conserved in each example of the particular protein molecule (5).

The α -helical disposition of polypeptides was first described in 1951 by Linus Pauling, predicting that it would be a stable structure, energetically favourable in proteins. This prediction almost immediately received experimental support and α -helices were since identified in the structure of numerous families of proteins that vary considerably not only by their overall secondary and tertiary structure composition but also, and most importantly, by their function.

Hydrophobic and amphipathic α -helices act as independent functional units in immunogenic or fusogenic polypeptides (6, 7). They also constitute important building blocks of larger, membrane interacting proteins. Moreover, certain cationic α -helices exhibit a combination of two singular properties, DNA condensation and membrane destabilizing capacities, and have proven to be excellent transfection vectors (8, 9).

The aim of this thesis was to study membrane associated peptides and proteins as for their interaction with large macromolecules such as the DNA and /or various lipid bilayers. Structural and thermodynamical studies were undertaken in parallel in order to collect information about the system and to understand its mechanism. Structural and mechanistic information is the basis of rational drug design and our ultimate goal would be to inspire the creation of new, more efficient molecules targeting specific points of the process of the peptides action.

In this thesis, four projects are described: structural investigations of membrane associated peptides reconstituted either in non-oriented or in oriented bilayers,

thermodynamic and structural studies of a transfection complex, and expression of a peptidic transfection vector in *E.coli* bacteria.

In Chapter 3 we discuss helix alignments and dynamics of membrane associated peptides from non-oriented ^{15}N chemical shift spectra:

The correlation times of small peptides associated with large macromolecules assemblies, such as phospholipid membranes, are to a large extent determined by the size of the complex. Tumbling is, therefore, considerably slower when compared to this same peptide in solution (10). In order to obtain information about the structure and dynamics of peptides associated with extended lipid bilayers, solid-state NMR spectroscopic methods have been developed.

To overcome the problems of low resolution, techniques such as fast spinning of the samples around the magic angle, and alignment of the samples with respect to the magnetic field direction are usually applied. Nevertheless, theoretical considerations predict that non-oriented samples are also capable of providing useful information about the dynamics and the orientation of α -helical peptides with respect to the membrane normal.

In this thesis, a novel approach has been experimentally tested, using two α -helical membrane associated peptides, the synthetic peptides h Φ 19W (transmembrane) and KL14 (in-plane), reconstituted in non oriented membranes, and to test such theoretical predictions and to evaluate a new method that aims to determine the orientation of α -helices with respect to the bilayer normal.

Although in powder samples the peptide is present at all possible orientations, movements around the longitudinal axis permits a rotational averaging of the ^{15}N chemical shift tensors around two different axes depending on the alignment of the

peptide in the bilayer. This, results in spectral line narrowing and orientation dependant solid state NMR line shapes.

Chapter 6 describes solid-state NMR studies on the diphtheria toxin T domain:

Changing from water soluble to a membrane associated state is also an essential feature of membrane penetration by bacterial toxins (*11-13*). The intracellularly acting toxins are generally bipartite proteins, containing the enzymatic and receptor-binding functions on separate polypeptides designated A and B respectively (*14*). The process by which toxins acting intracellularly translocate their enzymatic A moieties across the membrane within the cytosol is not well understood. In some members of this class, such as diphtheria, tetanus and anthrax toxins, the receptor binding B moiety has the ability to insert into membranes and form aqueous pores under conditions known to promote translocation (*11, 12*); However, the precise relationship between pore formation and translocation has not yet been clearly defined for any toxin.

Diphtheria toxin, a well studied example of AB toxins, is a single, 535-residue polypeptide containing three folding domains: the amino-terminal C, or catalytic domain (residues 1-185); an intermediate T, or transmembrane domain (residues 202-378); and the carboxy-terminal R, or receptor binding domain (residues 386-535). The catalytic domain is connected to the T domain by an arginine-rich loop and a readily reducible disulfide bridge (*15*).

The crystallographic structure of native diphtheria toxin (*15*) shows the T domain to consist of a bundle of 10 α -helices. This topology resembles the channel forming domains of certain colicins (*16*) and α -helical domains found in Bcl-xL family of mammalian proteins involved in the regulation of apoptosis (*17*). Studies in planar lipid

bilayers have shown that under low pH conditions ($\text{pH} \leq 6$) the isolated T domain is able to form cation- selective channels in the membrane (18).

Two long hydrophobic helices, TH8 and TH9, buried within the native T domain insert into the membrane bilayer when the domain converts to a transmembrane form (18). However, the conformation of the membrane associated T domain, and its role in translocation are poorly understood.

The T domain of diphtheria toxin is predominantly α -helical and plays a key role in the mechanism of action of the toxin. In this thesis it has been studied as for its topology, in reconstituted lipid bilayers and at various conditions by proton-decoupled ^{15}N solid state NMR. The results show the consequence of the constitution of the bilayer and the pH on the pore forming activity of the domain T.

In Chapter 4 we present thermodynamic and structural data of the study of a peptide transfection complex:

Amphipathic peptides are found in many species, including plants, insect, amphibians, and humans. Their membrane associating properties provide them bacteriocidal, fungicidal, virucidal and even tumoricidal activities. Membrane particularities in the composition of eukaryotic cells prevent their lysis (reviewed in (10)), conferring to some of the amphipathic peptides an interesting potential in the drug industry. The best studied of these peptides are probably the members of the bombinin-magainin family first found in toads and frogs, and cecropins isolated from the pupae of the cecropia moths (19).

These peptides are composed of 20 to 40 amino acid residues, some of with strongly basic character. They dissolve well in aqueous solution, where they assume random coil conformations. They also show strong affinity for phospholipid membranes, where they

assume right handed α -helical conformations (10). Edmundson helical wheel analysis shows that such helices are amphipathic, with polar and hydrophobic amino acid side chains separated on the opposite faces of the helix.

Amphipathic model peptides have been designed that exhibit pronounced antibiotic activities (20-23). Some peptide antibiotics designed in our laboratory are characterized by a hydrophobic face separated from a histidine-containing region. The polarity of histidine side chains is strongly dependent on the pH of the surrounding media, and many of these peptides exhibit pH-dependant transitions between transmembrane and in-plane alignments (21, 23).

Cationic synthetic peptides have also been used as transfection agents. Their sequences consist of a hydrophobic template rich in alanine and leucine, where cationic residues such as arginine, lysines and/or histidines are inserted. These peptides were designed based on existing compounds, mimicking the protamines DNA condensing properties (9), or the PEI proton sponge activity (24). Recent studies have shown that the number of cationic residues, their position in the sequence, and/or the pH at which the peptide transits from the transmembrane to the in-plane position are crucial for their gene delivery (24).

Several peptides of the LAH family present transfection capacities, the most efficient being the LAH4 peptide (24). This interactions of this peptide with membranes have been extensively studied over the past years (21, 23).

As the LAH4 peptide proved to be a gene transfection vector more efficient than the currently used gene delivery systems, thermodynamical and structural studies were undertaken in order to understand its interactions with the DNA molecules as well as the mechanism of action of the peptide during the transfection process.

In this study, various aspects of the transfection process have been considered, including the driving forces of the LAH4 - DNA interaction, the affinity, the structure of the complex, when it is assembled in reconstituted membranes, as well as the dynamics.

Solid state NMR provides information on the polypeptides secondary structure, their orientation, the dynamics, and topology, with respect to the membrane surface (21). In solid state NMR increasing the size of the molecular complexes does not automatically degrade relaxation parameters or line widths, so that sensitivity will only be diminished because of a smaller quantity of molecules in a fixed volume of material (25). Thus, large complexes may be investigated by solid state NMR without hindrance of the size factor.

However, examination of the structural details alone is not sufficient to understand the mechanism of biomolecular complex formation. Information about the energetic forces that drive complex formation, or that are responsible for maintaining the folded conformations of biological macromolecules in solution is also required.

In order to gain a fuller understanding of biological processes, it is necessary to combine structural data such as those obtained from NMR techniques, with information of the underlying thermodynamics of the process studied by a technique such as ITC. Therefore, the data provided by these two techniques may be used to explain and understand the biological function. This approach is necessary for example in drug design, where sufficiently detailed understanding of the molecular events that take place can lead to the design of more efficient agents that target specifically the aimed molecules.

Here peptide - lipid and LAH4/DNA complex - lipid interactions, as well as peptide - DNA interactions were studied. Different approaches and techniques were applied in order to obtain a more complete view on the peptides' actions. The results permit a detailed thermodynamic characterization of the LAH4 - DNA association, provide information about the secondary structure of the LAH4 peptide within the DNA-peptide

complex and in combination valuable insights of the transfection mechanism involving critical steps such as complex formation and DNA compaction, as well as complex delivery to the cytoplasm after endosomal acidification. All the data converge to the proposal of the LAH4 peptide mode of action during transfection. The information collected should allow the design of new synthetic, peptidic transfection agents presenting enhanced efficiency on the DNA compaction and on the lysis of the endosomal compartment.

Chapter 5 describes our efforts to express the LAH4 antibacterial peptide in *E.coli*:

The production of bioactive peptides, such as LAH4, is commonly achieved via solid phase chemical synthesis (26). However, to make use of the full potential of NMR methods, LAH4 peptide labeled with NMR active stable isotopes, in particular with ^{13}C , ^{15}N , and ^2H , is required. For such applications, solid phase chemical synthesis becomes excessively expensive. Genetic engineering followed by efficient expression of isotope labeled biomolecules in milligram amounts has been indispensable for recent successes in biological NMR applications. Our efforts have been thus concentrated in the elaboration of bacterial clones genetically engineered in order to express the LAH4 antimicrobial peptide.

Expression was achieved by fusing the LAH4 coding gene downstream to the Glutathion S-Transferase protein. The produced fusion protein was revealed to be insoluble, so that denaturation and refolding steps were necessary for its recovery. An affinity column under reduced conditions allowed purification of the fusion protein and a digestion step finally liberated the LAH4 peptide.

Characterization of peptide - lipid interactions by structural methods forms the basis from which mechanistic models for antibiotic and pore forming activities can be developed.

The mechanistic of action of the LAH4 peptide presented in this study is an example among others (10).

Chapter 2

Theoretical aspects

2.1 Introduction

In the first part of this chapter, we will introduce some quantum mechanics notions necessary to the description of solid-state Nuclear Magnetic Resonance (NMR) experiments. Solid-state NMR is a remarkably well described technique (27, 28). The case of static solid-state NMR will be discussed for oriented and non-oriented samples, as well as the case of magic angle spinning. Hence, in this thesis, only the notions necessary to the comprehension of the NMR experiments presented in the following chapters will be developed.

In the second part, the principles of thermodynamics applied in the Isothermal Titration Calorimetry (ITC) technique will be overviewed and a description of the calorimeter will be presented.

2.2 Solid-state NMR

2.2.1 Oriented samples

Reconstitution of isotopically labelled peptides into oriented membranes allows the orientational distribution of the labelled residues to be analysed with respect to the magnetic field (29). When the membranes are aligned with their bilayer normal parallel to the magnetic field, the main axis of rotational diffusion coincides with the magnetic field direction. This arrangement avoids the introduction of additional peptide orientations concomitant with broadened resonances from rotational diffusion.

The line shapes of these spectra are, therefore to a large extent determined by the orientational distribution of the peptides with respect to the magnetic field direction, as well as contributions from conformational heterogeneity and the dynamic interchange between different membrane topologies (21, 30).

Solid state NMR spectroscopy has been applied to a multitude of synthetic polypeptides that have been selectively labelled and reconstituted into oriented lipid bilayers. When the secondary structure at the site of the isotopic labelling is known, the anisotropic chemical shift provides information about the orientation of this domain with respect to the bilayer normal. The importance of the NH vector during the formation of secondary structures, together with the features of the ^{15}N amide chemical shift tensor allows one to deduce qualitative information about polypeptide topology in a straightforward manner(31, 32).

The size of the σ_{33} component of the amide ^{15}N chemical shift tensor is very different from σ_{11} and σ_{22} , and runs almost parallel to the NH vector (Fig.2.1). For α -helical polypeptides, the NH vector exhibits an orientation almost parallel to the helix axis.

These characteristics allow a direct translation of the ^{15}N chemical shift into the approximate orientation of the helix axis relative to the magnetic field. Provided that the ^{15}N labelled α -helix is reconstituted into oriented lipid bilayers with the bilayer normal parallel to the magnetic field direction, a chemical shift of >200 ppm is indicative of transmembrane orientation of the helix axis, while chemical shifts <90 ppm are observed when the peptide assumes a parallel orientation with respect to the bilayer surface (Fig. 2.2) (31, 32).

In oriented samples, when the helix axis is parallel to the bilayer normal, all of the amide sites have an identical orientation relative to the direction of the applied magnetic field, and therefore, all of the resonances overlap with the same chemical shift frequencies. Tilting the helix away from the membrane normal results in variations in the orientations of the amide N-H bond relative to the field. This is seen in the spectra as dispersions of both the heteronuclear dipolar coupling and the chemical shift frequencies.

In α -helical peptides the NH vector and the σ_{33} cover an angle of 18° and both are oriented within a few degrees of the helix long axis. Due to the size of σ_{33} and the orientation almost parallel to the helix axis, it is possible to measure an approximate alignment of the helix within oriented phospholipid bilayers by recording the ^{15}N chemical shift interaction.

In oriented samples, nearly all transmembrane helices are tilted with respect to the bilayer normal, and it is the combination of the tilt and the 18° difference between the tensor orientations in the molecular frame that makes it possible to resolve many resonances from residues in otherwise uniform helices (33).

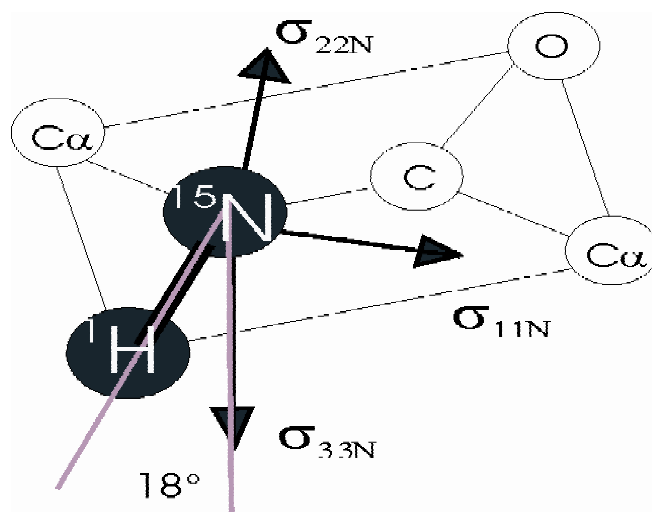


Figure 2.1: Orientations of the principal elements of the spin interaction tensors associated with ^{15}N in a peptide bond. σ_{11} , σ_{22} , and σ_{33} are the principal elements of the ^{15}N chemical shift interaction tensor, and the ^1H - ^{15}N dipolar coupling interaction is along the NH bond. σ_{33} is in the peptide plane and makes an angle of 18° with the NH bond. Adapted from (34).

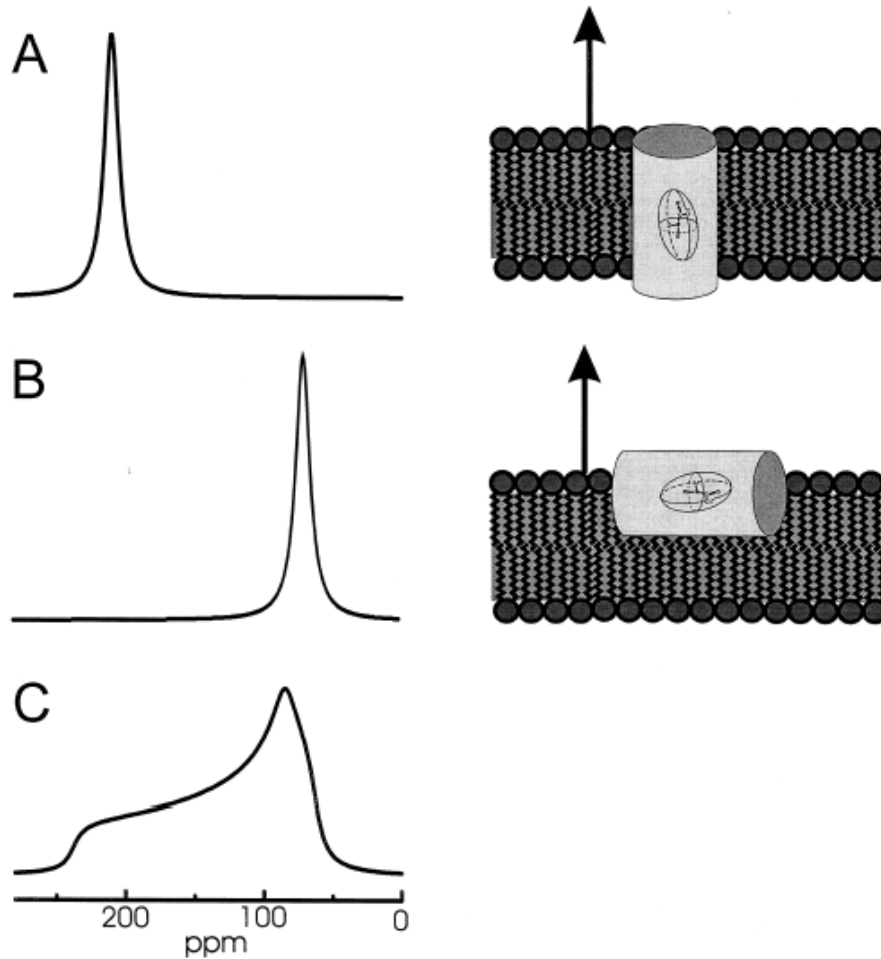


Figure 2.2: Calculated proton-decoupled ^{15}N solid-state NMR spectra of helical peptides ^{15}N -labelled at a single site and reconstituted into oriented membranes (illustrated to the right of the spectra). The membrane normal is aligned parallel to the magnetic field direction (arrows). (A) Transmembrane orientation of the helix axis. (B) Orientation of the peptide approximately perpendicular to the magnetic field direction. (C) Powder pattern line shape, where a random distribution of molecular orientations has been assumed. The ^{15}N chemical shift is scaled to liquid NH_3 . From (10).

Bilayers are on a molecular scale infinitely large in two dimensions and nearly all of the residues in the polypeptide chain are immobile on time scales longer than milliseconds. The relevant dipolar coupling and chemical shift interactions present in individual

backbone sites exhibit only partial motional averaging, and as a result, the samples give very broad and poorly resolved spectra in solid state NMR. Bilayer samples are suitable for the application of solid-state NMR methods where radio frequency irradiations replace molecular reorientation as the principal mechanism of averaging the dipolar couplings responsible for the broadening of the spectra. The solid state NMR that uses stationary, uniaxially aligned samples is particularly well suited for membrane proteins and peptides in lipid bilayers because the proteins are immobilized by the environment and can be highly aligned (10, 25, 35).

2.2.2 Non-oriented Samples

The perturbation of the Zeeman energy levels of a nuclear spin by the chemical shielding interaction results from induced electronic motions in the presence of an external magnetic field which in turn generates secondary magnetic fields that alter the strength of the applied field “felt” by the nuclear spin. The Hamiltonian governing this interaction for a nuclear spin A can be written as $H_{CS} = \hbar \gamma_A I_A \sigma B_0$ where I_A is the nuclear spin angular momentum vector and σ is the chemical shielding tensor, with all other terms having their standard meaning.

The chemical shielding has a directional dependence, it is thus an anisotropic parameter normally specified with reference to the an axis system in which the chemical shielding tensor is diagonal, known as the principal axis system, and is defined by the three principal components σ_{11} , σ_{22} , and σ_{33} , which designate the direction of least, intermediate and greatest shielding respectively and three Euler angles which orient the principal axis system of the chemical shielding tensor in the molecular frame. An important definition is that of the isotropic chemical shift given by $\sigma_{iso} = \frac{\sigma_{11} + \sigma_{22} + \sigma_{33}}{3}$,

where $\sigma_{11} \geq \sigma_{22} \geq \sigma_{iso} \geq \sigma_{33}$.

For a single crystallite with an arbitrary orientation with respect to the external magnetic field, all the molecules are aligned in the same direction in a crystalline lattice. Hence, the molecules will have a particular alignment in the magnetic field B_0 , and the magnitude of the chemical shielding interaction will be a function of the three principal components of the chemical shielding tensor as well as the direction of the magnetic field in the principal axis system of the chemical shielding tensor (Fig. 2.1) which can be specified by the

polar and azimuthal angle θ and ϕ respectively. Consequently, the orientation- dependant resonance frequency for a nuclear spin A can be written as $\nu(\theta,\phi) = \nu_L - \nu_{CS}$, where $\nu_L = \gamma_A/2\pi B_0$ and $\nu_{CS} = \nu_L(\sigma_{11}\sin^2\theta \cos^2\phi + \sigma_{22} \sin^2\theta \cos^2\phi + \sigma_{33}\cos^2\theta)$, where ν_L represents the A spin Larmor frequency.

In a powder sample, the molecules have a statistic distribution with respect to the magnetic field B_0 . All possible orientations (θ,ϕ) are present which gives rise to a characteristic line shape known as powder pattern. The chemical shift of a nuclear spin A can be converted to an absolute chemical shielding scale provided the magnitude of the absolute shielding in the experimental reference compound is known: $\delta_A \approx \sigma_{REF} - \sigma_A$. The three principal components of the chemical shift tensor can be obtained experimentally from the analysis of an NMR chemical shift powder pattern and are defined as the points of inflection $(\delta_{11}, \delta_{22},)$ and discontinuity respectively (δ_{33}) .

Figure 2.2 compares statistic and motionally averaged powder patterns. The powder pattern line shapes are indicators of the rate, direction, and mechanism of intra- and inter-molecular exchange processes, including motional averaging (36). When motional averaging around the membrane normal occurs, the powder pattern line shape can be used to extract the tilt angle of the peptide helix (37).

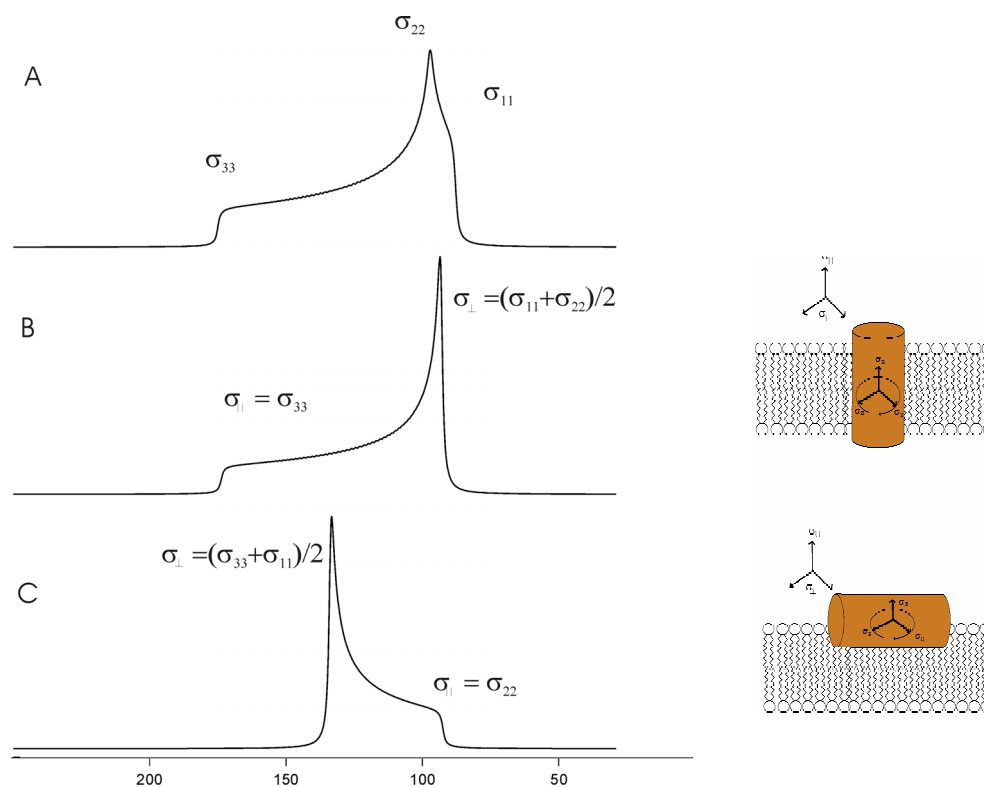


Figure 2.3: Calculated proton-decoupled ^{15}N chemical shift powder pattern (A) in the absence of motional averaging, (B) in case of motional averaging around the σ_{33} main tensor element, and (C) in case of motional averaging around the σ_{22} main tensor element. Averaging of the tensors around the bilayer normal is illustrated to the right of the spectra.

The anisotropic chemical shift interaction is mathematically described by second-rank tensors. In peptides, the properties of the ^{15}N chemical shift tensor are well defined. The ^{15}N σ_{22} and σ_{11} main tensor elements exhibit values in the approximately 85- and 65-ppm range respectively, while its σ_{33} component is characterized by a value of 230 ppm (Fig.2.2).

To first approximation, in an in-plane peptide the amide plane is parallel to the lipid bilayer and during the rotation, σ_{11} and σ_{33} should be averaged, thus spectra should

present a peak at $\sigma_{\perp} = (\sigma_{11} + \sigma_{33})/2 = 132.5$ ppm as well as values that span up to $\sigma_{||} = \sigma_{22} = 85$ ppm. On the other hand, a transmembrane peptide has the amide plane perpendicular to the lipid bilayer and the chemical shift tensors averaged will be $\sigma_{11} + \sigma_{22}$, so that spectra which present a peak at $\sigma_{\perp} = (\sigma_{11} + \sigma_{22})/2 = 75$ ppm and values up to $\sigma_{||} = \sigma_{33} = 200$ ppm are to be expected. Cooling the bilayer below the transition temperature decreases its fluidity. Thereafter, the gel phase of the lipid bilayer prevents peptides rotation and the powder pattern line shapes should be observed (Fig 2.3) (38).

2.2.3 Lipid phase transitions

Lipid bilayers are able to undergo transitions different lamellar phases depending, for each lipid, on the temperature and the hydration. The most studied lipid phase transition is between the lamellar gel and crystalline phases. However, lipid phase transitions have also been examined between other mesomorphic lipid forms.

Phase transitions can be induced in several ways, included changes in the pressure, temperature, ionic strength, or pH (39) The dominant mechanism driving the transition is the ordering of aliphatic tails, requiring a large entropy change. Therefore tail ordering is considered as the driving parameter and other forces like head group interactions are taken into account as secondary effects (40).

The gel phase $L\beta'$ (Fig.2.4) is normally formed at low temperatures, in the presence of water, although this is not strictly necessary. The thickness of the water layer depends on factors such as the water content and temperature, and the lipid headgroup size, polarity and charge. The hydrocarbon chains of DMPC are ordered parallel or tilted to the bilayer normal (41) essentially in the all-trans conformation but undergo hindered long-axis rotation on a time scale of 100 nsec. The headgroups are normally disoriented and the lateral correlations between adjacent layers are weak or non-existent.

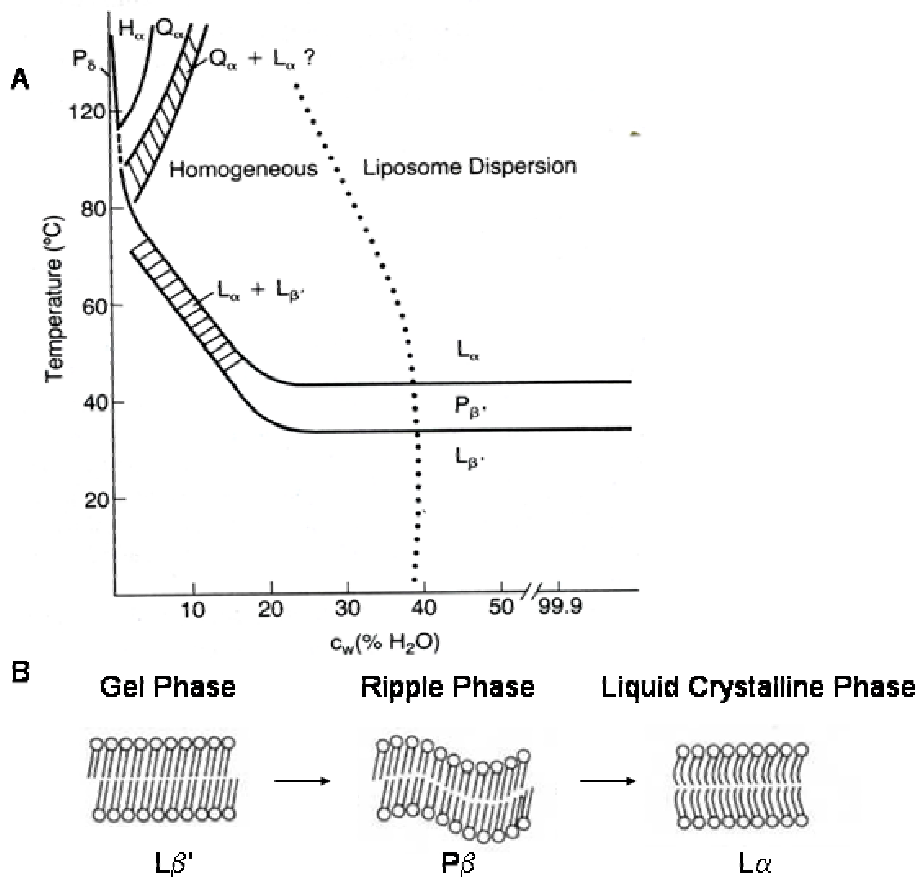


Figure 2.4: Membrane phase Transitions. (A) Phase diagram of dipalmitoyl phosphatidylcholine in water. The percentage of water is indicated on the abscissa with pure lipid on the left and a dilute liquid suspension on the right. Indicated are the Lamellar gel phase ($L_{\beta'}$), lamellar liquid crystalline phase (L_α), and the intermediate ripple phase ($P_{\beta'}$). At high temperature and low hydration, other phases can form (Q_α , cubic phase, H_α , hexagonal phase). The dotted line indicates the maximum absorption of water by the homogeneous lipid-water mixture. (B) Schematic showing the molecular organization of phosphatidylcholine upon heating. Adapted from (39).

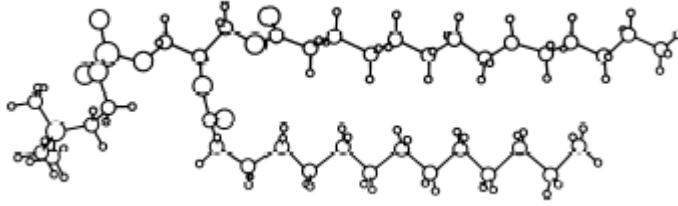


Figure 2.5: Molecular conformation in the lamellar phase of DMPC. From (42)

Upon heating, the cross-sectional area per chain characteristically increases to a limiting value of about 21 \AA^2 . Further heating leads to a liquid-like conformation, transforming to the lamellar $L\alpha$ phase. The $L\alpha$ phase (Fig. 2.4) is completely disordered and may be swollen by addition of water or oil up to a certain limiting spacing. For uncharged phospholipids, the maximum water layer thickness is typically in the range of 10-30 \AA (43). Figure 2.5 shows the molecular conformation in the lamellar crystalline phases of dimyristoylphosphatidylcholine (DMPC) used in our study. Although the fluid $L\alpha$ phase is the most important in biology, the study of the gel phase continues to be a valuable tool (41).

2.2.4 Magic Angle Solid state NMR

In solids, the molecules are generally held rather rigidly, so that dipolar interactions are not averaged to zero in the manner described for liquids (28, 44). If scalar couplings and shielding are ignored, the nuclear spin Hamiltonian becomes the sum of Zeeman and dipolar terms. Since Zeeman energies are much larger than dipole energies, the nuclear spin Hamiltonian for a two-spin heteronuclear AX spin system will be written:

$$h^{-1}\mathcal{H}_{NS} = -\left(v_A\hat{I}_{AZ} + v_X\hat{I}_{XZ}\right) + h^{-1}\mathcal{H}_{dd} \quad (28, 44)$$

where v_A and v_X are the appropriate Larmor frequencies, \hat{I}_j the nuclear spin operator for the nucleus j , R is the dipolar coupling constant, and θ is the angle between the vector and the magnetic field B_0 .

The magnetic dipolar Hamiltonian \mathcal{H}_{dd} of nuclei with spin I can be expressed as a scalar product of two second rank operators representing its spatial and spin symmetry, respectively.

$$h^{-1}\mathcal{H}_{dd} = -R\hat{I}_{AZ}\hat{I}_{XZ} \left(3\cos^2\theta - 1\right)$$

For powder samples all values of θ exist at random and the resulting spectrum forms a powder pattern as discussed in the chapter 1. The terms in the dipolar Hamiltonian which cause NMR line broadening for solids involve the geometric factor $(3\cos^2\theta - 1)$. Rapid isotropic tumbling, such as occurs in non-viscous solutions, averages this geometric factor to zero, thus explaining the very narrow lines observed for such solutions.

Experiments have been designed and performed in order to cancel out the dipolar Hamiltonian (27, 45, 46). They involve spinning the sample with the rotation axis tilted by an angle θ with respect to the magnetic field B_0 . The angle θ was chosen so that the

term $(3 \cos^2 \theta - 1) = 0$ for all orientations, which is the case when $\theta = 54.7^\circ$ (Fig.2.6).

This feature was first noted and exploited independently by Andrew (46) and by Lowe (47), who were interested in removal of dipole - dipole broadening.

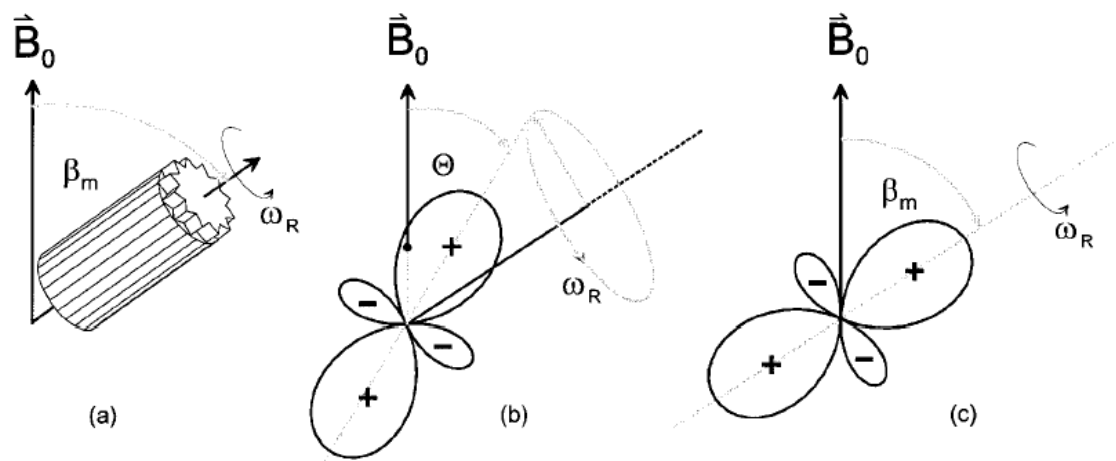


Figure 2.6: Magic angle spinning illustrated. (A) Geometric arrangement of the MAS experiment. The rotor axis is oriented along the “magic” angle of 54.78 to the magnetic field, and the sample is spun around this axis. Maximum spinning frequencies are between 5 and 35 kHz, depending on the rotor diameter and the hardware used. (B) For an intuitive understanding of the averaging of the spin interaction tensor by MAS, the anisotropic part is represented in the drawing by a plot of $P_2(\cos \theta) = (3 \cos^2 \theta - 1) / 2$. The measurable component σ_{zz} of the tensor is given by the intersection with the B_0 direction for simplicity, a symmetric tensor with $\eta=0$ is shown; the conclusions are valid in general). (C) By spinning the sample around the magic angle, the tensor is averaged to a symmetric tensor with σ_{33} axis aligned along the magic angle. In this case, the measurable σ_{zz} component of the anisotropic part of the interaction (intersection of $P_2(\cos \theta)$ with z axis) is zero. From (48).

The sample is filled in a rotor spinning around an axis inclined at the magic angle to the static magnetic field. Thus, just as for isotropic tumbling, the dipolar interaction is

averaged to zero, and the dipolar broadening eliminated giving much higher resolution. This situation is referred to as magic angle rotation (MAR) and 54.7° is called the magic angle.

The ^{15}N and ^{13}C chemical shifts have been used as an analytical tool to determine polypeptide main chain conformations (49). Optimization of sample preparation conditions to obtain microcrystalline samples has helped to yield remarkably high resolution MAS solid state spectra and partial assignments in small model proteins such as bovine pancreatic trypsin inhibitor (50) and the α -spectrin SH3 domain (51).

In MAS solid state NMR, orientational information relative to the membrane is lost, but determination of the peptides secondary structure, precise distance and torsional restraints are possible. Compared with solution NMR, it is possible to obtain measurements with greater accuracy and precision (0.1 - 0.2 Å) and longer distances. For ^{13}C - ^{13}C , the upper limit distance is ~ 6.5 Å, while for ^{19}F - ^{19}F , the upper limit is ~ 16 Å (52).

2.3 Isothermal Titration Calorimetry (ITC)

2.3.1 General thermodynamic considerations

The First Law of thermodynamics states that *the change in internal energy of a closed system is equal to the energy that passes through its boundary.*

The Second Law *relates the change in the entropy of a system (dS) during some process or reaction, to the heat absorbed by the system (dq) at a given temperature (T).* The law takes the expression:

$$dS \geq \frac{dq}{T}$$

Most chemical reactions are irreversible processes carried out at constant temperature and pressure. Under such conditions $dq=dH$ and dS constitutes a measure of spontaneity.

When $dS > \frac{dq}{T}$, the reaction is spontaneous. Substituting for dq , we have $dH - TdS > 0$.

The quantity $dH-TdS$ measures to which extent a reaction will proceed and is referred to as change in *Gibbs free energy*:

$$dG = dH - TdS \quad (2.1)$$

By application of the First Law to (2.1), an equation can be derived linking the standard free energy change (ΔG° under a pressure of 1 atm) and the equilibrium constant of the reaction (53).

Considering the general case of a chemical equilibrium:



The change in free energy will be (54):

$$\Delta G - \Delta G^o = RT \ln \frac{a_C^\gamma a_D^\delta}{a_A^\alpha a_B^\beta} \quad (2.2)$$

At equilibrium the *Gibbs free energy* (ΔG) is zero.

For pure liquids and solids, the activity coefficient is 1 and the activities are approximated to the molar concentrations and the equation (1.2) becomes:

$$\Delta G - \Delta G^o = RT \ln \frac{[C]^\gamma [D]^\delta}{[A]^\alpha [B]^\beta} \quad (2.3)$$

The equation (2.2) may be more generally written

$$-\Delta G^o = RT \ln \prod_j C_j^{\nu_j} \quad (2.4)$$

The product $\prod_j C_j^{\nu_j}$ is defined as the binding affinity constant of a reaction at equilibrium (K) and the above equation can be expressed as:

$$\Delta G = -RT \ln K \text{ or } K = e^{-\frac{\Delta G}{RT}} \quad (2.5)$$

The binding enthalpy primarily reflects the strength of the interactions of the ligand with the target macromolecule relative to those existing with the solvent. Thus, it quantifies Van der Waals, hydrogen bonding, and electrostatic interactions.

The entropy change, on the other hand, mainly reflects two contributions: changes in solvation entropy and changes in the conformational entropy. Upon binding, desolvation occurs, water is released and a gain in solvent entropy is observed. This gain is particularly important for hydrophobic groups. Moreover, the ligand and certain groups in the macromolecule lose conformational freedom, resulting in a negative change in conformational entropy. Different structural and chemical characteristics reflect themselves in different thermodynamic signatures (55).

2.3.2 ITC

In ITC, the calorimeter directly measures the energy associated with a chemical reaction produced by the mixing of two components, when precise amounts of reactant are injected into the reaction cell (56). This injection is performed by a spinning syringe, which at the same time mixes the components. Both the reaction and the reference cells are enclosed in an adiabatic shield, which is itself enveloped by a second adiabatic shield, in order to thermally isolate the two cells in a perfect manner (Fig 2.7).

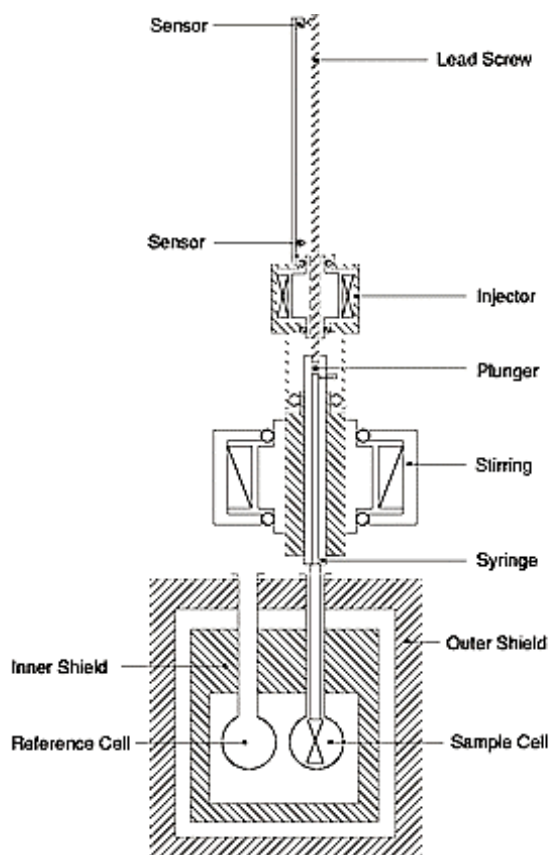


Figure 2.7: Diagram of ITC cells and syringe. The syringe rotates in place during the ITC experiment. The end of the syringe has been adapted to provide continuous mixing

in the ITC cell. The plunger is computer-controlled and injects precise volumes of ligand (<http://www.microcalorimetry.com>).

Temperature differences between the reference and the reaction cell are measured, calibrated to power units and displayed as a signal corresponding to the differential power between the reference and the reaction cell.

The chemical reaction created by each injection either releases or absorbs a given amount of heat (q_i) proportional to the amount of ligand that binds to the macromolecule in a particular injection, and the characteristic binding enthalpy (ΔH) for the reaction: $q_i = Vx\Delta Hx\Delta C_i$, where V is the volume of the reaction cell and ΔC_i the increase of the concentration of bound ligand after the i^{th} injection.

Modern ITC instruments operate by the heat compensation principle. An injection that results an exothermic reaction, causes a negative change in the differential power since the heat evolved chemically provides heat that the differential power feedback is no longer required to provide. The opposite is true for endothermic reactions.

Since the differential power DP has units of power, the time integral of the peak yields a measurement of thermal energy, ΔH . Thus, the measured signal is the amount of power ($\mu\text{cal/s}$) necessary to maintain constant the temperature difference between the reaction and the reference cells. The heat after each injection is therefore obtained by calculating the area under each peak. As the amount of uncomplexed protein available decreases progressively, the magnitude of the peaks becomes smaller until complete saturation is achieved. Once saturation is reached, subsequent injections produce similar peaks corresponding to dilution or mechanical effects that need to be subtracted from all the

injection peaks before analysis (55). It should be noted that after each injection, a reaction delay must be respected so that the system reaches equilibrium before a new perturbation.

ITC experiments have been performed on a VP-ITC instrument presenting an active cell volume of 1.4192 ml. The instrument may be stabilized in a range of temperatures between 2 and 80 °C. The mixing speed may vary from 0 to 545 rpm. The instrument detects binding constants between 10^2 and 10^9 M⁻¹.

2.3.3 The Association between Ligands and Macromolecules

Biochemical systems are rarely in equilibrium as matter is constantly entering and leaving cells, resulting in a steady state situation rather than a true equilibrium (53). However, using equilibrium thermodynamics, a good idea of which cell reactions are favourable *in vitro* can be obtained, thus providing us with the means to understand some energy balances involved in cellular processes.

If we consider the case of single set of identical sites for the reaction:



And we define the following magnitudes as:

K = apparent binding constant;

n = number of binding sites;

V_o = reaction cell volume

$[M_t]$, $[M_b]$ and $[M_f]$ = total, bound, and free concentrations of the macromolecule M in V_o

$[L_t]$, $[L_b]$ and $[L_f]$ = total, bound and free concentration of the ligand

θ = fraction of sites occupied by the ligand L

Then the apparent binding constant will be:

$$K = \frac{[ML]}{[M] \times [L]} = \frac{[Mb]}{[Mf] \times [Lf]} \quad (2.6)$$

As the fraction of sites occupied by the ligand L is:

$$\theta = \frac{[Mb]}{[Mt]} = \frac{[Mt] - [Mf]}{[Mt]} \quad (2.7)$$

And also

$$\theta = \frac{[L_t] - [L_f]}{n[Mt]} \Rightarrow [L_f] = [L_t] - n\theta[Mt] \quad (2.8)$$

The equation (2.6) becomes:

$$K = \frac{\theta}{[Lf](1-\theta)} \quad (2.9)$$

Combining the equations (2.8) and (2.9) gives:

$$([Lt] - n\theta[Mt])(1-\theta)K - \theta = 0 \Rightarrow \theta^2 - \theta \left(1 - \frac{1+[Lt]}{nK[Mt]} \right) + \frac{[Lt]}{n[Mt]} = 0 \quad (2.10)$$

The total heat content measured by the calorimeter at a fractional saturation θ is, as mentioned above:

$$Q = \sum_i q^i = n\theta[Mt]\Delta HV_o \quad (2.11)$$

Solving the binomial equation (2.10) for θ , and substituting it into the equation (2.11), gives:

$$Q = \frac{n[Mt]\Delta HV_o}{2} \left[1 + \frac{[Lt]}{n[Mt]} + \frac{1}{nK[Mt]} - \sqrt{\left(1 + \frac{[Lt]}{n[Mt]} + \frac{1}{nK[Mt]} \right)^2 - \frac{4[Lt]}{n[Mt]}} \right] \quad (2.12)$$

The parameter of interest though, is the change in the heat content from the end of the i-1 injection to the end of the i injection. The expression (2.12) becomes then, after correction of the volume ($\Delta V_i =$ injection volume):

$$\Delta Q_i = Q_i + \frac{dV_i}{V_o} \left[\frac{Q_i + Q_{i-1}}{2} \right] - Q_{i-1} \quad (2.13)$$

The equation (2.13) is used to analyze the data by MicroCal Origin software of the ITC instrument.

Fitting experimental data involves a comparison between a calculated and the experimental ΔQ_i of each injection for a given n, K, ΔH and improvement of these latter values by iteration until no further significant progress may occur.

In the current system, a concentrated solution of LAH4 peptide is injected into the reaction cell containing the DNA solution. The DNA solution contained low molecular double strand DNA fragments of, in average, 300 bp. It should be noted that as the binding affinity as well as the number of binding sites where the peptide is attached to the DNA both depend on the number of base pairs, the binding constant K and the number of sites n measured are, in our studies, specific of a DNA fragment with average size 300 bp.

2.4 Discussion

In this chapter we have overviewed the notions and principles of NMR and ITC techniques necessary to the understanding of the experimental data presented in this work. Solid-state NMR provides valuable information about the structure and dynamics of macromolecular complexes, while ITC measures the thermodynamical parameters characterizing macromolecular interaction.

A combination of different biophysical techniques such as solid-state NMR and ITC is necessary to better understand the function – structure relation of membrane bioactive proteins and peptides.

Chapter 3

Membrane peptide helix alignments and dynamics from non-oriented ^{15}N chemical shift spectra

3.1 Introduction

Nitrogen-15 solid state NMR spectroscopy has found widespread applications in structural studies of peptides and proteins. The chemical shift interaction has been found to be a sensitive probe of structural features such as peptide backbone conformation, secondary structure, hydrogen bonding, and dynamics in lipid bilayers. Due to the significance of the chemical shift in the study of polypeptide structure and dynamics, several reports have appeared in the literature using a variety of solid-state NMR techniques in order to characterize and understand the nitrogen chemical shift tensors of the amide fragment (29, 57, 58). Although the principal components of the chemical shift tensor are sensitive to subtle structural changes for other nuclei such as ^{13}C , it has been found that they show marked similarities throughout the wide range of polypeptides and secondary structures examined. For the amide nitrogen, the most shielded direction is approximately along the C-N bond with the intermediate component perpendicular to the amide plane (Fig. 2.1).

The nuclear interactions with the magnetic field are essentially anisotropic and, therefore, dependent on the orientation and conformation of the molecule with respect to the magnetic field direction (58).

The correlation times of small peptides associated with large macromolecules assemblies, such as phospholipid membranes, are to a large extent determined by the size of the complex. Tumbling is, therefore, considerably slower when compared to the same peptide in solution (10). In order to obtain information about the structure and dynamics of peptides associated with extended lipid bilayers, solid-state NMR spectroscopic methods have been developed.

The chemical shift anisotropy, the dipolar and quadrupolar interactions, often constitute the most pronounced features of solid-state NMR spectra. As a result, broad lines are obtained when solid-state NMR spectra are recorded from non-oriented samples, and consequently these signals often overlap and such spectra generally exhibit low resolution. However, the magnitude and the orientational dependence of nuclear interactions can be used to provide valuable information about the dynamics, the molecular structure, and the orientation of peptides associated with lipid bilayers.

To overcome the problems of low resolution, different approaches have been developed. Fast spinning of the samples around the magic angle, a technique that will be developed more in detail in the next chapter, alignment of the samples with respect to the magnetic field direction, multidimensional NMR spectroscopy and other techniques that decouple or select interactions between nuclear spins.

Once the problem of resolution is overcome, studying the characteristics of the ^{15}N chemical shift anisotropy of a peptide labelled with ^{15}N at a single site by solid state NMR provides valuable information about the structure, dynamics, and alignment of polypeptides.

Oriented samples are characterized by a restricted orientational distribution of alignments with respect to B_0 and therefore results in narrow lines.

Proton-decoupled ^{15}N solid-state NMR spectra of randomly oriented bilayer samples provide a valuable tool with which to analyse the global and local dynamics of membrane-bound polypeptides as well as their orientation with respect to the membrane normal.

The membrane associated peptides h Φ 19W and KL14, were used in order to test this new technique. The orientation of these two peptides has been previously described in oriented samples (59), it was found to be transmembrane for the peptide h Φ 19W and in plane for the KL14. Our studies on non oriented samples reached the same conclusion, confirming that the technique is applicable.

Non-oriented lipid bilayers were also studied as for their association to the amphipathic α -helical synthetic peptide LAH4 when complexed to low molecular weight DNA. Non-oriented samples containing the peptide LAH4 were studied providing information about the peptide re-orientational correlation times.

3.2 Materials and methods

Peptide synthesis

The peptides (KKK ALLA LLALA WALLAL LALLA KKK) hΦ19W, (KKL LKK AKKLL KKL) KL14 and (KKALL ALALH HLAHL ALHLA LALKK A) LAH4 were synthesized by solid phase peptide synthesis on a Millipore 9050 automatic peptide synthesizer by using standard synthesis cycles. A fourfold excess of Fmoc-protected amino acids (Calbiochem, L aufelfingen, Switzerland) was used during chain elongation and ¹⁵N-labeled Fmoc-protected alanine or leucine analogues were incorporated at the underlined positions of the peptides. After TFA cleavage of each peptide from the resin, their identity was determined by matrix-assisted laser desorption/ ionization mass spectroscopy (MALDI-MS) and the results fitted the theoretical molecular mass calculated from the peptide's primary sequence. The reverse-phase high-performance liquid chromatography (HPLC) was performed and the chromatograms were recorded at 214 nm using an acetonitril gradient in the presence of TFA. Both MALDI-MS and HPLC indicate a high degree of purity.

Preparation of non- oriented membrane samples

For solid-state NMR spectroscopy, oriented bilayers of lipid plus RK1 or KL14 were prepared by dissolving 50 mg of labelled peptide in water/ trifluoroethanol (TFE) and 400 mg of 1,2-Dimyristoyl-*sn*-Glycero-3-Phosphocholine (DMPC) in dichloromethane were added. Oriented bilayers of lipid plus LAH4 were prepared by dissolving 50 mg of labelled peptide in water/ trifluoroethanol (TFE) and diluted in Tris buffer. The pH was then adjusted to either 7.5 or 5.5 by addition of 0.5 N NaOH. Next a solution in dichloromethane 400 mg of 1,2-dimyristoyl-*sn*-glycero-3-phosphocholine (DMPC)

(Avanti Polar Lipids, Birmingham, AL) was added. A transparent film was obtained by evaporating the solvent, first under a stream of nitrogen, then in high vacuum overnight. Where appropriate 4 mg of salmon sperm low molecular weight DNA dissolved in a water/ Tris solution at pH 7.5 or 5.5 were added.

The samples were then spread on a glass plate, dried under vacuum and re-hydrated at 93% relative humidity. The material was finally scratched off the glass surface, transferred into small test tubes suitable for NMR measurements and sealed. Control samples were prepared by creating large multimeric vesicles (LMV) as described above, using the corresponding buffers at pH 5.5 and 7.5, in absence of DNA.

Solid-state NMR spectroscopy

The non-oriented samples were inserted in wide line solid-state NMR probe heads (60) and introduced into the magnetic field of a Bruker Avance wide-bore NMR spectrometer operating at 9.4 T. ^{15}N NMR solid-state spectra were recorded using a cross-polarization sequence with high-power proton decoupling. The following parameters were used: proton 90° pulse width of typically 8 μs , spin lock time of 1.6 ms, acquisition time of 3 ms and 256 data points acquired. An exponential line-broadening function of 150 Hz was applied to the free induction decay before Fourier transformation.

3.3 Results

α -Helical peptides were synthesized and labelled with [^{15}N]alanine or [^{15}N]leucine, reconstituted into non-oriented phospholipid bilayers, and investigated by solid-state NMR spectroscopy. The proton-decoupled ^{15}N solid-state NMR spectrum of KL14 labeled with [^{15}N]leucine-10 reconstituted in DMPC exhibit, at 310 K, ^{15}N chemical shifts between 142 ppm and 80 ppm (Fig. 3.1A). These powder pattern line shape values correspond, by approximation, to $\sigma_{\perp} = (\sigma_{11} + \sigma_{33})/2$ and $\sigma_{\parallel} = \sigma_{22}$. They are indicative of peptide alignments parallel to the membrane surface. On the other hand, the same sample, at 280 K, exhibits a wide powder pattern line shape with values ranging from 65 to 220 ppm (Fig 3.1B).

The proton-decoupled ^{15}N solid-state NMR spectrum of h 19W reconstituted into non-oriented DMPC membranes exhibits, at 310 K, ^{15}N chemical shifts between 75 ppm and 220 ppm (Fig. 3.1C). These powder pattern line shape values are related to, by approximation, $\sigma_{\perp} = (\sigma_{11} + \sigma_{22})/2$ and $\sigma_{\parallel} = \sigma_{33}$. Thus, the spectrum is indicative of a transmembrane orientation of the peptide helix relative to the membrane. At 280 K, a large powder pattern with values between 65 and 220 ppm is observed for the h 19W peptide reconstituted into non-oriented DMPC membranes (Fig.3.1D).

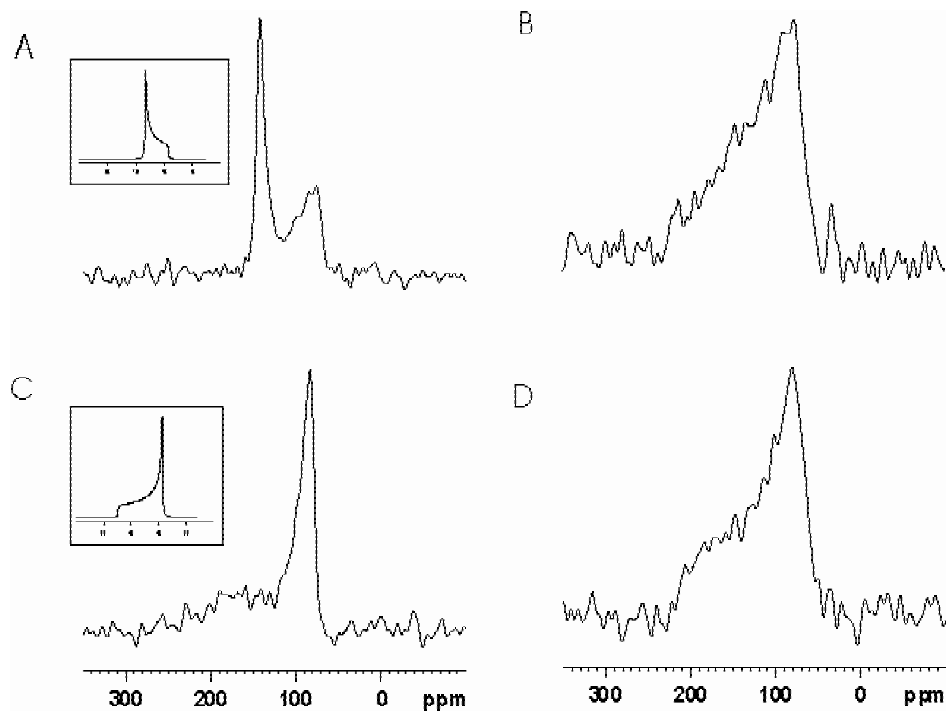


Figure 3.1: Proton decoupled ^{15}N solid state NMR spectra of ([^{15}N]leucine-10)-KL14 (A,B) and of ([^{15}N]leucine-15)-h 19W (C,D) when reconstructed into DMPC bilayers. Spectra A and C were obtained at 310K while spectra B and D were obtained at 280K. The insets show the respective calculated spectra.

Another interesting application of non-oriented samples in ^{15}N solid state NMR spectroscopy is the study of re-orientational correlation times and the peptides dynamic movement when associated to the membrane. As an example, the case of the α -helical peptide LAH4 will be described below.

Proton decoupled ^{15}N solid-state NMR spectra of ([^{15}N] alanine-13)-LAH4 reconstituted in non-oriented DMPC membranes have been recorded, complexed or not to DNA molecules and at different pH. The chemical shift dispersion observed for the powder pattern line-shape of LAH4 in DMPC bilayers at pH 7.5 extends from >200 ppm to approximately 65 ppm (Fig.3.2A). This chemical shift anisotropy resembles that observed for dry or frozen samples of model compounds or peptides (36, 61), indicating

that bilayer-association of LAH4 results in slow re-orientational correlation times when compared to the time-scale of the ^{15}N chemical shift interaction (10⁻⁴ second). This wide powder pattern line shape maintains its large distribution upon addition of the DNA (Fig. 3.2C), suggesting that the LAH4 peptide forms a large binary complex with the DNA where tight interactions between these two macromolecules hinder the backbone movement of the peptide.

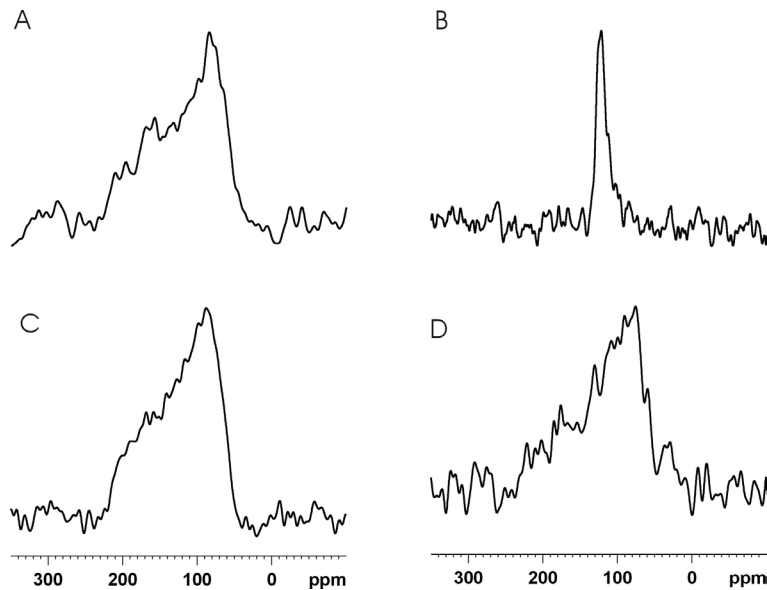


Figure3.2: Proton decoupled ^{15}N solid state NMR spectra of ([^{15}N] alanine-13)-LAH4 reconstructed into DMPC bilayers at pH 7.5 (A, C) and pH 5.5 (B, D), registered at 280K. Spectra C and D were obtained in presence of 4 mg salmon sperm low molecular weight DNA.

The size of LAH4/DNA complexes was thus measured by zeta-potential size experiments effectuated by our collaborators in Généthon - CNRS (UMR 8115, Evry, France). The results indicate that at pH 7 the complexes reach several micrometers in diameter when generated in 150 mM salt solutions whilst they are in the 100 nm range when assembled in a salt-free solution (5% glucose). Such a salt-dependent aggregation was also

described for other transfection agents, in particular for the cationic polymer polyethylenimine (62). Optical microscopy observation of the complexes at low pH also confirmed their large size.

The proton-decoupled ^{15}N solid state NMR spectrum of the (^{15}N] alanine-13)-LAH4 peptide reconstituted in lipid bilayers, at pH 5.5, exhibits a narrow anisotropic line shape with maximum at 120 ppm. This decrease in the chemical shift anisotropy observed at pH 5.5 is indicative of motional averaging due to rapid rotational correlation times (Fig. 3.2B) (21).

The proton decoupled ^{15}N solid state NMR spectrum of the LAH4 peptide associated to the DNA at pH 5.5, shows increased chemical shift anisotropy which results to a wide powder pattern indicating that bilayer-association of LAH4 results in slow re-orientational correlation time such as the one observed at pH 7.5 (Fig. 3.2D).

3.4 Discussion

The line shapes of proton-decoupled ^{15}N solid-state NMR spectra are strongly affected by molecular motion. Most of the backbone sites of bilayer-associated peptides are structured and therefore immobile on the time scale of the ^{15}N chemical shift interaction (10 kHz) and contribute to the characteristic amide powder pattern between about 220 and 65 ppm.

In the liquid crystalline phase $\text{L}\alpha$, the fluid mosaic model indicates considerable lateral and rotational diffusion within the bilayer (41). Although in non-oriented samples the peptide is present in all possible orientations, the fact that it is able to move around the bilayer normal results in rotational averaging along different axes and results in different averaged chemical shift tensors thereby reflecting the alignment of the peptide in the bilayer.

In order to validate the previously published predictions (38), α -helical peptides whose orientations relative to the phospholipid bilayer are well known were used as models. The KL14 sequence is composed of alternating lysine and leucine residues, when at the same time the h Φ 19W primary sequence contains an alternation of alanine and leucine amino acids interrupted by a tryptophan at the 13th position. These α -helical peptides were designed so they would be aligned respectively in-plane and transmembrane when inserted into lipid bilayers, affirmation of this assertion was provided by Aisenbrey et al, 2004 (59). The two peptides were synthesized, labelled with ^{15}N leucine, reconstituted in non-oriented phospholipid bilayers and investigated at different temperatures.

To reduce problems that would be associated with peptide aggregation, non-oriented samples were prepared from clear homogeneous solutions of peptide and lipid.

Furthermore, terminal lysines were attached as membrane surface anchors and helped to avoid peptide aggregation (63, 64).

Proton decoupled ^{15}N solid state NMR spectra of (^{15}N leucine-10)-KL14 on oriented DMPC membranes exhibit their maximal ^{15}N chemical shift <100 ppm, a line shape which is indicative of peptide alignments parallel to the membrane surface (59). The ^{15}N powder spectra of the KL14 peptide shown in Figure 3.1A exhibit, at the physiological temperature of 310K, values between 142 ppm and 80 ppm, which, when compared to the proton-decoupled ^{15}N chemical shift powder pattern simulated are in agreement with a motional averaging around the σ_{22} main tensor element (Fig. 2.3C). This motional averaging corresponds to an in-plane alignment of the peptide, relative to the membrane.

Proton decoupled ^{15}N solid state NMR spectra of (^{15}N leucine-15)-h Φ 19W on oriented DOPC membranes (Fig. 3.1C) exhibit ^{15}N chemical shift values >200 ppm indicating a transmembrane orientation (59). In the liquid crystalline phase of DMPC membranes, at 310K, proton decoupled ^{15}N solid state NMR spectra exhibit a sharp peak at 75 ppm as well as values up to 220 ppm, a pattern which corresponds indeed to the transmembrane orientation of the peptide when compared to the ^{15}N chemical shift simulated powder pattern averaged around the σ_{33} main tensor element (Figure 2.3B).

The spectra of the peptides are quite different at temperatures below the lipid phase transition. Lowering the temperature slows the dynamic movement of the lipids, preventing thus the rotational averaging of the movement. Indeed, when the membrane reaches the crystalline lamellar phase, at 280K for DMPC lipids, the typical wide powder pattern, expanding from 65 to 220 ppm, is obtained for non-oriented samples as expected (Fig. 3.1B, D). The spectra at this temperature were recorded in order to validate that in

the absence of motional averaging, the powder spectra find their wide spread distribution once more.

The membrane interaction of the LAH4 peptide has been thoroughly studied in the past (21, 23) and its orientation was shown to depend on the pH value of the peptides environment. Proton-decoupled ^{15}N solid state spectra of single-site ^{15}N labelled LAH4 incorporated into uniaxially oriented phospholipid bilayers were performed in order to determine the secondary structure of proteins and their orientation with respect to the bilayer surface (21, 31, 65-67). The spectra at low pH indicate an approximately parallel alignment of the α -helix with the bilayer surface (21). The amphipathic distribution of amino acid side-chains suggests that the polypeptide intercalates into the phospholipid interface in such a way as to bury the large majority of hydrophobic amino acid residues in the bilayer interior, while polar residues face the water phase. At neutral pH, the peptide spectra are characterized by a ^{15}N chemical shift of approximately 190 ppm, indicating a transmembrane orientation of LAH4 (31).

Below the transition temperature, the liquid gel phase $\text{L}\beta$ of the lipid bilayer thus prevents peptides rotation and the large powder pattern spreading from 65 to 220 ppm, should be replaced by characteristic narrower powder line shapes depending on the peptide orientation in respect to the bilayer normal (65).

Proton decoupled ^{15}N solid-state NMR spectra of (^{15}N alanine-13)-LAH4 reconstituted in non-oriented DMPC membranes have been recorded, complexed or not to DNA molecules and at different pH. The chemical shift dispersion observed for the powder pattern line-shape of LAH4 in DMPC bilayers at pH 7.5 (Fig. 3.2A) resembles to the one observed for dry or frozen samples of model compounds or peptides (36, 61), indicating

that bilayer-association of LAH4 results in slow re-orientational correlation times when compared to the time-scale of the ^{15}N chemical shift interaction (10⁻⁴ second).

In contrast, the decrease in chemical shift anisotropy observed at pH 5.5 is indicative of motional averaging due to rapid rotational correlation times (Figure 3.2C) (21). Several backbone sites of the membrane bound form of the LAH4 peptide interact more loosely with the lipids and are more mobile. This results in the narrow resonance band centred at the isotropic resonance frequency near 120 ppm (25).

The above observation is in good agreement with the results obtained from oriented samples. Indeed, at pH 7.5 the LAH4 peptide adopts a trans-membrane orientation surrounded by lipid molecules that prevent its motion. On the other hand, at pH 5.5 the in-plane orientation allows the peptide to move more freely. The isotropic averaging is therefore the result of rotational movement around the bilayer normal, as well as wobbling and/or tumbling movements in the inter-membrane space.

The powder pattern line shape observed for the LAH4 at pH 7.5 remains as wide upon addition of the DNA, suggesting that the LAH4 peptide forms a large binary complex with the DNA where tight interactions between these two macromolecules hinder the backbone movement of the peptide. The large size of LAH4/DNA complexes was also confirmed by zeta-potential measurements and optical microscopy.

On the other hand, when the LAH4 peptide is associated to the DNA at pH 5.5, the chemical shift anisotropy increases and a wide powder pattern is observed indicating that bilayer-association of LAH4 results in slow re-orientational correlation time such as the one observed at pH 7.5. This decrease of the motional dynamism further confirms the closer binding of the LAH4 molecules on the DNA helix.

The ^{15}N solid state NMR spectra of peptides in non-oriented membranes show that the motional averaging of the chemical shift tensors which compose the transversal axis of the peptides provide information on the peptide helix orientation relative to the membrane surface, provided that fast motional averaging around the membrane normal occurs. This principle was very successful for KL14 and hΦ19W, α -helical model peptides of the in plane and transmembrane orientations respectively. However, it proved to be less fruitful in the case of the LAH4 peptide, the acquired information on its dynamics was very general and difficult to interpret, while there was no information on the molecular orientation with respect to the membrane.

Proton-decoupled ^{15}N solid-state NMR spectra of non-oriented samples may be used to study the consequences of the binding between two macromolecules on their association to the membrane bilayer. This method may be applied for the study of various peptides. The preparation of the samples is less delicate and less time consuming. Moreover, the absence of glass plates allows enhanced filling of the coil, improved pH and hydration control of the sample, as well as better shimming conditions.

Chapter 4

Thermodynamic and structural study of a peptide transfection complex

4.1 Introduction

Increasing the efficiency and reducing the cytotoxicity of gene delivery system remains a major challenge but offer high benefits both for basic research and gene therapy. Recombinant viruses are the most studied vectors for the transfer of DNA into cells and they are the basis of the vast majority of ongoing clinical trials (68). Furthermore, biochemical studies and the structural characterization of these biological vectors has permitted the development of gene delivery systems made of greatly simplified components that mimic the advantageous aspects of viral transfection without its apparent side effects.

Non-viral gene delivery is achieved by a variety of compounds of unrelated structure including dendrimers (69), polylysine conjugates (70), linear and branched polycations (71, 72) blocked copolymers (73), cationic liposomes (74, 75) and peptides (8, 9). Among these systems, synthetic peptide based gene delivery is the least explored despite its great potential. Indeed, in contrast to most polymers, key parameters such as product identification and quality control are possible for polypeptides used in transfection experiments.

Peptides were initially used as cell targeting moieties (76), membrane destabilizing agents (77, 78), or nuclear localization elements (79). Cationic peptides are of particular interest as they can combine DNA condensation with membrane destabilizing capabilities. To our knowledge KALA was the first synthetic transfection peptide (8), a tetrameric repeat that was later improved by replacing the lysines by arginines (9). Furthermore, several peptides of the LAH4 family have proven to be efficient transfection agents (24), with low cytotoxicity and high bacteriotoxic activity (23).

The parent peptide (LAH4) with the sequence KKALL ALALH HLAHL ALHLA LALKK A was initially designed as a model peptide to study the interaction contributions that determine the membrane topology and the membrane-disrupting properties of some α helical amphipathic peptides, including the antibiotics magainins and cecropins (10, 21). Helical wheel projection shows that LAH4 is characterized by the separation of polar and hydrophobic residues at opposite helical surfaces (Fig. 4.1).

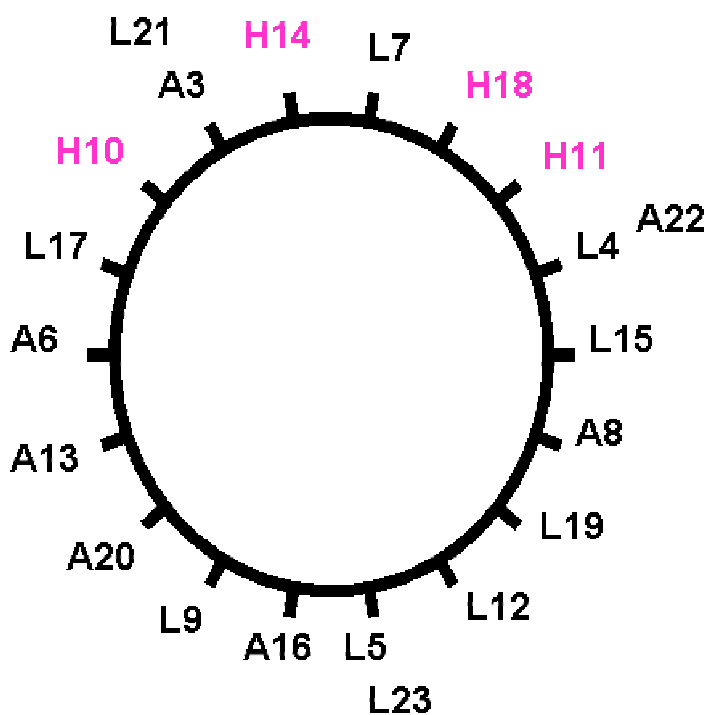


Figure 4.1: Edmundson helical wheel diagram of LAH4.

Whereas the cationic charge at physiologic pH confers DNA condensating properties in aqueous solution (80), the hydrophobic face of the peptide allows for efficient membrane interactions. In contrast to previous studies, where the interaction of LAH4 with membranes was investigated (21, 23), the present study focuses on the thermodynamic and biophysical parameters of the LAH4-DNA transfection complexes.

The key to understanding fully the mechanism of a reaction lies in combination of thermodynamic data with structural detail.

The micro calorimetric instrumentation currently available can provide a highly accurate measurement of the heat associated with the change in the considered system corresponding to the molar change in enthalpy (ΔH). Probing the extend of the occurred

change by the heat permits the determination of the equilibrium constant (K). Thus, determination of ΔH and K enables full characterization of the reaction considered.

While the association constant K informs us of the affinity and the specificity (δI) of the interaction, the enthalpy and the entropy of the reaction may permit the understanding of the driving forces of the reaction.

Biomolecules interact together via non-covalent bonds, namely hydrophobic interactions, electrostatic ones, hydrogen bonds and van der Waals forces.

The nature of hydrophobic interactions is based on the lack of strong, favorable interactions between polar water molecules and non-polar molecules. They have entropic and enthalpic contributions which vary considerably with the temperature, and they are driven by the minimization of the solvent-exposed non-polar (hydrophobic) surface area. Due to bond polarization resulting from differences in electronegativity, most covalent bonds are polarized and thus there is an effective charge on most atoms. Oppositely charged regions of polar molecules are attracted by electrostatic interactions.

Hydrogen Bonds are a special case of electrostatic interaction, resulting from the strong electronegativity of O and N. H-bonds are weak electrostatic interactions between two partially charged atoms, the donor and acceptor.

Van der Waals forces are weak attractive or repulsive interactions between any two atoms in close proximity. The physical basis is that each atom behaves like an oscillating dipole due to the movement of electrons around the nucleus, leading to coupled, transient dipoles of opposite charge.

The process of molecular recognition, and DNA binding by proteins and peptides, is governed by a hierarchy of interactions involving amino acid side chains. These are of three types: Stacking interactions between aromatic side chains and DNA bases,

Hydrogen Bonding interactions between hydrophilic side chains and nucleotides, and ionic interactions involving positively charged side chains and the phosphodiester backbone of DNA.

Isothermal Titration Calorimetry (ITC) has been employed successfully in previous studies to elucidate peptide - DNA (82-84) or peptide – membrane association (85-87). It has also been used to better understand the association of DNA with cationic lipids used in transfection experiments (88-90). Here we present, to our knowledge, for the first time, thermodynamic details characterizing the association of a peptide transfection vector with DNA. Furthermore, CD and solid state NMR spectroscopies provide complementary data that help in the structural interpretation of the ITC results and that ultimately lead us to propose a structural model of the multiple roles of the LAH4 peptide during transfection.

4.2 Thermodynamic Characterization of the LAH4/DNA complexes

4.2.1 Materials and Methods

Materials All chemicals were purchased at highest purity from commercial sources.

Peptide synthesis The peptide (KKALL ALLALH HLAHL ALHLA LALKK A) LAH4 was synthesized by solid phase peptide synthesis on a Millipore 9050 automatic peptide synthesizer by using standard synthesis cycles. A fourfold excess of Fmoc-protected amino acids (Calbiochem, L aufelfingen, Switzerland) was used during chain elongation and a $^{13}\text{C}_\beta$ -labeled Fmoc-protected alanine analog (Calbiochem, L aufelfingen, Switzerland) was incorporated at either position 6 or 13, respectively (underlined in the sequence shown above). After TFA cleavage from the resin, the identity and purity of the peptides was verified using matrix-assisted laser desorption/ ionization mass spectrometry (MALDI-MS) and reverse-phase high-performance liquid chromatography (HPLC). The HPLC chromatograms were recorded at 214 nm using an acetonitril/water gradient in the presence of 0.1% TFA.

Isothermal Titration Calorimetry was performed using a VP-ITC instrument with a cell volume of 1.4192 mL (MicroCal, Northampton, USA). The peptide and the salmon sperm low molecular weight DNA (Fluka, Buchs, Switzerland) were dissolved in phosphate saline buffer at pH 7.5 or 5.5, respectively. Care was taken to prepare the DNA and peptide solutions from the same batch of buffer in order to minimize mixing artifacts. All solutions were degassed under vacuum prior to use. At 240 seconds intervals 8 μL of

1 mM peptide stock solution was injected into a solution of 0.5 μ M DNA and the heat of association measured. The stirring rate was 300 rpm. The starting solutions in the calorimeter cell and in the syringe were kept at the same temperature (288, 298 or 308 °K, respectively). Control experiments were carried out under identical experimental conditions by injecting the peptide into PBS, or by injecting PBS into DNA solutions. The results of the titration experiments were analyzed using the MicroCal Origin software of the ITC instruments.

Determination of the standard thermodynamic functions: After each injection of peptide into DNA the heat of reaction is obtained. During the course of the experiment ΔH is measured in a concentration-dependent manner and the equilibrium constant K evaluated directly from the titration curve. The free energy of binding (ΔG) and the entropy change (ΔS) are thereafter determined using standard thermodynamic relationships: $\Delta G = -RT \ln K = \Delta H - T\Delta S$. The binding of LAH4 to DNA was evaluated using a model for a single independent binding site (91, 92). The temperature dependence of the enthalpy indicates the heat capacity of the association of the fully folded peptide with the fully folded DNA according to $\Delta C_p = d\Delta H/dT$. The equilibrium parameters reported were determined from two independent titrations at each experimental condition and agreed within 15%.

Native Gel Electrophoresis The peGFP vector used for the transfection experiments by Kichler et al, 2003 was digested by the *HinfI* enzyme and the fragments produced (1000, 500, 400, 300, 150, 100 and 75pb) were purified and used to test for binding with the LAH4 peptide.

The LAH4 peptide and the peGFP derived DNA were first solubilized in PBS buffer at the appropriate pH and mixed and at molar ratios of 0, 1, 2.5, 5, 7.5, 10, 25, 50 and 75 for the experiment at pH 7.5, or respectively 0, 0.001, 0.025, 0.05, 0.075, 0.01, 0.25, 0.5, 0.75 and 1 for the experiment at pH 5.5. The mixtures were incubated for 20 min at room temperature and loaded on a native agarose gel of 1 or 2 % depending on the size of the DNA fragment. To visualize the DNA, the gels were stained in 5 µg/ml ethidium bromide solution and the bands were detected by UV light (= 302 nm).

4.2.2 Results

ITC was used to directly measure the heat changes upon addition of small volumes of concentrated LAH4 to the reaction cell containing the DNA solution (Fig. 2.7). Integration yields the calorimetric binding enthalpy (ΔH) as a function of peptide concentration. The resulting titration curves were analyzed assuming a single type of binding site, directly providing both the association constant (K) and the peptide/DNA stoichiometry at saturation (N). The free energy change (ΔG) and the entropy change (ΔS) during complex formation are obtained using standard thermodynamic relationships. Titrations were performed in the temperature range 15-35°C in which both the peptide and the DNA are thought to undergo only minor conformational changes (82, 84, 93).

Although the enthalpy and entropy of the binding vary considerably under the different conditions tested, this variation is counter directional such that the free energy values (ΔG) remain roughly constant. This observation is true for most biological systems (94).

Figure 4.2a shows a typical DP signal as measured for the addition of LAH4 into the DNA solution at pH7.5, at different temperatures and variable concentrations. The reaction was in most cases endothermic with very low binding enthalpy (Table 4.1).

At pH 5.5, the reaction was exothermic for all conditions tested (Fig. 4.2b). The binding enthalpy observed at room temperature was high, fact that coincides with an important increase in the number of binding sites.

In Table 4.1 the thermodynamic parameters are assembled as a function of temperature and pH. The values of ΔG are all negative, favoring association, and in all cases this association process is entropy driven. However, the reaction is endothermic at pH 7.5 and exothermic at pH 5.5, the strong pH dependence of the enthalpy indicating different contributions at neutral and low pH.

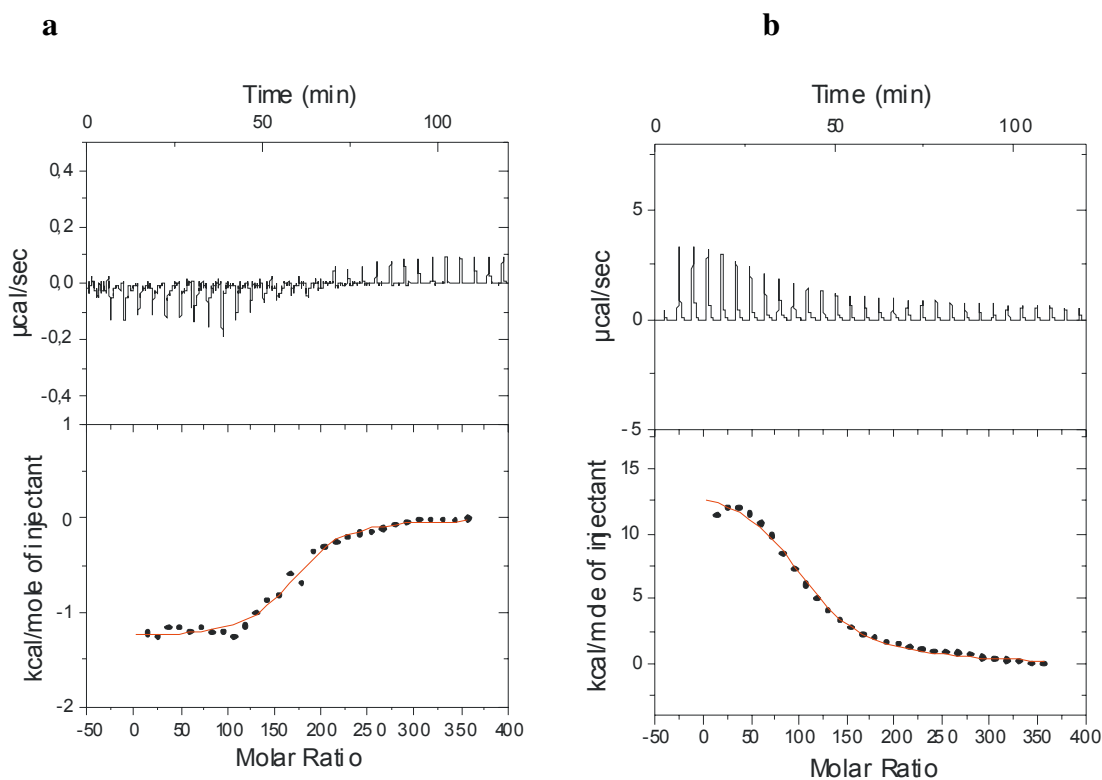


Figure 4.2: Isothermal titration of low molecular weight salmon sperm DNA (ca. 300 bp) with the LAH4 peptide. (a) pH 7.5 and (b) pH 5. Titration of 0.5 μM DNA with 1 mM LAH4 (upper panel). The peptide was added in 40 aliquots of 8 μl each, in phosphate-buffered saline at 25°C. Integration of these peaks and subtraction of the heats of dilution produces the binding isotherm shown in the lower panel. The points are fitted to a model for a single independent binding site.

In control experiments the enthalpy of the LAH4 dilution was determined (95-98), and subtracted from the total change in enthalpy due to the formation of the LAH4/DNA complex. In contrast, DNA dilution results in negligible heat changes under all conditions tested.

Temp (K)	pH	Conc (M)	ΔH (kJ/mol)	T ΔS (kJ/mol)	ΔG (kJ/mol)	KA (M ⁻¹)	N
308	7.5	1	5	25,76	-21	1,77E+05	143
298	7.5	1	-5	27,19	-33	5,02E+05	170,8
298	7.5	0,75	-7	23,33	-31	2,22E+05	129
298	7.5	0,5	-10	17,74	-28	7,69E+04	68,7
288	7.5	1	-6	21,69	-28	8,97E+04	208
308	5.5	1	2	31,40	-30	2,44E+05	51
298	5.5	1	58	88,11	-30	1,72E+05	107
298	5.5	0,75	54	84,91	-31	3,23E+05	99
298	5.5	0,5	41	72,44	-32	3,57E+05	88
288	5.5	1	6	34,58	-29	1,49E+05	34

Table 4.1: Thermodynamic parameters describing the interaction of LAH4 with DNA as a function of the temperature and pH obtained by ITC. Enthalpies were recorded as a function of the pH, LAH4 concentration and temperature. The binding enthalpy was determined directly from the ITC titration curves. From these experimentally determined parameters, the free energy of binding (ΔG) and the entropy change (ΔS) are obtained using the standard thermodynamic relationship $\Delta G = -RT \ln K = \Delta H - T\Delta S$.

The thermodynamic parameters thus obtained as a function of temperature and pH are shown in Table 4.1. The values of ΔG are all negative, favoring association, and in all cases this association process is entropy driven. However, the reaction is exothermic at pH 7.5 and endothermic at pH 5.5, this strong pH dependence being indicative of significant differences when the interaction contributions at neutral and low pH are compared to each other. Although the enthalpy and entropy changes during association vary considerably under the different conditions tested, this variation is counter directional such that the free energy values (ΔG) remain roughly constant (Table 4.1).

Such entropic-enthalpy compensation has been described for other biological systems and is discussed in reference (99).

Interestingly, the ITC data show twice as many binding sites on the DNA at pH 7.5 than at pH 5.5 at room temperature and at 1mM concentrations of the peptide. To understand these data one has to consider that at pH 7.5, the LAH4 lysines and the N-terminus are the only positively charged amino acids, conferring a nominal charge of +5 to the peptide, while at pH 5.5, the histidines are also protonated, and the peptide nominal charge increases to +9.

The LAH4-DNA association was also studied by migration of the complex on an agarose gel by native electrophoresis. Small fragments of different sequence produced by the digestion of the plasmid peGFP were added to different concentrations of LAH4 and the samples loaded and analyzed by agarose gel electrophoresis. The peGFP plasmid was chosen since it has already shown its capacity to interact with the LAH4 peptide, as demonstrated by its efficiency to act as a transfection vector (24).

Notably, the LAH4 peptide interacts with all the fragments tested, and generates large complexes that are not able to migrate through the agarose net (Fig. 4.3).

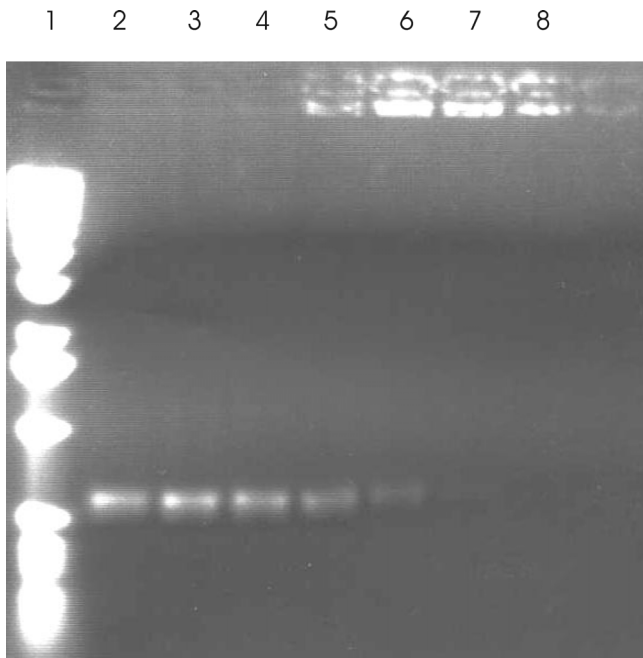


Figure 4.3: Gel electrophoresis analysis of LAH4/DNA complexes. LAH4 and peGFP derived 500bp DNA (1 mg/ml) were mixed at molar ratios of 0, 1, 2.5, 5, 7.5, 10, and 25 (Lanes 2-8) at pH 7.5 as described in the materials and methods section, incubated for 20 min and loaded on a native agarose gel of 1%. The migration of a standard 1Kb ladder is shown on the left (Lane 1).

This complex is retained at the slot at molar ratios $\text{LAH4} / \text{DNA} \geq 10$. It should be noted that retention of the complex corresponds to a state where the overall charge and topology of the complex prevents migration through the agarose matrix, rather than the saturation in binding.

Migrational properties of the complex did not show pronounced differences at the two pH values investigated, reflecting the low sensitivity of the method.

To further characterize the LAH4-DNA association, the conformational changes of the peptide during complex formation were studied by CD spectroscopy. CD spectra were

recorded as a function of pH and in the absence and presence of DNA under conditions comparable to those used during the ITC study. The experiments were undertaken by Dr Masae Sugawara (Fig.4.4).

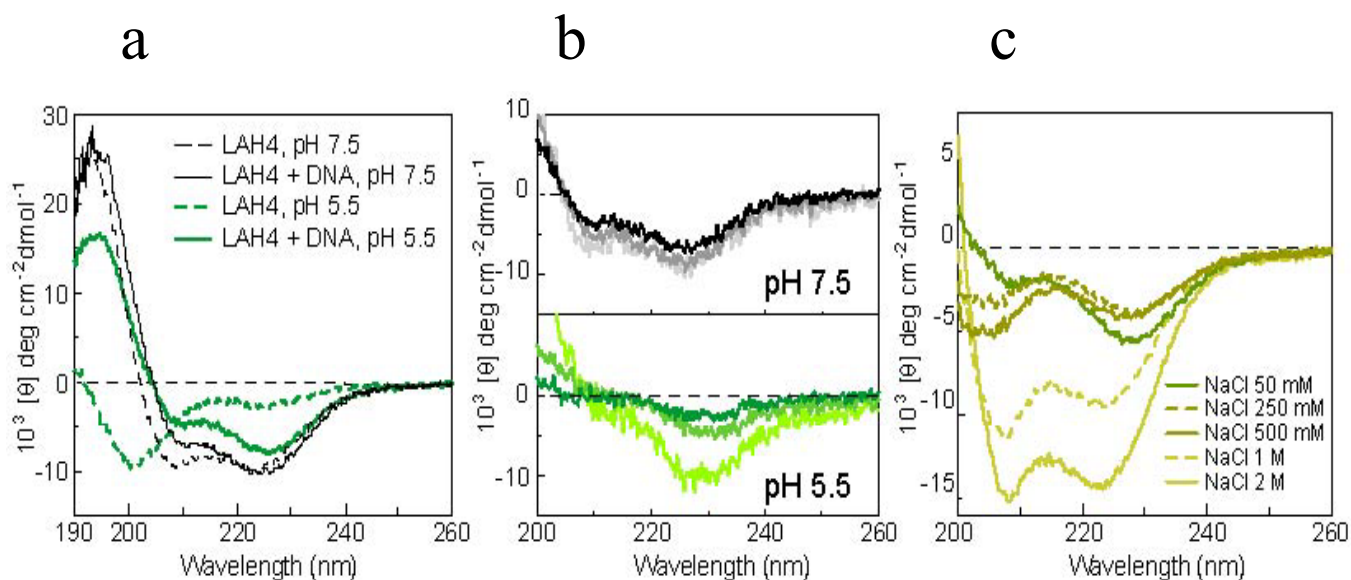


Figure 4.4: CD spectra of (a) LAH4 with or without DNA (300 bp) in 10 mM phosphate buffer at the indicated pH values. The molar ratio of LAH4/DNA was fixed at 240. (b) Titration of increasing amounts of LAH4 into a 0.044 mg/ml DNA solution at the pH values indicated. The molar ratio of LAH4/DNA is equal to 72 (—, —), 121 (—, —) and 168 (—, —). At pH 5.5, the LAH4/DNA complex precipitated within the quartz cell thereby displaying increased light scattering. C. The ionic force inducing spectral changes of LAH4-DNA complex at pH 5.5. The sample concentrations were fixed at 0.2 mg/ml LAH4 and 0.044 mg/ml DNA to respect the molar ratio of LAH4/DNA equal to 240.

In order to follow the conformational changes of the peptide during complex formation CD spectra were recorded under conditions comparable to those used during the ITC

study. The spectra shown in Figure 4.4 were acquired as a function of pH as well as in the absence and presence of DNA. Control experiments indicate that the dichroism of DNA can be neglected in the spectral region < 260 nm (data not shown) and the spectra are therefore directly indicative of the polypeptide secondary structures.

Quantitative analysis of the CD spectral line shapes indicates that in the absence of DNA LAH4 is predominantly random coil at low pH (5 % α -helix) but adopts 41 % helicity when the pH is increased (Fig. 4.4a). This is in perfect agreement with previous data (23). Notably, the lower solubility of LAH4 in aqueous buffer is reduced at neutral when compared to acidic pH. In analogy to the concentration-dependent formation of tetrameric helical aggregates of melittin (100, 101) we suggest that LAH4 also associates into small oligomers in order for the peptides to mutually cover their hydrophobic surfaces. This oligomerization is concomitant with the formation of amphipathic α -helical structures. The CD spectra of LAH4 recorded in the presence of DNA show two characteristic negative peaks near 208 and 222 nm, again indicative of α -helical secondary structure. Whereas at pH 7.5 the helicity of LAH4 is maintained upon association with DNA (41%), it increases considerably to reach 35 % at pH 5.5.

Figure 4.4b shows the results of a titration experiment where LAH4 was added to a DNA solution in a stepwise manner. At pH 7.5, the changes are small indicating that the secondary structure of LAH4 remains identical at all molar ratios LAH4/DNA tested. However, at pH 5.5, the LAH4 signal is lost when the LAH4/DNA molar ratio is increased. In parallel the optical density of the sample augments (data not shown), indicating that particles several 100 nm in size are formed that scatter the incident light beam. Subsequently the particles precipitate and are thereby removed from the incident

light beam. Notably this latter effect is reduced by increasing the salt concentration (Fig. 4.4c).

4.3 Structural characterization of the LAH4/DNA complexes

The secondary structure of LAH4/DNA transfection complexes was studied by proton-decoupled ^{13}C solid-state NMR spectroscopy. The solid state NMR technique was a tool of choice for large macromolecular complexes as the LAH4/DNA. The data show that the overall conformation of the peptide remains helical upon binding on the DNA molecules.

4.3.1 Sample preparation and proton-decoupled ^{13}C CP/MAS NMR

Dry powders of LAH4 peptide, salmon sperm low molecular weight DNA (Fluka, Buchs, Switzerland or a kind gift from Dr. Bruno Senger IBMC Strasbourg) or complexes thereof were compacted into 4 mm MAS rotors. For complex formation, LAH4 peptide and DNA were first dissolved in a minimum amount of water, mixed at the ratio of 1.2/1 (wt/wt) (pH5) and lyophilized.

Experiments were performed on a Bruker Avance wide-bore 400 MHz NMR spectrometer operating at 9.4 T. A commercial 4 mm double resonance MAS NMR probe operating at a frequency of 100 MHz for ^{13}C was used. Typical acquisition parameters were the following: 5 s recycle delay, 1 ms contact time, ^1H B1 field 72 KHz, and spinal 64 proton decoupling during acquisition. The number of scans is indicated in the figure caption. Samples were spun at 10 KHz MAS rate. The spectra were referenced relative to solid adamantane (38.2 ppm). All experiments were performed at ambient temperature. An exponential apodization function corresponding to a line broadening of 50 Hz was applied before Fourier transformation.

4.3.2 Results

Whereas the secondary structure analysis by CD spectroscopy works well for polypeptides or LAH4/DNA complexes that in aqueous solution remain dissolved or dispersed as small assemblies the method fails when large macromolecular structures form. We, therefore, studied the LAH4/DNA transfection complexes by proton-decoupled ^{13}C solid-state NMR spectroscopy. Numerous proteins and peptides have been studied using NMR techniques and correlations have been established between the CO, C_α and C_β ^{13}C chemical shifts and the secondary structure of the polypeptide chain (102, 103). For example, whereas the spectra of α -helical domains exhibit CO intensities at 176 ± 1 ppm, the carbonyls of pleated sheet structures resonate at 171 ± 1.5 ppm (102-104). In a related manner the chemical shift values of the Ala- C_β intensities occur at 15.5 ± 3 ppm or around 20 ppm for α -helical and β -sheet conformations, respectively (102-104).

Proton-decoupled ^{13}C solid-state NMR spectra of LAH4, DNA and the complex are shown in Figure 4.5, including the assignments of resonances that have been performed according to literature data (104-108).

Figure 4.5A indicates that LAH4 exhibits a well-defined peak intensities of the C_β chemical shift of eight alanines of the LAH4 sequence that add up to a maximum at 15.6 ppm, while the carbonyl carbons are situated at 176.1 ppm. We also prepared two peptides where the C_β carbon of alanine-6 and alanine 13 were selectively enriched with ^{13}C , and these sites exhibit resonances at 15.1 and 15.2 ppm, respectively. These data indicate that the LAH4 peptide as a whole, and residues 6 and 13 in particular, adopt α -helical structures in the solid lyophilisate.

Furthermore the proton-decoupled ^{13}C MAS NMR spectra of low molecular weight DNA at natural isotopic abundance was recorded in the solid state (Fig. 4.5B) and the peaks were assigned using literature data (107, 109).

Figure 4.5C shows the ^{13}C CP-MAS spectrum of the LAH4/DNA complex. When compared to a spectrum obtained by the summation of the individual recordings from the peptide and DNA (Figs. 3.7A and B) the chemical shift peak positions of the complex remain largely unaltered although some subtle changes such as line broadening are also observed. The obvious similitude of the ^{13}C chemical shifts obtained of the peptide alone (Fig. 4.5A) or within the complex (Fig. 4.5C) indicates that its predominantly α -helical character is preserved during complex formation. This is confirmed by the spectrum obtained from single-site labeled peptides which indicates that the C_β resonances remain unaltered at 15.6 ppm (Ala 6), as well as the CO peak continues to resonate at 176.3 ppm (not shown).

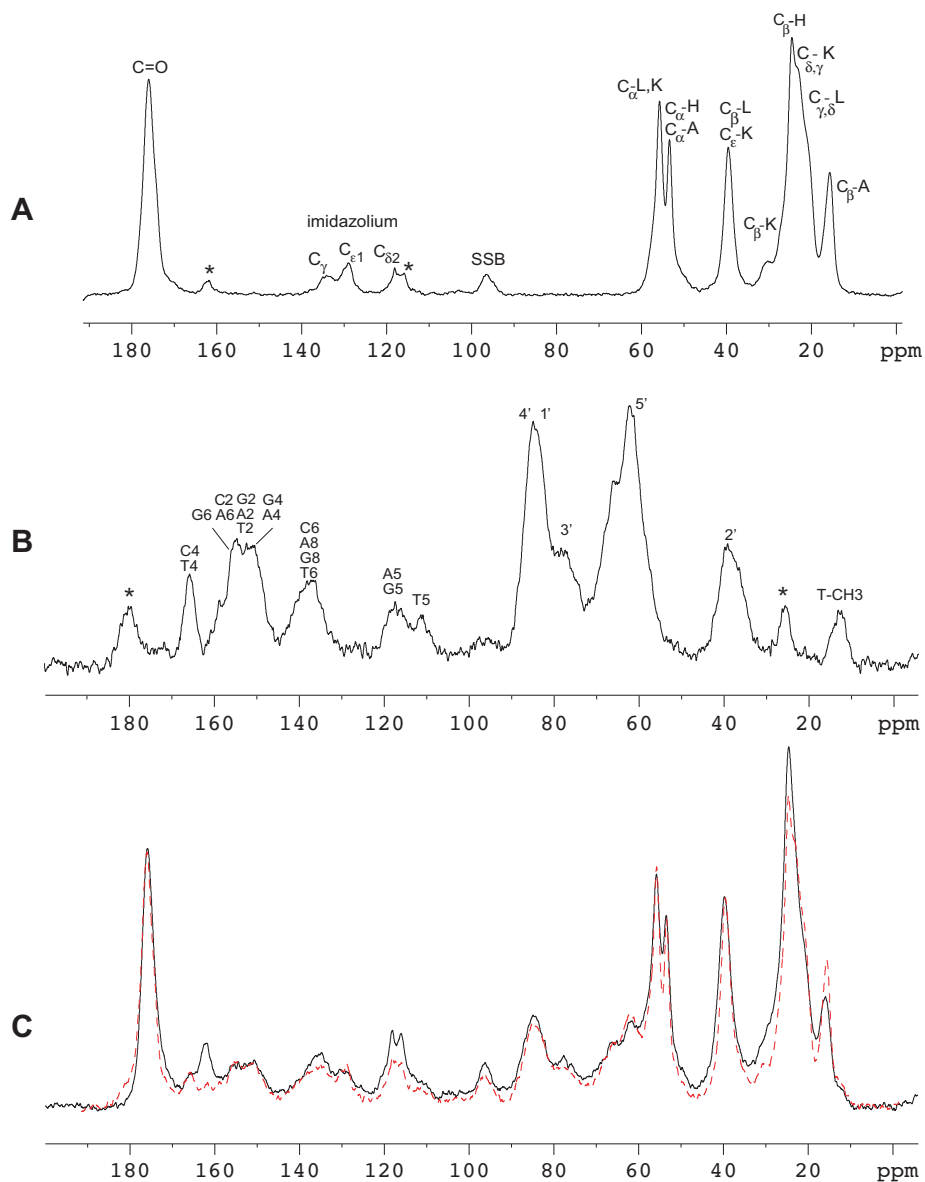


Figure 4.5: Proton-decoupled ^{13}C magic angle spinning (MAS) solid-state NMR spectra recorded at ambient temperature. Lyophilized powders of (a) the LAH4 peptide, (b) sonicated salmon sperm DNA (average size 4 kbp), and (c) a complex of LAH4 and DNA (solid line). The sum of spectra (a) and (b) is also shown for comparison (hatched line). SSB = spinning side band, * resonances from CF_3COOH (spectrum a), or from Tris-EDTA buffer (spectrum b), respectively.

4.4 Discussion

Transfection complexes composed of the amphipathic peptide LAH4 and DNA were formed and investigated by a variety of biophysical methods, including ITC, zeta-potential and size measurements, as well as CD- and solid-state NMR spectroscopies. The data indicate that the peptide maintains its strong propensity to form α -helical structures in the presence of DNA, also in membrane environments (23) and (Protein Structural Data Base entry 1Z5I) or in solutions at neutral pH (23). The best efficiency is obtained when LAH4 is mixed with DNA at a ratio 6:1 (wt/wt, or 1.4 peptides/bp), i.e. the number of lysine residues exceeds by far the number of phosphates. It is therefore not surprising that a large complex exhibiting an overall positive zeta-potential of 10 mV in the presence of 150 mM NaCl is formed. At the present time the structural details of the transfection complex, such as the interaction surface between DNA and peptide, are unknown, as classical structural techniques are hampered by the non-crystalline and non-soluble nature of the complexes.

Here ITC was used to analyze in a quantitative manner the interaction contributions that stabilize the complex and the stoichiometry at low and neutral pH. Although the characterization of a specific thermal signature for the different kinds of non-covalent interactions is difficult (99), the strong pH dependence of the binding enthalpy clearly indicates different contributions upon passage of the histidine pK values (21, 110).

At neutral pH the enthalpy contributions are close to zero, a thermodynamic signature attributed to electrostatic interactions (88, 111-113). Entropy loss is also observed upon DNA condensation, when the worm-like coiled structure of DNA collapses (80). In contrast, at lower pH, the endothermic enthalpies are unfavorable to binding, however, a gain in entropy is observed. This observation suggests that apart from electrostatic forces,

newly formed hydrophobic interactions contribute to the stabilization of the complexes (55), (114). The fast process of the association of cationic lipids to DNA molecules has been suggested as criteria for the distinction of the electrostatic interactions (115). Our results are consistent with this hypothesis as the LAH4 – DNA association equilibrium is reached within 1 min at all conditions tested. The electrostatic nature of the LAH4 - DNA binding has also been indicated by CD experiments at different ionic strength.

The binding affinity K of LAH4 to DNA is similar at both pH values investigated (Table 4.1), and differences in the appearance of the titration curves (Fig. 4.2) demonstrate the role of electrostatic interactions between the peptide and the DNA, an effect already described by Seelig et al. (1993) (86). Binding affinities exhibiting values lower than 10^6 M^{-1} are typical of unspecific electrostatic protein – DNA interactions (116). This is further affirmed by the free energy of the binding whose value is also typical of a non specific binding, an example of which is the binding of the lac repressor to a non specific DNA sequence (116).

Compared to polypeptides that bind to specific DNA sequences (98, 111), the results shown here indicate that a very high molar ratio of LAH4 is required to saturate the binding sites of DNA. The ITC data indicate that in the case of a 300 bp DNA fragment about 150 peptides can associate with the DNA. Notably the transfection complexes are formed at peptide:DNA ratios of 6:1 (wt/wt), thereby ensuring that at pH 7.5 most if not all of the available sites are occupied. The number of peptides is reduced to about half when the pH is decreased.

The density of peptides on the DNA double helix seems clearly too large to account for a tight and specific interaction of all peptides, or to correlate with a model where the helix is well-inserted within the major groove of the DNA. Instead one could imagine that several layers of peptides reside around the DNA, possibly by interacting with each other

through their hydrophobic surface (Fig. 4.6A). The CD data and analogies with other amphipathic peptides (*100*, *101*) suggest that at pH 7.5, LAH4 oligomers already exist in the aqueous phase and it is possible that these oligomers associate directly with the DNA. In this manner association is electrostatic without involving major changes in hydrophobic interactions in agreement with ITC data (Table 4.1).

In the most common form of DNA, the B form, the rise of the helix is $h = 3.4$ nm, the diameter of the helix is 1.08 nm and the number of residues per turn $n = 10$ (*1*). The length of the groove is, therefore, per turn, 3.6 nm.

In an α -helical peptide, there are $n = 3.6$ residues per turn, the diameter of the helix is 10 Å, and the rise of the helix is $h = 0.54$ nm per turn (*1*). The LAH4 peptide is composed of 26 residues, thus its length is 3.9 nm.

If we consider the salmon sperm low molecular weight DNA used in the ITC assay, it contains 300 bp, which corresponds to 30 turns. The length of the LAH4 peptide exceeds the length of the groove per turn of about 0.3 nm, but the rise of the DNA helix is sufficient for the close accommodation of 3.4 LAH4 peptides.

At pH 7.5, the ITC results foresee in average 150 molecules of peptide per 300 bp of DNA. This corresponds to 5 peptides per turn of helix. On the other hand, at acidic pH, the ITC results predict 100 molecules of peptide per 300 bp of DNA, which corresponds to 3.33 LAH4 peptides per turn. This coincides with the number of LAH4 peptides being placed closely in the DNA groove.

Alternatively a high density of peptides can be created by end-on association of the peptides with the DNA double helix. In this case one charged peptide terminus would be in contact with the DNA whereas the other one would be oriented away from the helix (Fig. 4.6B). In both models, the DNA would be covered by peptides exposing a positively charged surface which would be available for interactions with other DNA strands,

thereby condensating the long DNA into large globular aggregates. The charged surface permits the complex to stay soluble and helps association with negatively charged surfaces. Notably, DNA condensation has been demonstrated to be a critical feature for DNA stability and enhanced transfection efficiency (80). Similar thermodynamic driving forces (Table 4.1) albeit at a reduced peptide/DNA ratio was also observed for the adenoviral core peptide μ (mu) but not the spermatozoan protamine polypeptide that both shows DNA condensating properties (83).

Cationic peptides are frequently used to charge-neutralize and condense DNA to form toroids or rod structures (80). Toroid formation can apparently be achieved with trivalent cations (117), spermidine (118), protamine (119), poly(L-lysine) (120) and polyethyleneimine (71, 121). Hence, efficient DNA condensation and neutralization is a necessary prerequisite for enhanced gene delivery.

An important result from the ITC studies is that upon addition of charges to the LAH4 sequence upon acidification of the environment the capacity of DNA to bind these cationic peptides decreases considerably. Although the net charge of the complex does not much change during this process these modifications in composition lead to structural alterations and a reduction in the solubility of the complex (Fig. 4.4). However, with one peptide per 4 bp a tighter packing of helices into the major groove is possible in agreement with the observed alterations in enthalpy and entropy associated with complex formation (Table 4.1). The thermodynamic profile observed at pH 5.5 is indicative that both electrostatic and hydrophobic interactions contribute during complex formation suggesting tighter packing interactions between the LAH4 and the DNA molecules. Indeed, based on x-ray diffraction data Azorin et al (122) have proposed a model whereby α -helical peptides with 30% of their residues presenting a positive charge closely interact with the DNA. Their data suggest that poly (Lys-Ala-Ala) follows a

helical path around the DNA major groove where the distance between the peptide charged side chains and the DNA phosphates amounts to 4 - 5 Å.

At pH 5.5, over 30 % of the residues in LAH4 possess a positive charge. These residues are distributed evenly along the length of the molecule compensating favorably the negative charges on the DNA. The surface of interaction between the LAH4 and the DNA molecules may be enhanced by supplementary electrostatic as well as classical hydrophobic interactions. Both types of interaction are entropy driven (85, 114), in accordance with the ITC results (Table 4.1).

The transition between the two states, at neutral and low pH, is energetically favorable. The LAH4 - DNA binding is dominated by a multiplicity of weak and non covalent interactions that determine the thermodynamic stability of the process. This process takes place within limited free energy windows and all perturbations are absorbed by compensation between the enthalpy and the entropy so as to maintain constant the free energy of the system (99), leading to favorable transition between the two states.

Fominaya et al (9) have already suggested the existence of at least two forms of the transfecting peptide RAWA, each responsible for a different activity: the complexed peptide binds to the membrane whereas the free modifies the membrane's permeability.

Previous studies have shown the formation of the DNA - peptide complex is very much dependent on the LAH4 amino acid sequence and tertiary structure (24). They have also indicated an endosome mediated delivery of the complex to the cytoplasm, a usual way of entering cells for most transfection vectors (123). The data presented in this study have brought a better understanding of the transfection mechanism, enlightening key steps of the process such as the complexation of the DNA and the delivery of the complex into the cytoplasm.

It would be interesting to study the binding of the LAH4 peptide on DNA molecules of different size in order to see whether the thermodynamic characteristics of the described reaction are preserved or not. Another interesting feature would be the thermodynamical study of the association of the peptide and of the complex on lipid surfaces that would provide further information about the action of the LAH4 peptide in the transfection mechanism.

In order to achieve good transfection efficiency the proton pumps of the endosome have to be active (24), (123). Here we show that about half of the peptides initially associated with the transfection complex are released upon acidification of the endosome. These cationic peptides are highly amphipathic in nature and membrane-active. Membrane-partitioning constants in the $10^3 - 10^4 \text{ M}^{-1}$ range have been measured for LAH4 in the presence of POPC or mixed zwitterioning / acidic liposomes, respectively (124), indicating good to high affinity also for the endosomal membranes. These data allow one to estimate that when compared to the number of endosomal lipids a large excess of peptides is released from the complex and associates with the membrane. At such high concentrations amphipathic peptides are known to develop detergent-like and membrane-lytic activities (10). With the disruption of the endosomal membrane the peptide ensures not only compaction but also access of the transfection complex to the cytoplasm.

Several models have been proposed for the binding and lysis of the endosomal membrane. The helix of the LAH4 peptide strongly interacts with phospholipid membranes of diverse composition and exhibits parallel orientation as well as maximum effectiveness as a bilayer disrupting molecule (23). The disruption of the bilayer can be explained either by the detergent-like separation of hydrophobic and charged/polar residues within the amphipathic LAH4 helix (10). When the peptide concentration in the

membrane is increased, lysis may occur as has been observed for other amphipathic molecules (125).

In summary, thermodynamic and structural parameters that describe the first steps of the transfection show the existence of two dynamic states of the LAH4 peptide and the importance of the transition between them for its action. The transfection mechanism can be presented as a process involving at least six steps (Figure 4.7). The LAH4 peptides bind in large excess to the plasmid DNA by non-specific interactions generating voluminous complexes. These complexes are taken up by endocytosis, as it is the case of other transfection vectors (123). When the pH inside the endosome drops, the maximum number of LAH4 molecules bound to the DNA is reduced thereby liberating a major fraction of peptides. These LAH4 molecules interact with the endosomal membrane provoking its lysis, and the DNA can be delivered to the cytoplasm. Other processes, which are so far much less well understood, help in the transfer of DNA to the nucleus, where the genetic information is expressed.

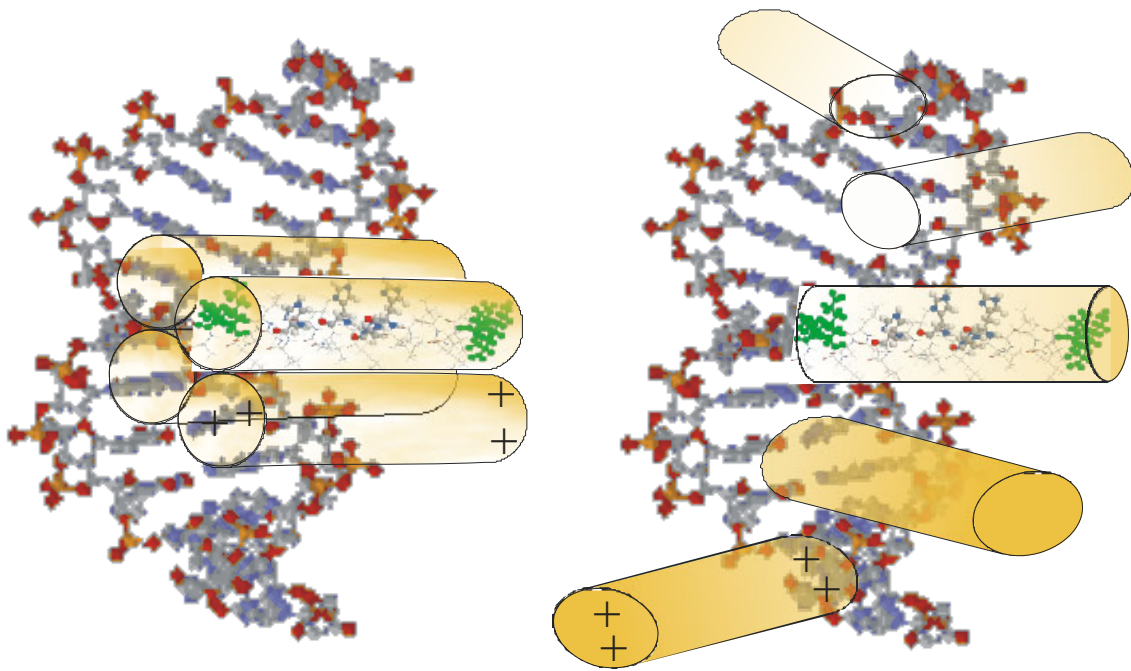


Figure 4.6: Schematic illustrations of how the high coverage of DNA with LAH4 could be explained. A Multimeric (a) and a monomeric association model (b) are shown.

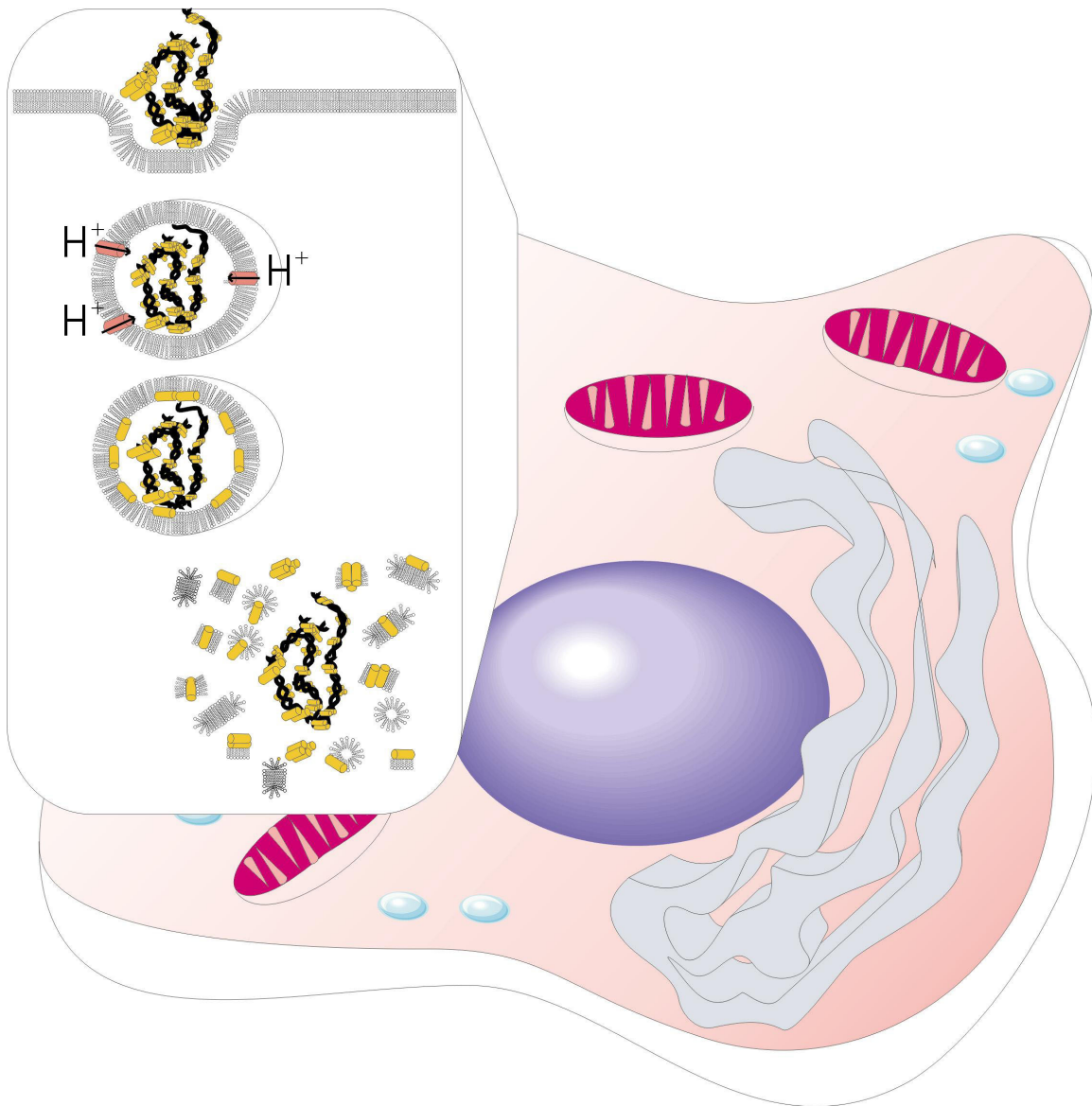


Figure 4.7: The mechanism of transfection of eukaryotic cells by the LAH4/DNA complexes. (a) Complex formation and compaction of the DNA molecules by interactions with LAH4, (b) endocytosis of the large LAH4/DNA complexes, (c) acidification of the endosome concomitant with the release of LAH4, (d) Partitioning of the free LAH4 peptides into the membrane and lysis, (e) Complex delivery to the cytoplasm and intracellular routing, transport to the nucleus and expression.

Chapter 5

Expression of the LAH4 peptide in *E.coli*

5.1 Introduction

NMR is a powerful method for characterizing the structure, dynamics, and interactions of biological macromolecules. However, to make use of the full potential of NMR methods, biomolecules labelled with NMR active stable isotopes, in particular with ^{13}C , ^{15}N , and/or ^2H , are required. Multidimensional, multinuclear, NMR experiments reduce signal overlap, greatly simplify resonance and cross peak assignments, and allow for spectral editing or filtering schemes (126).

The production of bioactive peptides and small protein fragments is commonly achieved via solid phase chemical synthesis (26). This technique is used for the quantitative scale production of unlabelled peptides or peptides with selective isotopic labelling. However, such techniques become unviable and prohibitively expensive, at least to an academic laboratory, when large-scale production is needed, or when uniform isotope labelling is required for NMR studies. Large peptides are also very difficult to synthesize by solid phase chemical synthesis.

Genetic engineering followed by efficient expression of isotope labelled biomolecules in milligram amounts has been indispensable for the recent success of biological NMR applications. Much effort has been devoted to recombinant expression and refolding of medium size proteins (127) and short peptides (128).

During the last decades, expression of various antibacterial polypeptides has been achieved using different expression strategies. These approaches include direct expression in cell free systems (129) or prokaryotic cells (130, 131), and most commonly, expression mediated by a fusion partner (130, 132-136). Gene fusions have been successfully engineered coding for hybrid proteins with the target peptides being part of a larger protein (137, 138), which are sufficiently stable and well characterized for recombinant production. Fusion partners provide also affinity tags (139-141), make proteins more soluble (142), or enable the formation of disulfide bonds (143). They are also commonly used in order to diminish the toxicity of the antibacterial peptides against host cells (130, 132-136). Proteins that express well and allow the rapid purification by affinity chromatography are attractive fusion partners.

Antibacterial peptides are particularly difficult to express in *E.coli* because of their toxicity towards this organism (23). Martemyanov et al (144), as well as Xie et al (145), published, in the same year, the expression of the first antibacterial peptides as fusion proteins. Cecropin CMIV from *Bombyx mori* was expressed in fusion with the IgG binding domain of the Staphylococcal protein A by Xie et al (145). Three antimicrobial peptides, cecropin, magainin and bombinin were expressed in *E.coli* with protein A as a fusion partner by Martmyanov et al (144). Later on, the antimicrobial peptide P2 was genetically engineered, and expressed as a fusion protein with the bovine protein prochymosin as a fusion partner at its amino terminus (146). High-level expression of small antimicrobial peptides such as bombinin, indolicidin and melittin was achieved by fusing the peptide DNA sequences downstream to a truncated fragment of the PurF gene, coding for the amidophosphoribosyltransferase *E.coli* protein (147). A magainin

derivative, the MSI-344 peptide, was also produced in *E.coli* as a fusion protein, by utilizing the same fusion partner (148).

In this work, we present the results of our efforts to express the designed antimicrobial peptide LAH4. This project arose due to the need of a detailed structural analysis of the LAH4 peptide in its membrane-associated form, or in the transfection complex, by the NMR techniques. Indeed, recent studies have shown LAH4 peptide to be a competent transfection agent (24, 123), and a detailed view of the mechanism of action would be a considerable advantage. The LAH4 peptide is a synthetic peptide that doesn't exist in nature, and it is the first time that efforts are being made to express the peptide *in vivo*.

Different approaches such as expression of LAH4 from pET-3d vector and pTol vectors with the periplasmic protein TolA as a fusion partner have been undertaken for this thesis, but the only strategy that produced results was the fusion of LAH4 with the GST protein, using the Gateway system from Invitrogen.

5.2 Constructs

The fusion gene was constructed by a combination of DNA single strand synthesis with the PCR technique as first presented by Chen in 1993 (149). A synthetic single strand containing the gene sequence of the LAH4 peptide as deduced from the primary structure according the *E.coli* codon usage table was conceived and purchased. The synthesis of the complementary strand and the amplification of the gene were performed by PCR (Fig 5.1). After several steps, the newly constructed LAH4 gene was cloned downstream to the GST coding gene, so as to produce a fusion protein containing the GST fusion partner on the N-terminal extremity.

The Gateway system is based on recombination reactions allowing the λ phages integration and excision inside the *E.coli* genome (Fig.5.2). This method permits the directional cloning of a PCR product in a donor vector by an enzyme called topoisomerase. The PCR product contains the gene of interest, and a cleavage site. The product of this cloning is called an entry vector, and contains the recombination site attP and is used as a matrix for a recombination reaction with a destination vector containing the recombination sites attL. This reaction between the recombination sites attP and attL is catalyzed by the enzyme LR clonase and produces the expression vector.

The present system was chosen in order to avoid the use of restriction enzymes and ligases. It reduces significantly the number of steps necessary for the expression of a protein. Most interesting of all, it allows the production of an N-terminal tagged fusion protein, with Glutathione S-transferase (GST) as a fusion partner.

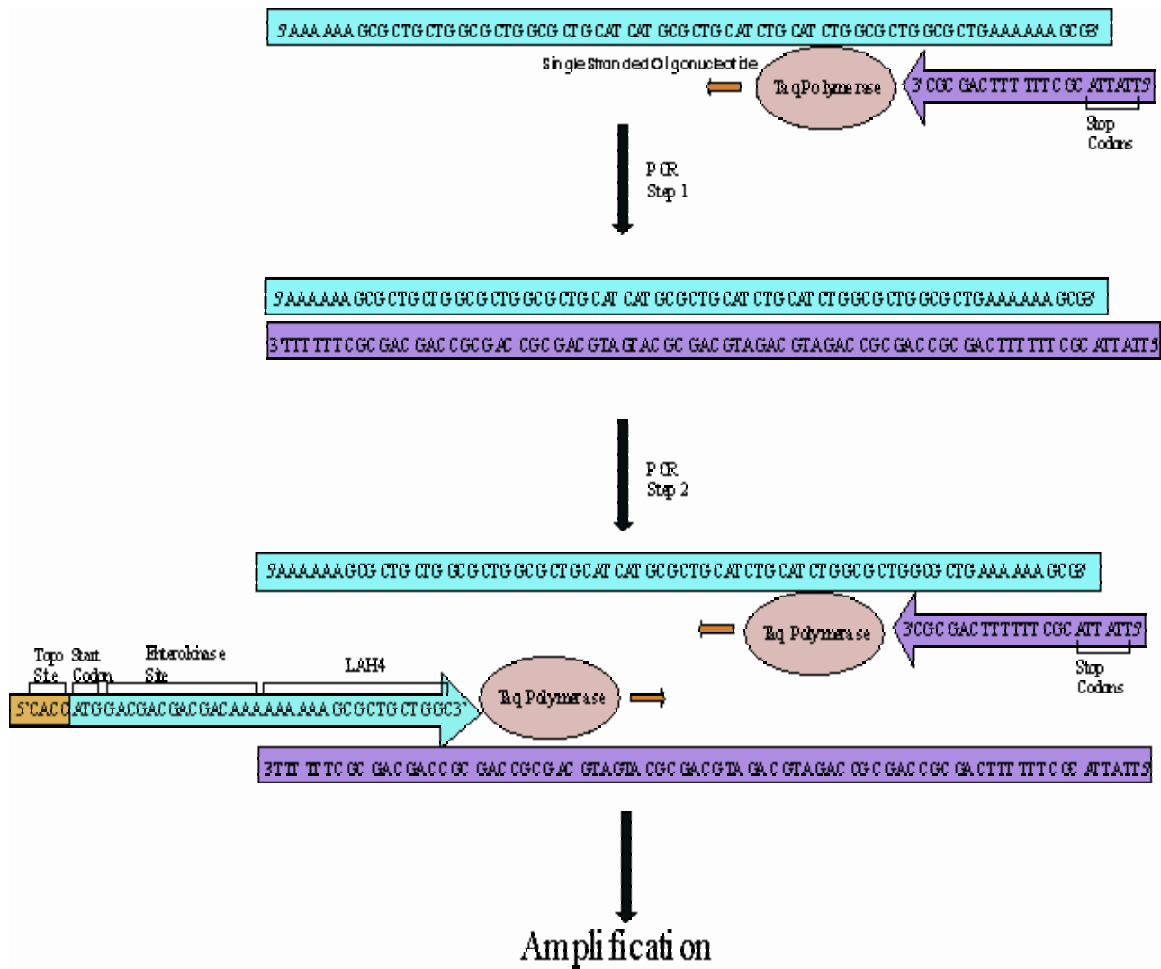


Figure 5.1: Schematic representation of the LAH4 gene synthesis by PCR. During the first step, the synthetic 3' oligonucleotides anneal with the single stranded synthetic template DNA, carrying partially complementary sequences and serve as primers to the Taq polymerase enzyme who catalyses the DNA synthesis according to the complementarities principle. The double stranded LAH4 synthetic gene is thus produced and amplified, during the second step, following melting, annealing and polymerization cycles as described in the material and methods section. The PCR product is directionally cloned in the pENTRY vector in a site flanked by two attL recombination sites (Fig. 4.2).

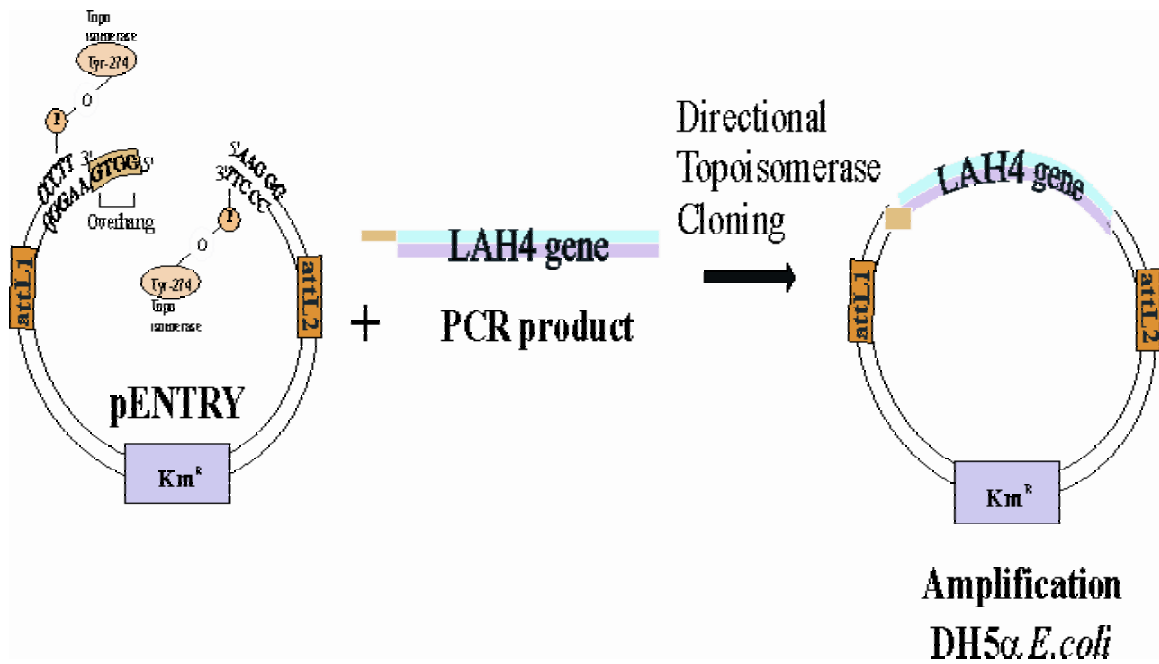


Figure 5.2: Directional cloning of the PCR product containing the LAH4 gene, by topoisomerase reaction. The 5' single stranded overhang of the pENTRY vector recognizes the 3' single stranded end of the PCR product, anneals and stabilizes it in the correct orientation.

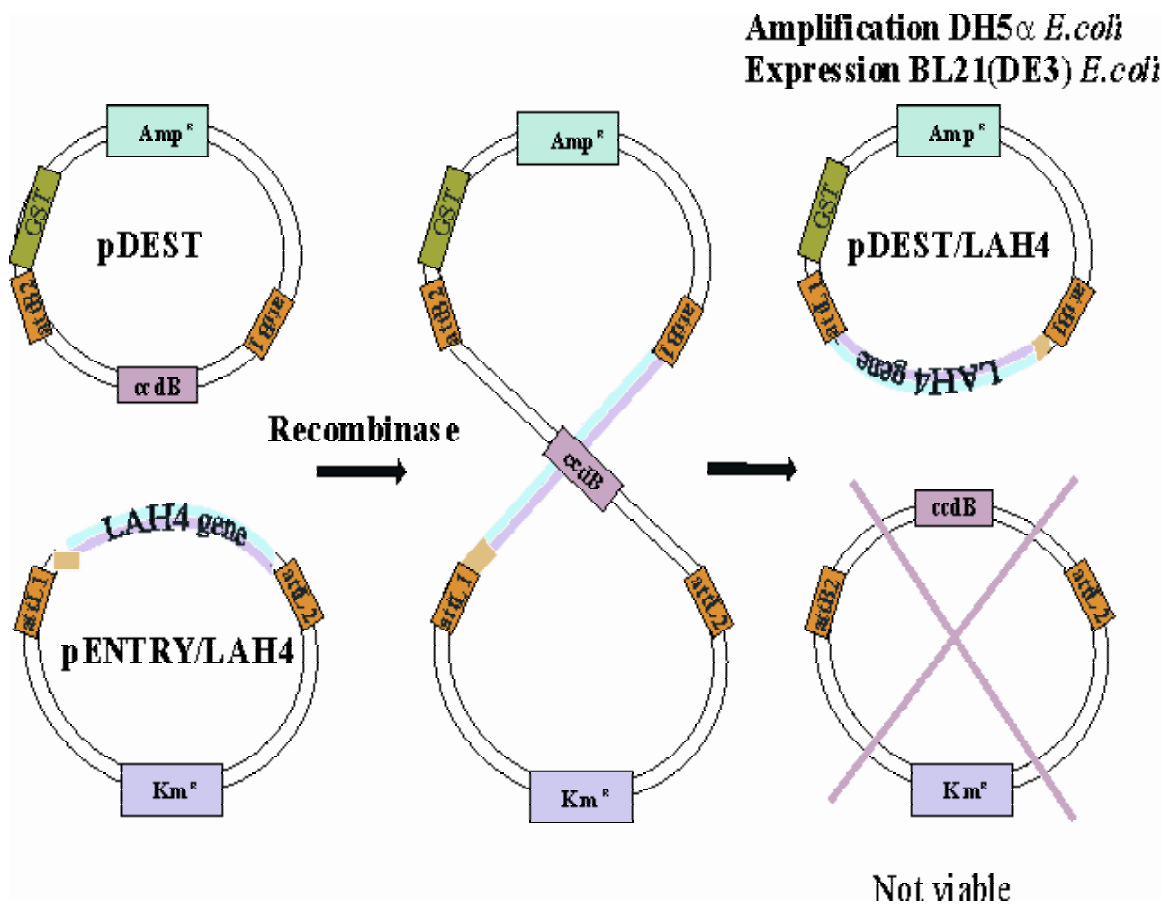


Figure 5.3: Schematic representation of the construction pDEST/LAH4 plasmid containing the inserted LAH4 gene. The site-specific recombination between the attL sites of the entry vector and the attB sites of the destiny vector is achieved using a bacteriophage λ recombinase enzyme. Double selection of the pDest carrying the insert is obtained by the ccdB toxin coding gene and by ampiciline resistance.

5.3 Materials and methods

Construction of the expression vector

A synthetic single strand DNA of 128 bp was purchased from the Department of Pathology in Yale. The synthetic single strand contained the gene sequence of the LAH4 peptide as deduced from the primary structure according the *E.coli* codon usage table (www.kazusa.or.jp/codon). The 5' primer (CACC ATG GACGACGACGACAAA AAA AAA GCG CTG CTG GC, 40 bp) was designed to provide a four base pair sequence CACC complementary to the pENTR vector overhang, the initiation codon and the enterokinase cleavage site, in addition to a 17 bp sequence complementary to the synthetic strand containing the LAH4 sequence. The 3' primer (TTA TTA CGC TTT TTT CAG CGC, 21 bp) contained a 15 bp sequence complementary to the LA gene and two stop codons. The two primers were purchased from MWG Biotech (Ebersberg, Germany). The synthesis of the complementary strand and the amplification of the gene were performed by PCR (149). The PCR reaction occurred within 30 cycles of 3 steps: DNA melting, 30 sec at 94°C, annealing, 30 sec at 52°C, and polymerization, 1 min at 72°C steps.

The PCR product was directionally cloned into the pENTRTM/D-TOPO® vector (Invitrogen, Carlsbad, CA) by a topoisomerase reaction. The product was used to transform the One shot® top10 chemically competent *E.coli* strain (Invitrogen). After amplification the vector was purified on an anion exchange column, and a recombinase reaction was performed with the pDESTTM15 vector (Invitrogen) in order to express the LAH4 peptide in fusion with an N-terminal Glutathione S-transferase part. The

recombinase reaction was performed with 4 µg of Proteinase K in TE buffer (10 mM Tris HCl, 1 mM EDTA, pH 8).

Expression

The *E.coli* strain BL21 (DE3) (Novagen, Darmstadt, Germany) was transformed chemically, by heat shock, with the pDESTTM15 plasmid containing the insert. Cells were grown either in Luria-Bertani-medium or in a modified minimum media for ¹³C labeling with [¹³C₆] D-glucose (Eurisotop, Saint Aubin, France) as the sole carbon source.

5ml cultures were grown in shake flasks at 37 °C overnight in Luria-Bertani (LB) media supplemented with 50 µg/ml ampicilin, followed by a 100 fold dilution in to LB ampicilin medium. These cultures were induced by addition of 1 mM isopropyl thiogalactoside (IPTG) (Sigma-Aldrich, St Louis, USA) for 2 h. After centrifugation at 4500 g for 20 min at 4 °C the cell pellet was stored at -20 °C.

The modified minimum medium contained 56,5 mM Na₂HPO₄, 22 mM KH₂PO₄, 85 mM NaCl, 18.7 mM NH₄Cl, 0.1 mM CaCl₂, 1 mM MgSO₄, 10 µg/ml thiamine, 10 µg/ml biotin, 50 µg/ml ampicilin and 16 mM D-glucose uniformly ¹³C labeled; the pH was adjusted to 7.4.

Cells were grown in 50 ml of medium at 37 °C overnight. The culture was diluted 20 fold with medium and grown to late exponential phase at 37 °C. Expression was induced at OD₆₀₀ = 0.8 with 1 mM IPTG overnight. Cells were harvested by centrifugation at 4500 g for 20 min at 4 °C.

Solubilization

Pelleted cells were washed with ice cold Mouse Tonicity Phosphate-Buffered Saline (MTPBS) buffer (150 mM NaCl, 16 mM Na₂HPO₄, 4 mM NaH₂PO₄, 3 mM NaN₃, pH 7.3) containing 1 mM Pheny Methyl Sulphonyl Fluoride (PMSF). After a short centrifugation (4500 g for 5 min at 4 °C), they were resuspended in ice cold MTPBS buffer containing 0.1 mM PMSF and a protease inhibitor cocktail.

The cells were lysed by French Press (2000 psi) and the insoluble material containing the fusion protein pelleted by centrifugation (48000 g, 15 min, 4 °C). The pellet was treated for 1 h with 8 M urea in a 50 mM sodium bicarbonate buffer (pH 9) containing 1 mM dithiothreitol and 1 mM EDTA at room temperature.

The insoluble material was removed by centrifugation (48000 g, 15 min, 4 °C) and the supernatant transferred to a dialysis tubing cellulose membrane of 13 kDa cut-off (Sigma-Aldrich, St Louis, USA) and dialyzed against 4 M urea, 50 mM sodium bicarbonate, 1 mM dithiothreitol, 1 mM EDTA pH 9 at room temperature for 1 h. The solution was then dialyzed twice with 2 M urea, 50 mM sodium bicarbonate, 1 mM dithiothreitol, 1 mM EDTA pH 9 at 4 °C for 1 h, and finally, with 50 mM sodium bicarbonate, 1 mM dithiothreitol, 1 mM EDTA pH 9 at 4 °C for an hour and then again overnight. Insoluble material was discarded by centrifugation (48000 g, 15 min, 4 °C) and the fusion protein contained in the supernatant was purified by affinity column chromatography.

Purification

10 mL hydrated glutathione agarose beads (Sigma-Aldrich, St Louis, USA) were washed with water and equilibrated with MTPBS buffer at room temperature. The dialyzed material was applied to the column for 1 h, the beads were washed with MTPBS and the fusion protein eluted with glutathione agarose elution buffer (20 mM glutathione in MTPBS, 1 mM dithiothreitol, 1 mM EDTA). The fusion protein was concentrated using

Centriprep YM-10 concentrators (Millipore, Bedford, MA) and dialyzed in distilled water. The elution of the pure fusion protein was analyzed by discontinuous SDS-PAGE as described below.

Cleavage

The fusion protein was digested with various concentrations of enterokinase MAX ranging from 0.01 to 4 u (Invitrogen, Carlsbad, CA) in 30 μ l of reaction buffer (50 mM Tris-HCl, 1 mM CaCl₂, 0.1 % Tween-20 pH 8 (v/v)). The reaction was incubated at 37 °C overnight.

SDS-Polyacrylamide Gel Electrophoresis

Protein samples were analyzed by discontinuous SDS-PAGE according to Laemmli (1970). Samples were denatured by boiling for 3 min, and then used for electrophoresis on 8 % or 15 % SDS/polyacrylamide gels (150). Protein staining was performed with Coomassie brilliant blue.

5.4 Results

We expressed the antibiotic peptide LAH4 in *E.coli* bacteria in order to produce uniformly labelled ^{13}C and ^{15}N samples suitable for NMR spectroscopy.

The exogenous coding sequence of LAH4 was produced by PCR using a single strand oligonucleotide as template and two primers (Fig.5.1), and inserted by topoisomerase reaction to the pENTR vector (Fig.5.2).

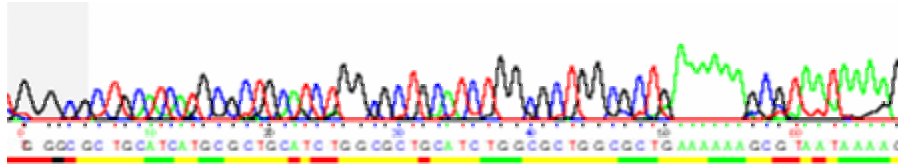
After amplification of the plasmid in One shot® top10 chemically competent *E.coli*, PCR and sequence analysis verified the insertion and integrity of the sequence (Fig. 5.4).

Recombination of the attL sites of the entry vector with the attB sites of the destiny vector provides the final expression vector, with the LAH4 inserted gene downstream to the GST coding gene, and under the control of the T7 promotor (Fig.5.3). Selection of the destiny vectors containing the insert is achieved in a double manner. A positive selection of the pDEST vectors with the ampiciline resistance gene excludes the pENTRY vectors carrying the LAH4 gene, as well as a negative selection by the ccdB gene, a gene coding for a toxic protein, excludes all the vectors not containing the LAH4 insert. The pDEST vector was once more amplified and its sequence analysed before transformation in the expression bacterial strain.

E.coli BL21 (DE3) was transformed with the expression vector pDEST and grown in LB medium. The fusion protein was expressed after induction with IPTG and the optimum expression in 2 L shaker flasks occurred after a 2 h induction with 1 mM IPTG at 37 °C. The SDS-PAGE analysis under reducing conditions shows that the molecular weight of

GST-LAH4 was about 30 kDa, which agrees with the predicted value of 29.633 kDa from the gene sequence.

A



B

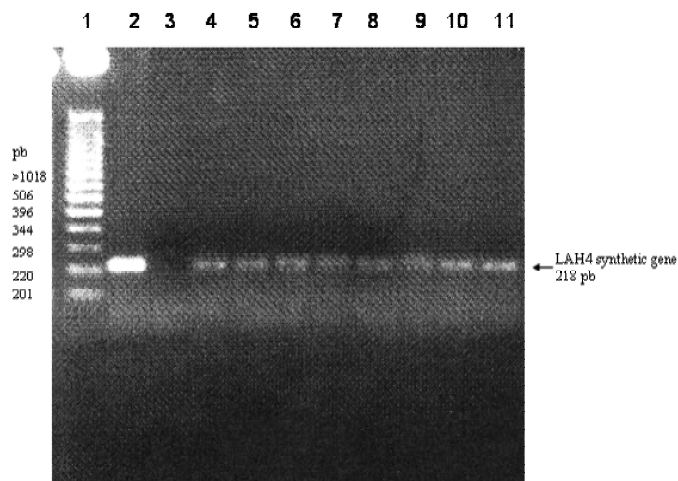


Figure 5.4: LAH4 gene insertion analysis of the pDEST plasmid. (A) Sequence analysis (B) PCR analysis: DNA molecular weight marker, from top to bottom: 12 K; 11 K; 10 K; 9 K; 8 K; 7 K; 6 K; 5 K; 4 K; 3 K; 2K; 1.6 K; 1K; 506; 396; 344; 298; 220; 201 bp (Lane 1); Positive control of the PCR reaction, using the pENTRY as template (Lane 2); Negative control of the PCR reaction, without plasmid DNA (Lane 3); PCR reaction using the DNA extracted from 7 different *E.coli* colonies as template (Lanes 4-11)

Prolongation of the induction did not increase the yield of the fusion protein production. After 2 h of induction the bacterial growth stopped and the optical density at 600 nm

remained constant or even decreased in some cases. On the contrary, bacteria in control cultures continue to grow for another 8 h. These results show that the LAH4 peptide maintains its antibacterial activity, or at least a part of it, even when it is fused with a large protein of 23 kDa such as the GST.

Following protein expression, the cells were lysed by French Press lysis, and soluble and insoluble proteins of the lysate were separated by centrifugation. Almost all of the GST-LAH4 protein was found in the insoluble fraction, i.e. in inclusion bodies (Fig. 5.5). Lowering the temperature of incubation as well as decreasing the IPTG concentration are common techniques to solubilize otherwise insoluble proteins (151). Unfortunately, they did not prove efficient in the case of the GST-LAH4 construct. Hence, solubilization and refolding steps were necessary after lysis of the cells.

The solubilization of inclusion bodies was carried out in 8 M urea rather than in guanidium hydrochloride, as it has been shown that the resulting high salt concentration in the latter hinders the refolding of certain GST fusion proteins (152).

The pathways leading to conformational maturation are not completely understood (153), but it is well known that the generation of the correct disulfide bonds is a key reaction in the folding process as it introduces a significant stabilizing force (154). GST possesses two disulfide bonds per monomer, while the precursor bears only one such linkage (155). Thus, the composition of the refolding buffer was critical, and addition of a thiol reagent and a pH higher than 8.0 were essential for the regeneration of GST activity (152).

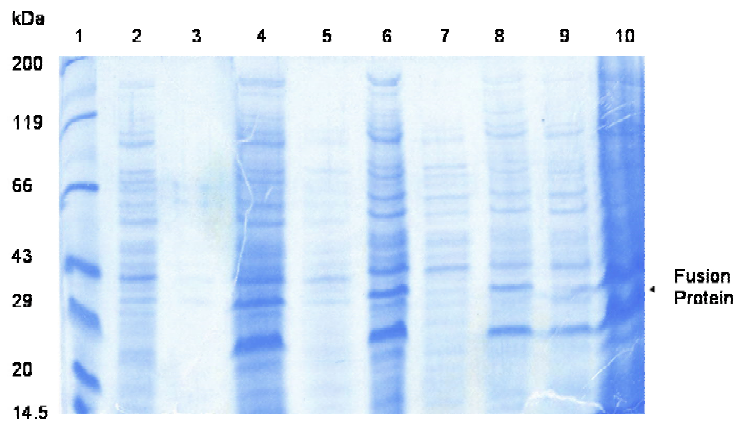


Figure 5.5: Solubilization test of the fusion protein. Protein molecular weight marker, from top to bottom: 200, 119, 66, 43, 29, 20, and 14,5 kDa (Lane 1); Non induced cell lysate (Lane 2); Lysate supernatant after 2 h induction (Lane 3); lysate pellet after 2 h induction (Lane 4); Supernatant after 2 M urea treatment of the cell pellet (Lane 5); Pellet after 2 M urea treatment (Lane 6);); Supernatant after 4 M urea treatment (Lane 5); Pellet after 4 M urea treatment (Lane 6);); Supernatant after 2 M urea treatment of the cell pellet (Lane 7); Pellet after 2 M urea treatment (Lane 8); Supernatant after 8 M urea treatment pellet (Lane 9); Pellet after 8 M urea treatment (Lane 10).

The fusion protein was then purified by passage through a glutathione affinity agarose column. This technique allows a one-step purification of recombinant proteins under physiological conditions to preserve their structure and bioactivity. In order to maintain the functional structure of the GST fusion part, the same buffer as in the refolding processes was used for the affinity purification. The affinity column was first equilibrated with the DTT and EDTA containing buffer, at pH 9. Then the crude protein solution was loaded onto the column followed by washing steps to remove impurities. Elution buffer

containing glutathione resulted in the release of pure GST-LAH4 protein. The pure fusion protein was analysed by SDS-PAGE 8 % (Figs. 5.6 and 5.7).

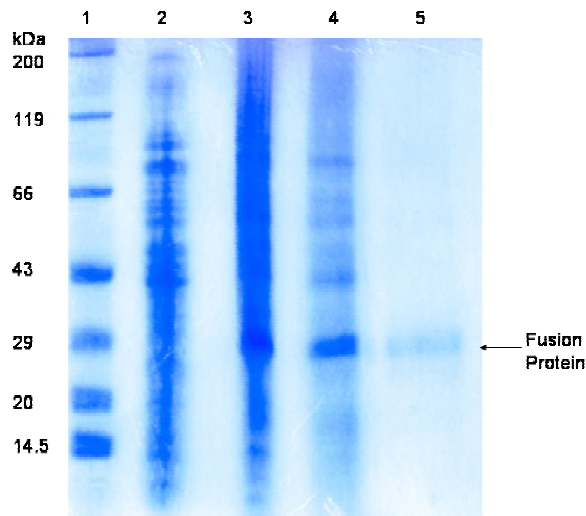


Figure 5.6: Purification of the GST-LAH4 fusion protein. Protein molecular weight marker, from top to bottom: 200, 119, 66, 43, 29, 20, and 14,5 kDa (Lane 1); cell lysate prior to induction (Lane 2); cell lysate after overnight induction (Lane 3); 8M urea solubilization and refolding of membrane and inclusion bodies (Lane 4); GST-LAH4 fusion protein purified by affinity column (Lane 5).

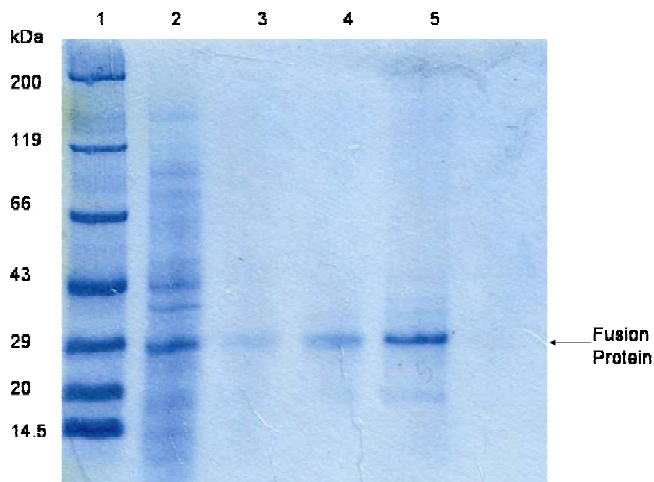


Figure 5.7: Purification of the GST-LAH4 fusion protein by affinity column. Protein molecular weight marker, from top to bottom: 200, 119, 66, 43, 29, 20, and 14,5 kDa (Lane 1); cell lysate prior to purification (Lane 2); Deposition of 0.2, 0.5, and 1 mg/ml purified fusion protein (Lanes 3-5)

In order to liberate the antibiotic peptide LAH4, the fusion protein was cleaved specifically by a serine protease. Incubation with enterokinase was overnight at the optimal temperature published for enzyme activity (37 °C, ref). Figure 5.8 shows the products of the fusion protein cleavage reaction achieved by various concentrations of enterokinase. The cleaved LAH4 peptide is not visible on the gel due to its low quantity (2 µg expected).

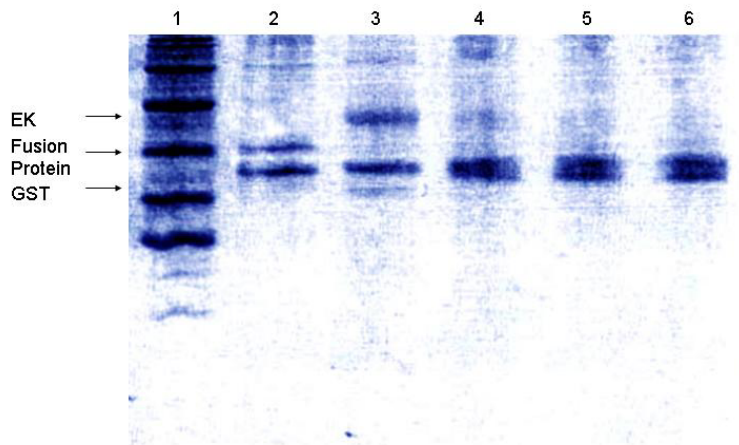


Figure 5.8: Enterokinase (EK) digestion of the fusion protein. Protein molecular weight marker, from top to bottom: 200, 119, 66, 43, 29, 20, and 14,5 kDa (Lane 1); Negative control with no enzyme (Lane2); Digestion of 20µg fusion protein with 4u EK (Lane 3); 1u EK (Lane 4); 0.1u EK (Lane 5) and 0.01u EK (Lane 6).

The expression was finally undertaken in minimal medium M9. Optimization of the temperature and the time of induction had once more to be determined as the growth rate of *E.coli* in minimal medium is decreased. As a 2 h induction was found not to be sufficient, overnight induction produced approximately the same amount of fusion protein as the induction in LB media. The following steps, purification and cleavage, followed the same procedures as described above.

In our system of expression, the production of the fusion protein attained a concentration of 1.5 mg/ml, and the purification yields 2.5 mg per L of minimal medium.

5.5 Discussion

In spite of the wealth of information, expression of fusion proteins is a complex process and does not always follow simple predictions. It is necessary to test several strategies with different fusion tags in search for a highly efficient protocol that works for a given peptide.

The construction of the fusion gene by combination of DNA single strand synthesis with the PCR technique (149), proved to be a low cost, highly efficient method. The recombinant vectors provided by Gateway technology offer a time saving and highly competent system, which allows expression in various prokaryotic and eukaryotic organisms.

Reoccurring causes of unsuccessful efforts are proteolytic digestion of the exogenous protein and toxicity to the cells. Antibiotic peptides often belong to the second category (147, 156). The attempt by Piers et al (157) to produce small antimicrobial cationic peptides with a N-terminal signal were unsuccessful, while the same peptides were expressed stably in different fusion systems (157). Unsuccessful were also our attempts to produce the peptide without a fusion partner, while small fusion proteins were inefficient.

Peptide antibiotics, as antimicrobial reagents, have potentially high bacteriocidal activities thereby killing the host organisms. To avoid this harmful effect of expressed molecules and to meet the requirement of the subsequent purification strategy, the following points were taken into account in selecting the carrier molecule for the expression of the LAH4 peptide: (1) the carrier molecule should be hydrophilic, (2) it must not be harmful to the host bacteria expressing large quantities of it, and (3) there

should be a unique chemical or protease cleavage site between the fusion protein and the expressed peptide (136).

To avoid the harmful effects on the expression host, *E.coli*, the antimicrobial peptide LAH4 was expressed as a fusion protein with the glutathione S-transferase protein (26 kDa). This well described fusion partner (158, 159) has not only permitted the expression of our peptide, which proved in our hands unsuccessful by a direct approach, or in fusion with the considerably smaller periplasmic protein TolA (11.6 kDa), but also offers a straightforward simple purification procedure. The fusion partner, thus, played a key role in the expression: as the mass of the peptide represents only 10 % of the GST mass, the fusion partner covered partially the toxicity of the peptide.

The supernatant fraction from the cell lysate showed no detectable amount of the fusion protein in the soluble form, hence limiting the loss of material in the first purification step. Moreover, localization of the fusion protein in insoluble inclusion bodies has the advantageous effect to protect the bacteria from the antimicrobial peptides and also to avoid proteolysis of the expressed protein (135).

The affinity column showed very good yields of retention, witnessing excellent recovery of the GST three-dimensional structure regarding the refolding chosen process.

In our system of expression, the production of the fusion protein attained a concentration of 1.5 mg/ml. After optimization of the purification conditions 2.5 mg per L of minimal medium are obtained. Those levels are not very high compared to the expression of other recombinant peptides. Indeed, an average yield of peptide production in the various systems compared by Koenig et al (128) is 10 mg /L of minimum media, but it is noteworthy that the peptides described are not antibacterial. Our yield of 2.5 mg seems in

line with previous observations made with antibacterial peptide constructs. Martemyanov et al (144) isolated 3 mg of fusion protein from 2 L of culture (which corresponds to about 0.15 mg of pure peptide), while Haught et al (146) produced 0.37 mg of pure peptide from 1 L of bacterial culture.

The identity of recombinant antimicrobial peptide LAH4 produced must be determined by matrix-assisted laser desorption/ ionization mass spectroscopy (MALDI-MS), and its purity must be analyzed by reverse-phase high-performance liquid chromatography (HPLC). Lastly, the peptide must be tested as for its antibacterial activity and transfection efficiency.

As the choice of the fusion partner is evidently one of the key parameters in the determination of the yields of production of a genetically engineered peptide, and the selection of the host appears to be of great importance, our ability to change the expression vector by a single step recombination reaction may reveal to be very useful. It would certainly be very interesting to test our construct in different species, for example in *S. cerevisiae*, in order to increase the production yields, as the LAH4 peptide is not toxic to eukaryotic organisms.

Chapter 6

Solid state NMR studies on the diphtheria toxin domain T

6.1 Introduction

Diphtheria toxin (DT) is secreted as a 58 kDa polypeptide, which must be proteolytically cleaved to act on sensitive cells (160). Mild trypsinolysis yields two fragments, a NH₂-terminal fragment (21 kDa) termed A or DTA, and a COOH-terminal fragment (37 kDa) termed B or DTB, linked together by a disulfide bond. The fragment B is responsible for receptor binding and for mediating the translocation of the A fragment into the cytoplasm. There, DTA carries out the ADP-ribosylation of elongation factor EF-2, resulting in the inhibition of protein synthesis and cell death (160, 161).

Entry of DTA into the cytoplasm occurs from the endosomal compartment, following receptor mediated endocytosis. *In vitro* studies have shown that inside the endosomes, DT undergoes conformational changes as the pH decreases that result in exposure of previously buried hydrophobic regions, but allow secondary structure to be largely conserved (162, 163). Under such conditions, the toxin is able to insert into lipid vesicles and to form voltage-gated ion channels estimated to be large enough (18 Å in diameter), to allow passage of the extended DTA (18, 164-166).

Determination of the crystallographic structure in 1992, and refining at 1994 (15, 167), revealed that the protein is composed of three folding domains: the catalytic (C) domain,

corresponding to DTA; an intermediate α -helical domain, designated translocation or transmembrane (T) domain; and the receptor binding (R) domain (Fig. 6.1). The last two domains correspond to the amino and carboxy -terminal respectively of DTB.

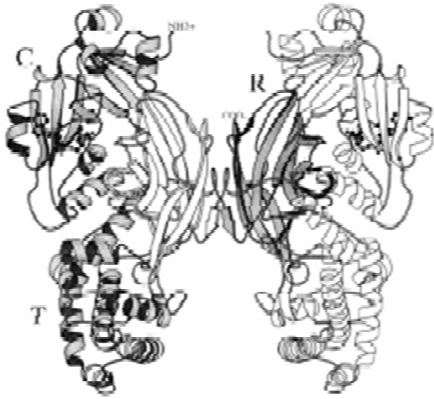


Figure 6.1: Diphtheria toxin dimer structure according to M.J. Bennett et al (167).

Ribbon representation of the 2.0 Å resolution model of the dimeric DT. One polypeptide chain is grey, while the other is white. The termini of one polypeptide chain are labelled NH_3^+ and COO^- . The domains are indicated by the letters C (catalytic, residues 1-190), T (transmembrane, residues 191-378), and R (receptor binding, residues 379-535).

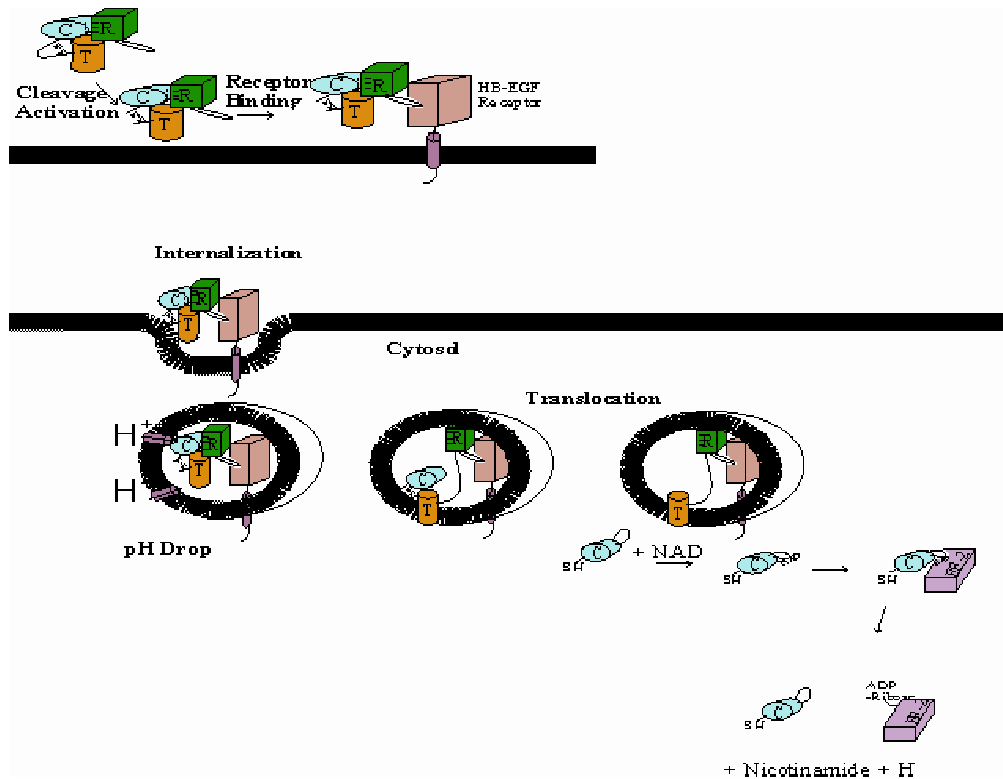


Figure 6.2: Mechanism of intoxication by the diphtheria toxin. The 3 domains of the DT molecule are labeled C, T and R. Proteolysis of the disulfide-linked surface loop activates the toxin. Three salt bridges between the C and R domains are indicated by the symbols - and +, representing acidic and basic residues, respectively. Receptor binding by a hairpin loop - shown protruding from the surface of the R domain - and internalization of the toxin. pH drop triggers conformational changes and protonation of acidic residues in the C domain weakening the salt bridges between the C and R domains and resulting to the formation of an open monomer. The domain T interacts with the membrane and provokes translocation of the C domain into the cytoplasm after disulfide bond reduction. The toxic reaction involves the sequential binding of substrates. NAD binds first and may cause a conformational change in a loop covering the active site cleft, which allows EF-2 to bind. After the transfer of ADP-ribose to EF-2 (inactivating EF-2), the C domain undergoes subsequent rounds of catalysis.

Diphtheria toxin binds to a specific heparin binding epidermal growth factor receptor (HB-EGF) precursor expressed in DT sensitive cells. The interaction is realized via the receptor-binding domain R, and is pH sensible. During intoxication of cells, the toxin reaches the early endosomes through the clathrin - coated pathway (168). The low pH of the endosome provokes dissociation of the DT prior to the translocation of the enzymatically active fragment of DT into the cytosol (169), as well as conformational changes of the domain T from a soluble state with a stable tertiary structure to a functional membrane inserted state (170) which achieves the translocation of the catalytic domain towards the cytosol (Fig.6.2).

The T domain is implied in pH dependant membrane interactions and has been shown to be sufficient for channel formation (18, 171). The domain is composed of nine helices (TH1-TH9), arranged in three layers according to crystallography data (15). The innermost layer consists of a long buried helical hairpin containing a highly hydrophobic helix (TH8) and one of amphipathic character (TH9). The second layer consists of helices TH5, TH6, and TH7, which form another hydrophobic hairpin that wraps around the TH8/9 hairpin. The third and outmost layer, consisting of helices TH1, TH2, and TH3, contains a high density of charged residues, which maintain the domain in water -soluble form (166).

Membrane insertion of proteins and peptides requires a refolding process that is poorly understood at the molecular level, but the membrane interfacial region is expected to play a critical role in the refolding event (172).

The membrane interacting domain T of the diphtheria toxin has been reconstituted in lipid vesicles and aligned mechanically between glass plates in order to be investigated as for its structure and topology by solid-state NMR techniques.

6.2 Material and Methods

The diphtheria's toxin domain T peptide was kindly provided by Dr. A.Chenal from the Département d'Ingénierie et d'Etudes des Protéines CEA -Saclay 91191 Gif sur Yvette cedex. The recombinant domain T was expressed in bacteria as described by Nizard et al, 1998(173), in minimal media with ^{15}N NH_4Cl as sole source of nitrogen.

Preparation of Oriented Samples

100 mg of 1-palmitoyl-2-oleoyl-*sn*-glycero-3-phosphocholine (POPC) alone or mixed with 1-palmitoyl-2-oleoyl-*sn*-glycero-3-[phospho-rac-(1-glycerol)] (Sodium Salt) (POPG) (Avanti Polar Lipids, Alabaster, AL) at wt:wt ratio of 8:2 were dissolved in 1 ml of dichloromethane (Sigma Aldrich, St Louis, MO). The solvent was evaporated under a gentle stream of nitrogen and the lipids further dried under vacuum overnight. Thereafter the resulting films were solubilized in 10 mM sodium acetate buffer pH 6. Mechanical agitation of the solution produces multilamellar vesicles (MLV). These were extruded through 100 nm membranes (Avestin, Ontario, Canada) to produce large unilamellar vesicles (LUV) (174).

The LUV preparations were mixed with 2.5 mg of domain T solubilized in 10 mM sodium acetate buffer pH 7 and the pH adjusted to 6 or 4, respectively, using HCl 0.5 mM.

The mixture is concentrated with Macrosep Centrifugal Devices, 10 kDa cut off (PALL, East Hills, NY) and spread onto 30 ultrathin cover glasses (9 x 22 mm; Paul Marienfeld GmbH & Co. KG, Lauda-Königshofen, Germany), first dried in air, and thereafter

equilibrated at 93 or 100 % relative humidity. The glass plates were stacked on the top of each other, stabilized with Teflon tape and sealed with plastic wrappings.

Solid-state NMR spectroscopy

The oriented samples were inserted in flat-coil solid-state NMR probe heads (60) and introduced into the magnetic field of a Bruker Avance wide-bore NMR spectrometer operating at 9.4 T. ^{15}N solid-state NMR spectra were recorded using a cross-polarization pulse sequence with high-power proton decoupling. The following parameters were used for the cross-polarization sequence: proton 90° pulse width of typically 8 μs , spin lock time of 1.6 ms, acquisition time of 3 ms and 10 K data points acquired. For the Hahn echo sequence the parameters used were the following: proton 90° pulse width of typically 13 to 16 μs , spin lock time of 5 ms, acquisition time of 13 ms and 10000 data points acquired. An exponential line-broadening function of 150 Hz was applied to the free induction decay before Fourier transformation. The ^{15}N spectra were referenced relative to NH_4Cl .

Prior to the ^{15}N experiments, the orientation of the LUV in the hydrated peptide/lipid samples was checked using a standard ^{31}P single pulse proton decoupled experiment at 9.395 T (121.4 MHz), providing information about the orientation of the ^{31}P chemical shift tensors for the phosphate headgroups in the phospholipids. The ^{31}P spectra were referenced relative to liquid H_3PO_4 .

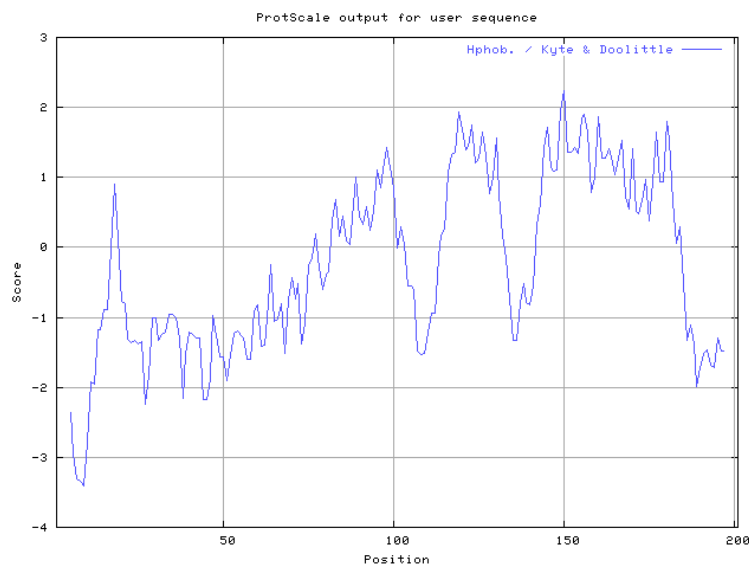


Figure 6.4: Analysis of the hydrophatic character of the domain T polypeptide using the Kyte-Doolittle scale.

The uniformly labelled ^{15}N recombinant domain T was reconstituted into oriented lipid vesicles in various conditions and investigated by solid state NMR spectroscopy.

At neutral pH, the insertion of the domain T is a function of lipid composition. When DT is reconstituted into POPC lipid bilayers and equilibrated at 93% r.h. the proton-decoupled ^{31}P solid-state NMR spectrum is indicative of liquid crystalline phospholipid bilayers which are well-aligned with their long axis parallel to the magnetic field direction (Fig.6.6). The proton-decoupled ^{15}N solid-state spectrum of the same sample labelled uniformly with ^{15}N shows a wide distribution of alignments of the NH vectors (230 – 60 ppm). This is not surprising when considering that the spectrum is a composition of 201 amide residues, 14 Histidine side chains, 13 Lysine side chains, 11 Asparagine, 6 Glutamine and 2 Arginine side chains. It should be noted however, that the cross-polarisation efficiency is a function of the efficient dipolar couplings between proton and nitrogen nuclei and therefore also on the local mobility of the sites.

When the hydration of the same sample is increased by equilibration at 100% humidity an additional peak at 125 ppm appears, where the chemical shift corresponds to the isotropic signal intensity of the amide residues. The relative signal intensity is much enhanced when the spectrum is recorded using a Hahn –echo pulse sequence instead of the cross polarisation technique. This observation is indicative of a high mobility of these amide residues due to the increase in intermembrane space, and therefore, a loose binding of large parts of the proteins to POPC lipid bilayers under these conditions.

In the presence of 20% POPG in the large unilamellar vesicles, the ^{15}N signal ≥ 170 ppm increases indicating that the ratio of NH bonds with alignments parallel to the membrane normal, such as e.g. those in transmembrane helices increases (Fig. 6.5). Similar alterations are observed for POPC-associated T-domain when the pH of the medium is acidified (Fig. 6.5). Under these conditions the CP-detected fraction of signal intensities at the isotropic chemical shift position is less pronounced when compared to spectra recorded at pH 6.

Proton decoupled ^{15}N solid-state NMR spectra of the domain T incorporated in POPC/POPG lipids at low pH exhibit a line shape comparable to that of the protein at higher pH in the presence of this lipid mixture. When the sample is equilibrated at 100% r.h., the intensity > 140 ppm decreases only slightly and the CP-detected signal intensity at the isotropic chemical shift region is insignificant, which contrast the observations made at the sample conditions discussed before. Unfortunately the Hahn-echo spectra from the series of samples do not allow to quantitatively evaluate this change between protein tightly associated with the membrane and those residues undergoing isotropic motion due to the low signal-to-noise inherent in the pulsed solid-state NMR approach.

Furthermore, an additional peak situated at 174 ppm is observed, in particular in the presence of POPC/POPG membranes at pH 4. This chemical shift value is compatible to

a peptide with α -helical secondary structures tilting by 15 - 35° relative to the bilayer normal or with the resonances of histidine side chains.

Together the spectra shown in Figure 5.4 indicate a tighter lipid association of the domain T protein when the pH is decreased and/or in the presence of POPG lipids.

It is noteworthy that in the proton decoupled ^{15}N , the <100 ppm chemical shifts are present for all the conditions tested indicating that a certain number of helices remain in plane at low pH and in the presence of anionic lipids. These findings are supported by the ^{31}P spectra, which for the same samples, at 93 % relative humidity, contain a single relatively narrow resonance at 29 ppm for the POPC samples and two relatively narrow resonances at 28 and 17 ppm for the POPC/POPG samples. This profile was well preserved at 100 % relative humidity for all the samples except one, the sample where both low pH and presence of POPG conditions meet (Fig. 6.6D).

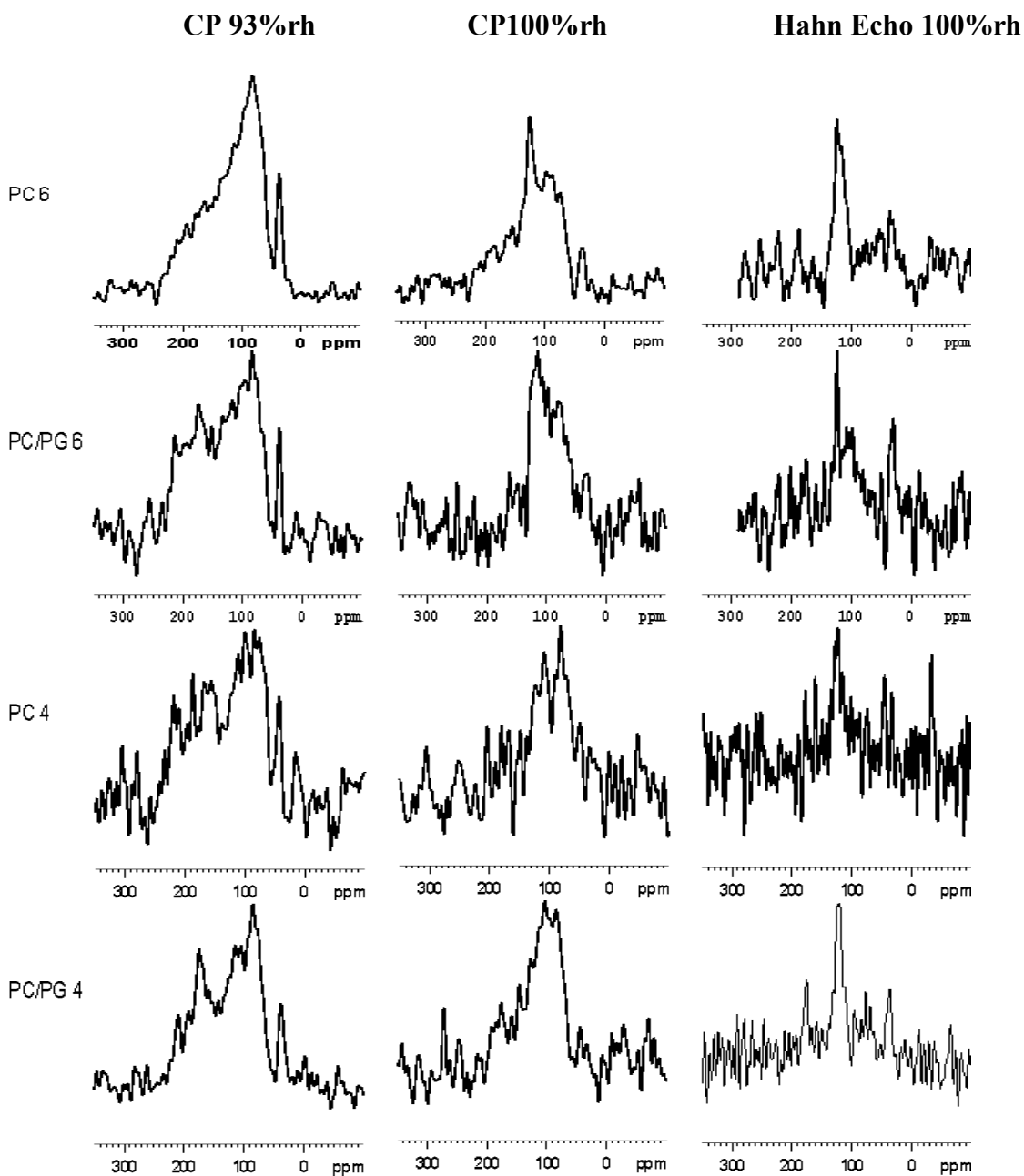


Figure 6.5: Cross Polarization (CP) at 93 and 100 % r.h. and Hahn Echo at 100 % r.h. of proton decoupled ^{15}N solid state NMR spectra of diphtherias toxin domain T reconstituted in oriented POPC (PC) or POPC/POPG (PC/PG) large unilamellar vesicles (LUV at wt:wt ratio of 8:2) in sodium acetate buffer 10 mM, pH 6 or 4.

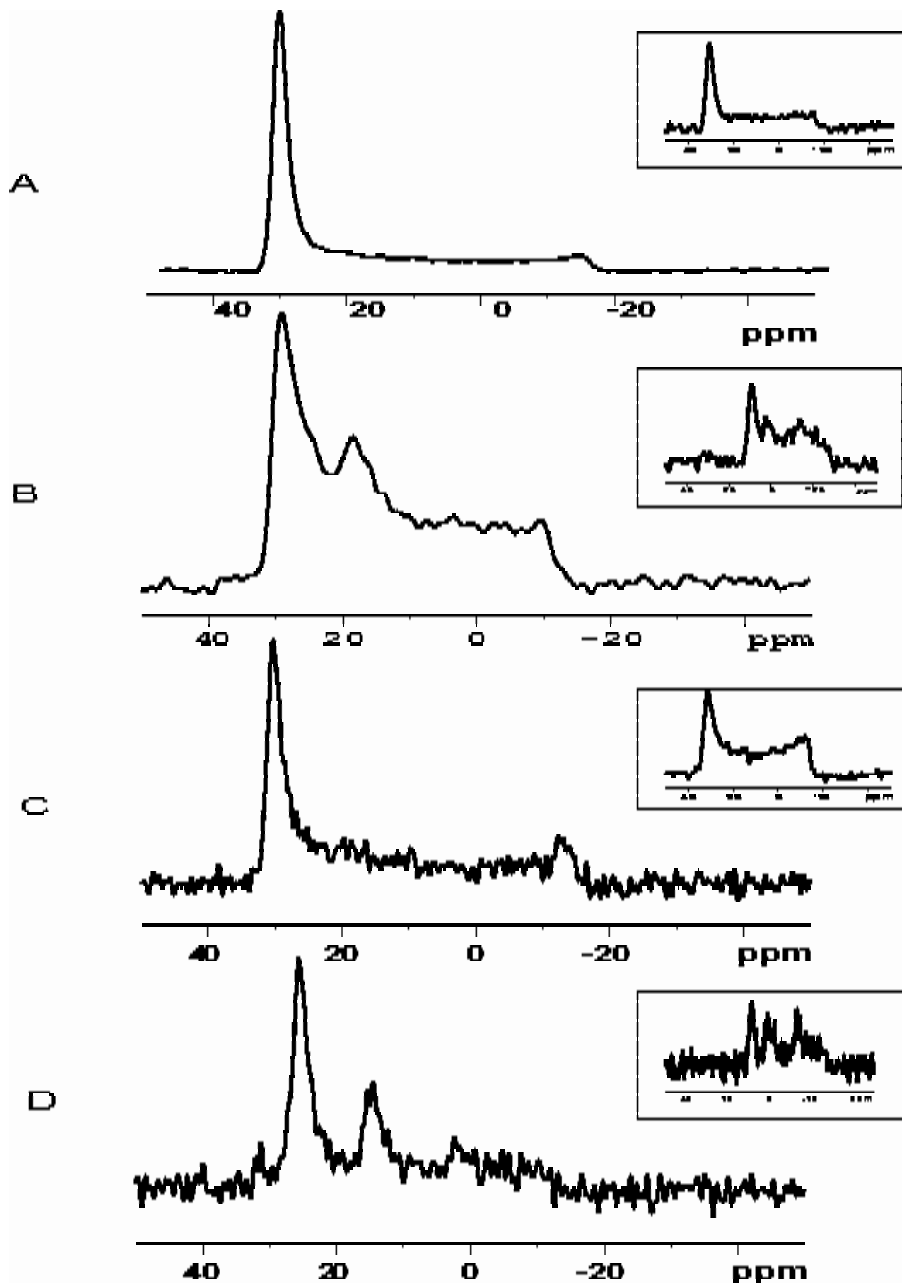


Figure 6.6: ^{31}P single pulse solid state NMR spectra at 93 % r.h. of diphtherias toxin domain T reconstituted in oriented POPC large unilamellar vesicles (LUV at wt:wt ratio of 8:2), in sodium acetate buffer 10 mM at pH 6(A), POPC/POPG at pH 6 (B), POPC pH 4 (C), and POPC/POPG pH4 (D). The insets show spectra at 100 % r.h. in the respective conditions.

6.4 Discussion

While the structure of soluble diphtheria toxin domain T at neutral pH has been clearly identified (15), conformational changes, provoked by the pH decrease, yielding a functional, membrane associated state whose structure is less well known. This latter state arises from changes in the balance of electrostatic attractions and repulsions between the N terminal part of the diphtheria toxin domain T and the membrane (175).

Numerous studies underline the important role played by the helices TH8/9 in the pore formation at low pH, and their transmembrane orientation is widely accepted.

Mutational analysis of the helical hairpin region of diphtheria toxin transmembrane domain, shows a marked reduction of cytotoxicity when the substitution mutations take place in the TH8/9 hairpin rather than in the TH5/6/7 hairpin (176).

D'Silva et al proposed a model in 2000 (177), conceived out of hydrophobic photolabeling data, where a tetramer of domains T interact with their hydrophobic helices TH8 and TH9, and their amphipathic helices TH1 to form the transmembrane toxin pore. Concerning the amphipathic helix TH1, the hydrophobic regions contact the hydrophobic core of the membrane, while the basic side chains interact with the anionic lipids. Thus, translocation occurs to equilibrate electrostatic and hydrophobic distribution on both sides of the membrane (175). Translocation of the TH1 – TH4 part seems necessary for the translocation of the catalytic domain (178).

The behaviour of hydrophobic helices TH 5/6/7, is less well understood. Hydropathy analysis suggests that these helices might have the potential to insert as a second transmembrane hairpin, one side of which would be formed by a transmembrane helix 5,

and the other side by a single transmembrane sequence formed by the combination of helices 6 and 7, either of which is too short to span the bilayer.

However, the sequence of the helix 5 - 7 region also has properties that make transmembrane insertion less likely. First, the helix 5 is not strongly hydrophobic (Fig. 5.4). Second, helices 5 and 6 are separated by a fairly large loop region containing several polar and charged residues, which might result in a thermodynamic barrier to insertion of the hairpin (179). Last, helices 6 and 7 are separated by a kink formed by proline - glycine sequence, which is somewhat unfavourable for transmembrane insertion (15) but does not prevent the α -helix formation in low dielectric environments such as the membrane.

Rosconi et al (180) have established that the membrane inserted T domain can exist in two distinct conformations. In the P state hydrophobic helices 5-9 lay close to the membrane surface, while in the TM state they insert more deeply, but never reach the transmembrane state. Bilayer width, bilayer curvature, T domain concentration, and interaction with molten globule-like proteins affect which state predominates (179).

Proton decoupled ^{15}N solid state NMR spectra of the domain T incorporated in POPC membranes at neutral pH, exhibit a typical powder pattern line shape at 93 % r.h., indicating coexistence of all polypeptide orientations in space, while at 100 % r.h., a strong anisotropic peak indicates important dynamic movements of the polypeptides backbone. These results are consistent with the polypeptide soluble form at pH 6, where the hydrophobic core is hidden and the domain T interacts via hydrophobic forces with the membrane (175). Its amphipathic N terminal part is largely solvated due to the repulsive electrostatic interactions between the T domain and the membrane.

Diminution of the anisotropic signal intensity, and deterioration of the signal to noise ratio in the presence of POPG in the membrane, as well as when the pH value is decreased, suggests a deeper insertion concomitant to a destabilization of the lipid bilayer structure.

Appearance of an additional peak at 175 ppm, in particular in the presence of POPC/POPG membranes at pH 4, may be interpreted in two ways. This chemical shift value is compatible to a peptide with α -helical secondary structures tilting by 15 - 25° relative to the bilayer normal or with the isotropic resonances of histidine side chains.

¹⁵N CP spectra of alamethicin, a small α -helical peptide presenting an important ion channel formation activity, labelled at one position present a single narrow resonance at the same position (181), exhibit chemical shift values of 172.7 ± 5 ppm when labelled on Ala⁶, and 176.7 ± 5 ppm when labelled on Val¹⁵. These values, in α -helical structures, correspond to tilt angles of 10-23° and 21-29° relative to the lipid bilayer, for Ala⁶ and Val¹⁵ respectively.

On the other hand, previous studies of the ¹⁵N chemical shift tensors in L-His•HCl•H₂O (182) have shown that the average chemical shift imidazole shielding tensors exhibit values of 179.2 ppm and 192.8 ppm for N3 and N2, respectively.

Histidines are present predominantly in highly mobile fragments in the diphtheria toxin domain T. The His tag in the N terminal segment, the C terminal and also in the loops connecting helices TH 1 - 2, TH 3 - 4 and TH 8 - 9 contain histidines. There are only two histidines in helical regions and these are in helix 3 and 9.

As a pronounced signal intensity at this chemical shift value is also observed at 100 % r.h. using a pulsed Hahn-echo sequence we suggest that it corresponds to the fourteen histidine residues in the sequence, including the six histidines of the N-terminal tag.

The large distribution of the chemical shifts at 93 % r.h., as well as the strong anisotropic character of polypeptide backbone at 100 % r.h. suggest that while part of the domain T inserts into the membrane, the rest of it remains highly mobile. The conformational changes provoked by the pH decrease are also observed by addition of POPG lipids in the physiological pH. The polypeptide passes from a globular structure where the hydrophobic core is surrounded by its polar parts, to a state where the hydrophobic helices slide into the membrane and inter-helical loops are unmasked.

Further studies, comprising selectively labelled domain T, should be undertaken in order to locate precisely each helix with respect to the lipid bilayer and to identify the complete topology of the diphtheria toxin domain T functional state when associated with the membrane.

^{13}P solid state NMR spectra at 93 % relative humidity, exhibit relatively narrow peaks typical of preparations containing oriented bilayers. ^{13}P NMR recorded spectra provide an estimate of the degree of the membrane orientation of the phospholipid head groups. The fast axial rotation of the phospholipids around their long axis averages the ^{31}P chemical shift anisotropy to a symmetric tensor where the tensor singular axis (σ_{\parallel}) coincides with the rotation axis (29). Liquid crystalline bilayers of pure phosphatidylcholine oriented with the bilayer parallel to the magnetic field direction exhibit resonances at $\sigma_{\parallel} = 30$ ppm. Signals in the region > 30 ppm arise from phospholipids with molecular orientations deviating from parallel to the magnetic field directions (29).

The narrow lined profile indicating well-oriented bilayers was preserved at 100 % relative humidity for all the samples except one, the sample where the conditions of low pH and presence of POPG lipids meet. The ^{31}P spectra of this sample suggest that the

lipid order in the bilayer is very much degraded. Thus, insertion of the domain T provokes misalignment of the lipid membranes. Hence, coexistence of these two factors, pH lowering and POPG presence, allow a better insertion of the diphtheria toxin domain T into the membrane.

Previous studies have shown that the bilayer width and curvature, the T domain concentration, and interaction with molten globule-like proteins are important factors for the insertion of the domain T into the membrane (179). Our results reveal that the membrane composition also plays an important role in the insertion of the T domain. We propose that the disordering of the lipid bilayer induced by the T domain may contribute to the translocation of the catalytic domain across the membrane.

Chapter 7

General Conclusions

NMR spectroscopy offers exciting perspectives to investigate the structure, dynamics, interactions and topologies of polypeptides associated with large macromolecular aggregates. Three different systems have been studied during my thesis work permitting exploration of the above stated perspectives.

A novel technique was experimentally tested and validated. Solid-state NMR studies on peptides reconstituted on non-oriented membrane bilayers have shown that motional averaging of the chemical shift tensors provides information on the peptide dynamics and orientation relative to the membrane normal. Non-oriented sample preparation that we developed is less time consuming and needs less delicate manipulation. This method is applicable for various peptides exhibiting membrane-associating properties.

The membrane-associating domain T of the diphtheria toxin has also been studied as for its membrane inserting properties at low pH and in presence of the anionic lipid POPG. Rosconi et al (*180*) established a two conformational state model of the domain T. Bilayer width, bilayer curvature, T domain concentration, and interaction with molten globule-like proteins affect which state predominates (*179*).

Solid-state NMR studies on oriented samples have shown that both pH and anionic lipids play an important role in the insertion and the disorientation of the lipids, responsible for the translocation of the catalytic domain C.

The conformational changes provoked by the pH decrease are also observed by addition of POPG lipids at physiological pH. The polypeptide passes from a globular structure where the hydrophobic core is surrounded by its polar parts, to a state where the hydrophobic helices slide into the membrane and inter-helical loops are unmasked. The ^{31}P spectra shows that the lipid order in the bilayer is very much degraded when the sample is subjected to both low pH and anionic lipid presence conditions, suggesting that insertion of the domain T provokes misalignment of the lipid membranes.

Solid-state NMR data together with other biophysical techniques reveal a large panel of information, all necessary to better understand the structure – function correlation of membrane bioactive proteins and peptides.

The present study allows for a detailed characterization of the LAH4 peptide action during the first steps of transfection. The formation of the binary complex LAH4/DNA was thoroughly studied, as well as its interaction with reconstituted membrane bilayers. The binary complex formation LAH4/DNA was investigated as for its thermodynamical properties and structural characteristics at both physiological and low pH, as the pH drop sets off the liberation of the DNA into the cytoplasm (183).

MAS NMR spectroscopy studies of the peptide in absence and in presence of DNA demonstrate that the α -helical character of the peptide is preserved upon DNA complexation. These data were supported by CD spectroscopy studies, which also provided evidence about increased LAH4 helicity at low pH.

However, to make use of the full potential of the NMR techniques, uniformly labelled LAH4 is required. Therefore, different expression strategies were tested, and the fusion GST partnership privileged. The LAH4 coding sequence was deduced from the *E.coli* codon usage table, and a single stranded DNA oligonucleotide was designed and

purchased, which served as a template for the construction of the complementary strand and the amplification of the gene by PCR. The PCR product was cloned first to an amplification vector and then transferred by recombination to the expression vector, downstream to the GST coding sequence. The vector was used to transfect chemically competent BL21(DE3) *E.coli* cells, who expressed the protein after induction.

The fusion protein was purified and cleaved, so as to release the LAH4 peptide. Currently, our effort is concentrated to the optimization of the cleavage reaction and the high level production of the peptide.

The ITC data allowed the establishment of the association parameters of the LAH4/DNA interaction. The data reveal that the association constant is not affected by the pH drop, and that its value is typical of a non-specific DNA – protein interaction based mainly on electrostatic interactions. The electrostatic nature of the driving forces of the interaction was also confirmed by the values of the enthalpic and entropic components in the association at neutral pH, while additional reinforcing hydrophobic interactions entered into play at low pH. Further evidence about the non-specific and electrostatic nature of the LAH4/DNA interaction was provided by CD spectroscopy and migrational electrophoresis studies.

The type of interactions between the peptide and the DNA, through the definition of their surface of interaction determines the stoichiometry of the reaction and the number of binding sites. At neutral pH, high density of peptide is achieved via electrostatic interactions either over their length in the form of multimers or via their N terminal extremities with the DNA groove. When the pH drops, peptide is released. At pH 5.5, over 30 % of the residues in LAH4 possess a positive charge. These residues are evenly distributed along the length of the molecule compensating favourably the negative charges on the DNA. The surface interaction between the LAH4 and the DNA molecules

is thus enhanced by supplementary electrostatic interaction, and additional hydrophobic forces reinforce this binding, resulting in tighter packing interactions between reduced number of LAH4 peptides and the DNA.

¹⁵N proton-decoupled spectra of non-oriented tertiary complex of LAH4/DNA reconstituted in lipid bilayers, present the same wide powder pattern line shape at both neutral and low pH. These patterns are indicative of slow re-orientational correlation times, in the order of 10 sec, when compared to the time-scale of the ¹⁵N chemical shift interaction. They suggest that the LAH4 peptide forms a large binary complex with the DNA where tight interactions between these two macromolecules hinder the backbone movement of the peptide. The large size of LAH4/DNA complexes was also confirmed by zeta-potential measurements and optical microscopy.

Integrating the information that we have collected from the peptidic transfection vector using the different techniques has brought a more detailed comprehension of the transfection mechanism.

During the first steps of the transfection, the LAH4 peptides bind in large excess to the plasmid DNA by non-specific electrostatic interactions, generating voluminous complexes. These complexes are internalized by endocytosis (183), and when the pH drops inside the endosomes, additional interactions between the macromolecules reduce the maximum number of LAH4 peptides bound to the DNA, thereby liberating a major fraction of peptides. The free LAH4 molecules interact with the endosomal membrane and provoke its lysis, delivering by this way the DNA to the cytoplasm.

The LAH4 peptidic vector has been proposed as an attractive alternative to the recombinant viruses based gene delivery systems which they are the basis of the vast majority of ongoing clinical trials (68). Product identification and quality control, low

cytotoxicity, and more efficient elimination rates would be some of the advantages offered by peptidic gene delivery system. Moreover, enhanced specificity could be achieved by a targeting sequence, easily grafted on the peptide. However, although the actual transfection efficiency of the LAH4 peptide higher than the efficiency of the current non-viral transfection vectors, it is not high enough compared to recombinant viral vectors.

A common distinctive feature observed for membrane active peptides is their ability to disturb bilayers integrity, either by disruption or pore formation (10). The resulting openings in the lipid bilayer lead to the collapse of the lipid structure and can explain the delivery of the DNA in the case of the LAH4 peptide or of the catalytic domain A in the case of the domain T of the diphtheria toxin in the cytoplasm. Rationalization of the drug design is based on structural and functional information. The more detailed is our knowledge of the process we want to enhance or to inhibit, the more specifically we can act. A detailed understanding of the mechanism of the membrane perturbation action of these two peptides will allow for the rational design of new antibiotics in the future.

References

1. Mathews, C., K., van Holde, K., E. (1990) *Biochemistry*, The Benjamin/Cummings Publishing Company.
2. Alberts, B., Bray, D., Lewis, J., Raff, M., Roberts, K., Watson, J., D. (1994) *Molecular Biology of the Cell*, Third ed., Garland publishing Inc.
3. Opella, S. J. (1997) *Nat Struct Biol* 4, 845-8.
4. Griffin, R. G. (1998) *Nat Struct Biol* 5, 508-12.
5. Mathews., C., K., van Holde, K., E. (1990) *Biochemistry*, The Benjamin/Cunmmings Publishing Co.
6. Bevins, C. L., and Zasloff, M., 395-414.
7. Boman, H. G. (1991) *Cell* 65, 205-7.
8. Wyman, T. B., Nicol, F., Zelphati, O., Scaria, P. V., Plank, C., and Szoka, F. C., Jr. (1997) *Biochemistry* 36, 3008-17.
9. Fominaya, J., Gasset, M., Garcia, R., Roncal, F., Albar, J. P., and Bernad, A. (2000) *J Gene Med* 2, 455-64.
10. Bechinger, B. (1999) *Biochim Biophys Acta* 1462, 157-83.
11. Oh, K. J., Senzel, L., Collier, R. J., and Finkelstein, A. (1999) *Proc Natl Acad Sci U S A* 96, 8467-70.
12. Miller, C. J., Elliott, J. L., and Collier, R. J. (1999) *Biochemistry* 38, 10432-41.
13. Shatursky, O., Heuck, A. P., Shepard, L. A., Rossjohn, J., Parker, M. W., Johnson, A. E., and Tweten, R. K. (1999) *Cell* 99, 293-9.
14. Gill, D., M.,. (1978) (Jeljaszaszewich, Ed.) pp 291-322, J. & Wadstrom, T. (Academic London).

15. Choe, S., Bennett, Mj, Fujii, G, Curmi, Pm, Kantardjieff, Ka, Collier, Rj, Eisenberg, D. (1992) *Nature* . 357, 216-222.
16. Parker, M. W., Pattus, F., Tucker, A. D., and Tsernoglou, D. (1989) *Nature* 337, 93-6.
17. Muchmore, S. W., Sattler, M., Liang, H., Meadows, R. P., Harlan, J. E., Yoon, H. S., Nettlesheim, D., Chang, B. S., Thompson, C. B., Wong, S. L., Ng, S. L., and Fesik, S. W. (1996) *Nature* 381, 335-41.
18. Kagan, B., Finkelstein, A, Colombini, M. (1981) *Proc Natl Acad Sci U S A* 78, 4950-4.
19. Steiner, H., Hultmark, D., Engstrom, A., Bennich, H., and Boman, H. G. (1981) *Nature* 292, 246-8.
20. Blondelle, S. E., and Houghten, R. A. (1992) *Biochemistry* 31, 12688-94.
21. Bechinger, B. (1996) *J Mol Biol* 263, 768-75.
22. Wieprecht, T., Dathe, M., Krause, E., Beyermann, M., Maloy, W. L., MacDonald, D. L., and Bienert, M. (1997) *FEBS Lett* 417, 135-40.
23. Vogt, T. C., and Bechinger, B. (1999) *J Biol Chem* 274, 29115-21.
24. Kichler, A., Leborgne, C., Marz, J., Danos, O., and Bechinger, B. (2003) *Proc Natl Acad Sci U S A* 100, 1564-8. Epub 2003 Jan 31.
25. Marassi, F. M., Ramamoorthy, A., and Opella, S. J. (1997) *Proc Natl Acad Sci U S A* 94, 8551-6.
26. Merrifield, B. (1995) (B, G., Ed.) pp 94-170, Academic Press, San Diego.
27. Maricq, M., M., Waugh, J., S. (1979) *J Chem Phys* 70, 3300-3316.
28. Mehring, M. (1983) *Principles of High Resolution NMR in solids*, Second ed., Springer-Verlag.

29. Bechinger, B., Kinder, R., Helmle, M., Vogt, T. C., Harzer, U., and Schinzel, S. (1999) *Biopolymers* 51, 174-90.
30. Bechinger, B. (1997) *Proteins* 27, 481-92.
31. Bechinger, B., Kim, Y., Chirlian, L. E., Gesell, J., Neumann, J. M., Montal, M., Tomich, J., Zasloff, M., and Opella, S. J. (1991) *J Biomol NMR* 1, 167-73.
32. Bechinger, B., Gierasch, L. M., Montal, M., Zasloff, M., and Opella, S. J. (1996) *Solid State Nucl Magn Reson* 7, 185-91.
33. Opella, S. J., Nevzorov, A., Mesleb, M. F., and Marassi, F. M., 597-604.
34. Opella, S. J., Nevzorov, A., Mesleb, M. F., and Marassi, F. M. (2002) *Biochem Cell Biol* 80, 597-604.
35. Opella, S. J., Stewart, P. L., and Valentine, K. G. (1987) *Q Rev Biophys* 19, 7-49.
36. Lazo, N. D., Hu, W., and Cross, T. A. (1995) *J Magn Reson B* 107, 43-50.
37. Bechinger, B., Sizun, C. (2003) *Concepts Magn Reson* 18A, 130-145.
38. Bechinger, B., Sizun, C. (2003) *Concepts Magn Reson* 18A, 130-145.
39. Gennis, R., B. (1989) *Biomembranes - Molecular structure and function*, Springer-Verlag.
40. Möhwald, H. (1995) in *Handbook of Biological Physics* (Lipowsky, R., Sackmann, E., Ed.) pp 161-211.
41. Nagle, J. F., and Tristram-Nagle, S. (2000) *Biochim Biophys Acta* 1469, 159-95.
42. Pascher, I., Lundmark, M., Nyholm, P. G., and Sundell, S. (1992) *Biochim Biophys Acta* 1113, 339-73.
43. Seddon, J., M., Templer, R., H. (1995) in *Handbook of Biological Physics* pp 97-160.

44. Harris, R., K. (1986) *Nuclear Magnetic resonance spectroscopy*, Longman Group UK Limited.
45. Andrews, E., R., Bradbury, D, Eades, R., G., Wynn, V., T. (1958) *Phys Lett* 4, 99-100.
46. Andrew, E., R., Bradbury, D, Eades, R., G., Wynn, V., T. (1959) *Nature* 183, 1802-1803.
47. Lowe, I., J. (1959) *Phys Rev Lett* 2, 285.
48. Hafner, S., Spiess, H., W. (1998) *Concepts in Magnetic Resonance* 10, 99-128.
49. Ando, I., Kameda, T., Asakawa, N., Kuroki, S., Kurosu, H. (1998) *J Mol Struct* 441, 213-230.
50. McDermott, A., Polenova, T., Bockmann, A., Zilm, K. W., Paulson, E. K., Martin, R. W., and Montelione, G. T. (2000) *J Biomol NMR* 16, 209-19.
51. Pauli, J., van Rossum, B., Forster, H., de Groot, H. J., and Oschkinat, H. (2000) *J Magn Reson* 143, 411-6.
52. Torres, J., Stevens, T. J., and Samsó, M. (2003) *Trends Biochem Sci* 28, 137-44.
53. Price, N. C., Dwek, R. A. (1991) *Principles and problems in physical chemistry for biochemists*, Second Edition ed., Oxford Science Publications.
54. Atkins, P. W. (1994), Oxford University Press.
55. Leavitt, S., and Freire, E. (2001) *Curr Opin Struct Biol* 11, 560-6.
56. MicroCal, I.
57. Saïto, H. (1986) *Magn Reson Chem* 24, 835-852.
58. Watts, A. (1999) *Curr Opin Biotechnol* 10, 48-53.
59. Aisenbrey, C., Bechinger, B. (2004) *J Am Chem Soc* 126, 16676-83.

60. Ramamoorthy, A., Marassi, F. M., Zasloff, M., and Opella, S. J. (1995) *J Biomol NMR* 6, 329-34.
61. Oas, T. G. H., C.J., Dahlquist, F.W., Drobny, G.P. (1987) *J Am Chem Soc* 109, 5962-5966.
62. Wightman, L., Kircheis, R., Rossler, V., Carotta, S., Ruzicka, R., Kursa, M., and Wagner, E. (2001) *J Gene Med* 3, 362-72.
63. Subczynski, W. K., Lewis, R. N., McElhane, R. N., Hodges, R. S., Hyde, J. S., and Kusumi, A. (1998) *Biochemistry* 37, 3156-64.
64. de Planque, M. R., Kruijtzter, J. A., Liskamp, R. M., Marsh, D., Greathouse, D. V., Koeppe, R. E., 2nd, de Kruijff, B., and Killian, J. A. (1999) *J Biol Chem* 274, 20839-46.
65. Bechinger, B., Zasloff, M., and Opella, S. J. (1993) *Protein Sci* 2, 2077-84.
66. Cross, T. A., 672-96.
67. Smith, B. O., Downing, A. K., Dudgeon, T. J., Cunningham, M., Driscoll, P. C., and Campbell, I. D. (1994) *Biochemistry* 33, 2422-9.
68. Anderson, W. F. (1998) *Nature* 392, 25-30.
69. Haensler, J., and Szoka, F. C., Jr. (1993) *Bioconjug Chem* 4, 85-93.
70. Michael, S. I., and Curiel, D. T. (1994) *Gene Ther* 1, 223-32.
71. Boussif, O., Lezoualc'h, F., Zanta, M. A., Mergny, M. D., Scherman, D., Demeneix, B., and Behr, J. P. (1995) *Proc Natl Acad Sci U S A* 92, 7297-301.
72. Ferrari, S., Moro, E., Pettenazzo, A., Behr, J. P., Zacchello, F., and Scarpa, M. (1997) *Gene Ther* 4, 1100-6.
73. Wolfert, M. A., Schacht, E. H., Toncheva, V., Ulbrich, K., Nazarova, O., and Seymour, L. W. (1996) *Hum Gene Ther* 7, 2123-33.

74. Gao, X., and Huang, L. (1995) *Gene Ther* 2, 710-22.
75. Behr, J. P. (1994) *Bioconjug Chem* 5, 382-9.
76. Hart, S. L., Collins, L., Gustafsson, K., and Fabre, J. W. (1997) *Gene Ther* 4, 1225-30.
77. Midoux, P., Mendes, C., Legrand, A., Raimond, J., Mayer, R., Monsigny, M., and Roche, A. C. (1993) *Nucleic Acids Res* 21, 871-8.
78. Plank, C., Oberhauser, B., Mechtler, K., Koch, C., and Wagner, E. (1994) *J Biol Chem* 269, 12918-24.
79. Zanta, M. A., Belguise-Valladier, P., and Behr, J. P. (1999) *Proc Natl Acad Sci U S A* 96, 91-6.
80. Bloomfield, V. A. (1996) *Curr Opin Struct Biol* 6, 334-41.
81. von Hippel, P., Berg, O. G. (1986) *Proc Natl Acad Sci U S A* 83, 1608-12.
82. Dragan, A. I., Klass, J., Read, C., Churchill, M. E., Crane-Robinson, C., and Privalov, P. L. (2003) *J Mol Biol* 331, 795-813.
83. Keller, M., Tagawa, T., Preuss, M., and Miller, A. D. (2002) *Biochemistry* 41, 652-9.
84. Lundback, T., Hansson, H., Knapp, S., Ladenstein, R., and Hard, T. (1998) *J Mol Biol* 276, 775-86.
85. Seelig, J. (1997) *Biochim Biophys Acta* 1331, 103-16.
86. Seelig, J., Nebel, S., Ganz, P., and Bruns, C. (1993) *Biochemistry* 32, 9714-21.
87. Ortega, A., Lambotte, S., and Bechinger, B. (2001) *J Biol Chem* 276, 13563-72. Epub 2001 Jan 16.
88. Lobo, B., Koe, Gs, Koe, Jg, Middaugh, Cr. (2003) *Biophys Chem* 104, 67-78.

89. Pector, V., Backmann, J, Maes, D, Vandenbranden, M, Ruyschaert, Jm. (2000) *J Biol Chem* 275, 29533-8.
90. Seelig, J., Nebel, S, Ganz, P, Bruns, C. (1993) *Biochemistry* 32, 9714-21.
91. Ackers, G. K., Johnson, M.L., (1998) *Methods in Enzymology*, Vol. 295, Academic press.
92. Leavitt, S., Freire, E. (2001) *Curr Opin Struct Biol* 11, 560-6.
93. Forstner, M., Berger, C., and Wallimann, T. (1999) *FEBS Lett* 461, 111-4.
94. Cooper, A., Johnson, Cm, Lakey, Jh, Nollmann, M. (2001) *Biophys Chem* 93, 215-30.
95. Krylov, D., Olive, M, Vinson, C. (1995) *EMBO J* 14, 5329-37.
96. Zitzewitz, J., Bilsel, O, Luo, J, Jones, Be, Matthews, Cr. (1995) *Biochemistry* 34, 12812-9.
97. Wendt, H., Berger, C, Baici, A, Thomas, Rm, Bosshard, Hr. (1995) *Biochemistry* 34, 4097-107.
98. Berger, C., Jelesarov, I, Bosshard, Hr. (1996) *Biochemistry* 35, 14984-91.
99. Cooper, A., Johnson, C. M., Lakey, J. H., and Nollmann, M. (2001) *Biophys Chem* 93, 215-30.
100. Lauterwein, J., Bosch, C., Brown, L. R., and Wuthrich, K. (1979) *Biochim Biophys Acta* 556, 244-64.
101. Terwilliger, T. C., and Eisenberg, D. (1982) *J Biol Chem* 257, 6010-5.
102. Luca, S., Filippov, D. V., van Boom, J. H., Oschkinat, H., de Groot, H. J., and Baldus, M. (2001) *J Biomol NMR* 20, 325-31.
103. Cornilescu, G., Delaglio, F., and Bax, A. (1999) *J Biomol NMR* 13, 289-302.
104. Kricheldorf, H. R., Müller, D. (1983) *Macromolecules* 16, 615-623.

105. Howarth, O. W., Lilley, D.M.J. (1978) *Prog. NMR Spec.* 12, 1-40.
106. Saito, H., Ando, I. (1989) *Ann. Rep. NMR Spec.* 21, 209-290.
107. LaPlante, S. R. e. a. (2001) *Biophys. Chem.* 90, 219-232.
108. Kalinowski, H. O. e. a. (1984) *¹³C-NMR-Spektroskopie Thieme Verlag, Stuttgart.*
109. Leupin, W., Wagner, G., Denny, W. A., and Wuthrich, K. (1987) *Nucleic Acids Res* 15, 267-75.
110. Aisenbrey, C., Kinder, R., Goormaghtigh, E., Ruysshaert, J.M., Schinzel, S., and März, J., & Bechinger, B. (2005).
111. Dragan, A., Klass, J, Read, C, Churchill, Me, Crane-Robinson, C, Privalov, Pl. (2003) *J Mol Biol* 331, 795-813.
112. Seelig, J. (1997) *Biochim Biophys Acta* 1331.
113. Ross, P., Subramanian, S. (1981) *Biochemistry* 20, 3096-102.
114. Ross, P. D., and Subramanian, S. (1981) *Biochemistry* 20, 3096-102.
115. Pector, V., Backmann, J., Maes, D., Vandenbranden, M., and Ruyschaert, J. M. (2000) *J Biol Chem* 275, 29533-8.
116. von Hippel, P. H., and Berg, O. G. (1986) *Proc Natl Acad Sci U S A* 83, 1608-12.
117. Arscott, P. G., Li, A. Z., and Bloomfield, V. A., 619-30.
118. Lin, Z., Wang, C., Feng, X., Liu, M., Li, J., and Bai, C. (1998) *Nucleic Acids Res* 26, 3228-34.
119. Li, S., and Huang, L. (1997) *Gene Ther* 4, 891-900.
120. Laemmli, U. K. (1975) *Proc Natl Acad Sci U S A* 72, 4288-92.
121. Behr, J. P. (1994) *Bioconjug Chem* 5, 382-9.
122. Azorin, F., Vives, J., Campos, J. L., Jordan, A., Lloveras, J., Puigjaner, L., Subirana, J. A., Mayer, R., and Brack, A. (1985) *J Mol Biol* 185, 371-87.

123. Kichler, A., Leborgne, C., Coeytaux, E., and Danos, O. (2001) *J Gene Med* 3, 135-44.
124. Vogt, T. C., and Bechinger, B. (1999) *J Biol Chem* 274, 29115-21.
125. Bechinger, B. (2005) *Biochim Biophys Acta* 1712, 101-8. Epub 2005 Apr 1.
126. Walters, K. J., Ferentz, A. E., Hare, B. J., Hidalgo, P., Jasanoff, A., Matsuo, H., and Wagner, G., 238-58.
127. Gardner, K. H., and Kay, L. E., 357-406.
128. Koenig, B. W., Rogowski, M., and Louis, J. M. (2003) *J Biomol NMR* 26, 193-202.
129. Martemyanov, K. A., Spirin, A. S., and Gudkov, A. T. (1997) *FEBS Lett* 414, 268-70.
130. Huang, Y., Liu, F. P., Zhou, T. H., and Zhu, J. M. (2001) *Sheng Wu Gong Cheng Xue Bao* 17, 207-10.
131. Weng, H. B., Niu, B. L., Meng, Z. Q., and Xu, M. K. (2002) *Sheng Wu Gong Cheng Xue Bao* 18, 352-5.
132. Martemyanov, K. A., Spirin, A. S., Gudkov, A. T. (1996) *Biotechn Lett* 18, 1357-1362.
133. Kim, S. H., Park, B. S., Yun, E. Y., Je, Y. H., Woo, S. D., Kang, S. W., Kim, K. Y., and Kang, S. K. (1998) *Biochem Biophys Res Commun* 246, 388-92.
134. Hwang, S. W., Lee, J. H., Park, H. B., Pyo, S. H., So, J. E., Lee, H. S., Hong, S. S., and Kim, J. H. (2001) *Mol Biotechnol* 18, 193-8.
135. Lee, J. H., Kim, J. H., Hwang, S. W., Lee, W. J., Yoon, H. K., Lee, H. S., and Hong, S. S. (2000) *Biochem Biophys Res Commun* 277, 575-80.

136. Rao, X. C., Li, S., Hu, J. C., Jin, X. L., Hu, X. M., Huang, J. J., Chen, Z. J., Zhu, J. M., and Hu, F. Q. (2004) *Protein Expr Purif* 36, 11-8.
137. Itakura, K., Hirose, T., Crea, R., Riggs, A. D., Heyneker, H. L., Bolivar, F., and Boyer, H. W. (1977) *Science* 198, 1056-63.
138. Goeddel, D. V., Kleid, D. G., Bolivar, F., Heyneker, H. L., Yansura, D. G., Crea, R., Hirose, T., Kraszewski, A., Itakura, K., and Riggs, A. D. (1979) *Proc Natl Acad Sci USA* 76, 106-10.
139. Crowe, J., Dobeli, H., Gentz, R., Hochuli, E., Stuber, D., and Henco, K., 371-87.
140. Smith, D. B., and Johnson, K. S. (1988) *Gene* 67, 31-40.
141. Anderluh, G., Gokce, I., and Lakey, J. H. (2003) *Protein Expr Purif* 28, 173-81.
142. LaVallie, E. R., DiBlasio, E. A., Kovacic, S., Grant, K. L., Schendel, P. F., and McCoy, J. M. (1993) *Biotechnology (N Y)* 11, 187-93.
143. Stewart, E. J., Aslund, F., and Beckwith, J. (1998) *EMBO J* 17, 5543-50.
144. Martemyanov, K., Spirin, As, Gudkov, At. (1996) *Biotechn Lett* 18, 1357-1362.
145. Xie, W., Qiu, Q., Wu, H., and Xu, X. (1996) *Biochem Mol Biol Int* 39, 487-92.
146. Haught, C., Davis, G. D., Subramanian, R., Jackson, K. W., and Harrison, R. G. (1998) *Biotechnol Bioeng* 57, 55-61.
147. Lee, J. H., Kim, J. H., Hwang, S. W., Lee, W. J., Yoon, H. K., Lee, H. S., and Hong, S. S. (2000) *Biochem Biophys Res Commun* 277, 575-80.
148. Hwang, S., Lee, Jh, Park, Hb, Pyo, Sh, So, Je, Lee, Hs, Hong, Ss, Kim, Jh. (2001) *SO - Mol Biotechnol* 18, 193-198.
149. Chen, C., Mao, J., Zhang, M., and Dai, J., 63-70.
150. Schagger, H., and von Jagow, G. (1987) *Anal Biochem* 166, 368-79.
151. Liao, H. H. (1991) *Protein Expr Purif* 2, 43-50.

152. Volkel, D., Blankenfeldt, W., and Schomburg, D. (1998) *Eur J Biochem* 251, 462-71.
153. Dill, K. A., and Chan, H. S. (1997) *Nat Struct Biol* 4, 10-9.
154. Fischer, B., Sumner, I., and Goodenough, P. (1992) *Arzneimittelforschung* 42, 1512-5.
155. Cameron, A. D., Sinning, I., L'Hermite, G., Olin, B., Board, P. G., Mannervik, B., and Jones, T. A. (1995) *Structure* 3, 717-27.
156. Rao, X. C., Li, S., Hu, J. C., Jin, X. L., Hu, X. M., Huang, J. J., Chen, Z. J., Zhu, J. M., and Hu, F. Q. (2004) *Protein Expr Purif* 36, 11-8.
157. Piers, K. L., Brown, M. H., and Hancock, R. E. (1993) *Gene* 134, 7-13.
158. Smith, D. B., and Johnson, K. S. (1988) *Gene* 67, 31-40.
159. Volkel, D., Blankenfeldt, W., and Schomburg, D. (1998) *Eur J Biochem* 251, 462-71.
160. Collier, R. J. (1975) *Bacteriol Rev* 39, 54-85.
161. Strauss, N., and Hendee, E. D. (1959) *J Exp Med* 109, 145-63.
162. Blewitt, M. G., Chao, J. M., McKeever, B., Sarma, R., and London, E. (1984) *Biochem Biophys Res Commun* 120, 286-90.
163. Cabiaux, V., Brasseur, R., Wattiez, R., Falmagne, P., Ruyschaert, J. M., and Goormaghtigh, E. (1989) *J Biol Chem* 264, 4928-38.
164. Zalman, L. S., and Wisnieski, B. J. (1984) *Proc Natl Acad Sci U S A* 81, 3341-5.
165. Gonzalez, J. E., and Wisnieski, B. J. (1988) *J Biol Chem* 263, 15257-9.
166. Silverman, J. A., Mindell, J. A., Finkelstein, A., Shen, W. H., and Collier, R. J. (1994) *J Biol Chem* 269, 22524-32.
167. Bennett, M. J., Choe, S., and Eisenberg, D. (1994) *Protein Sci* 3, 1444-63.

168. Lemichez, E., Bomsel, M., Devilliers, G., vanderSpek, J., Murphy, J. R., Lukianov, E. V., Olsnes, S., and Boquet, P. (1997) *Mol Microbiol* 23, 445-57.
169. Brooke, J. S., Cha, J. H., and Eidels, L. (1998) *Biochem Biophys Res Commun* 248, 297-302.
170. D'Silva, P. R., and Lala, A. K. (2000) *J Biol Chem* 275, 11771-7.
171. Cabiaux, V., Phalipon, A., Kaczorek, M., Collier, R. J., and Ruyschaert, J. M., 273-7.
172. Ladokhin, A. S., and White, S. H. (2001) *J Mol Biol* 309, 543-52.
173. Nizard, P., Liger, D., Gaillard, C., and Gillet, D. (1998) *FEBS Lett* 433, 83-8.
174. Mayer, L. D., Hope, M. J., and Cullis, P. R. (1986) *Biochim Biophys Acta* 858, 161-8.
175. Chenal, A., Savarin, P., Nizard, P., Guillain, F., Gillet, D., and Forge, V. (2002) *J Biol Chem* 277, 43425-32.
176. Silverman, J. A., Mindell, J. A., Finkelstein, A., Shen, W. H., and Collier, R. J. (1994) *J Biol Chem* 269, 22524-32.
177. D'Silva, P. R., and Lala, A. K. (2000) *J Biol Chem* 275, 11771-7.
178. Oh, K., Senzel, L., Collier, Rj, Finkelstein, A. (1999) *Proc Natl Acad Sci U S A* 96, 8467-70.
179. Rosconi, M. P., and London, E. (2002) *J Biol Chem* 277, 16517-27. Epub 2002 Feb 21.
180. Rosconi, M. P., Zhao, G., and London, E. (2004) *Biochemistry* 43, 9127-39.
181. Bak, M., Bywater, R. P., Hohwy, M., Thomsen, J. K., Adelhorst, K., Jakobsen, H. J., Sorensen, O. W., and Nielsen, N. C. (2001) *Biophys J* 81, 1684-98.
182. Harbison, G., Herzfeld, J., Griffin, R.,G. (1981) *J Am Chem Soc* 103, 4752-4754.

183. Kichler, A., Leborgne, C., Marz, J., Danos, O., and Bechinger, B. *SO - Proc Natl Acad Sci U S A* 2003 Feb 18;100(4):1564-8. Epub 2003 Jan 31.

Publications

- L. Prongidi, P. Bertani, M. Sugawara, J. Raya, A. Kichler, B. Bechinger
Self-promoted cell entry of peptidic transfection complexes
Submitted
- L. Prongidi, B. Bechinger
Membrane peptide helix alignments and dynamics from non-oriented ¹⁵N chemical shift spectra
In preparation

Posters

- Lydia Prongidi, Masae Sugawara, Philippe Bertani, Antoine Kichler, Burkhard Bechinger
Etudes structurales et interactionnelles de LAH4, nouveau vecteur de transfection
GERM 2005, mars 2005, Poster
- L. Prongidi, P. Bertani, M. Sugawara, J. Georgescu, A. Kichler, B. Bechinger
Mechanistic studies of the peptide transfection vector LAH4
28th European CF conference en Crete, juin 2005, Poster
- L. Prongidi, P. Bertani, M. Sugawara, J. Georgescu, A. Kichler, B. Bechinger
Mechanistic studies of the peptide transfection vector LAH4
Symposium International Progrès en chimie supramoléculaire à Strasbourg, juillet 2005
- Lydia Prongidi, Philippe Bertani, Antoine Kichler, Burkhard Bechinger
Le nouveau vecteur de transfection LAH4
4e Colloque de Vaincre la Mucoviscidose à Paris, mai 2004, Poster

- F.Vierling, J.Meullemeestre, F.Brisach, H.Dkhissi, L.Domon, J.Durand, C.Frison, C.Hamann, M.Hanbali, P.Heller, M.Lejeune, P.Mobian, N.Peybernes, L.Prongidi, M.Rombourg, H.Risler, E.Shneider, P.Schall, V.Wernert
Expériences et montages de Travaux Pratiques de Chimie : Génie Biologique, Mesures Physiques, IUT Louis Pasteur Schiltigheim, ULP, Strasbourg I
Journées Portes Ouvertes, IUT Louis Pasteur Schiltigheim, ULP, Strasbourg I, mars 2004
- F.Vierling, J.Meullemeestre, F.Brisach, H.Dkhissi, L.Domon, J.Durand, C.Frison, C.Hamann, M.Hanbali, P.Heller, M.Lejeune, P.Mobian, N.Peybernes, L.Prongidi, M.Rombourg, H.Risler, E.Shneider, P.Schall, V.Wernert
Spectrométrie d'absorption de systèmes ternaires d'oxydo-réduction ; Aspects thermodynamiques et cinétiques
Journées Portes Ouvertes, IUT Louis Pasteur Schiltigheim, ULP, Strasbourg I, mars 2004
- Lydia Prongidi, Philippe Bertani, Antoine Kichler, Burkhard Bechinger
Etude structurale du nouveau vecteur peptidique de transfection LAH4 par RMN du solide
3^e Colloque de Vaincre la Mucoviscidose à Paris, mai 2003, Poster

RESUME:

Les peptides constituent un moyen simplifié d'étudier le fonctionnement des protéines et des moyens thérapeutiques potentiellement très intéressants. Ce travail a permis l'investigation de deux peptides, le peptide synthétique LAH4 et le domaine T de la protéine diphtérique en interaction avec d'autres macromolécules.

Le peptide LAH4 conçu et synthétisé par notre laboratoire, présente les propriétés générales des peptides amphipathiques et se lie également fortement à l'ADN permettant son transfert dans les cellules en tant que vecteur de transfection. Dans le but de mieux comprendre l'activité du peptide LAH4 pendant la transfection, j'ai examiné ses propriétés biophysiques par ITC (isothermal titration calorimetry), CD (Circular Dichroism) et RMN du solide. Les résultats montrent que la structure en hélice- α du peptide est maintenue après complexation de l'ADN. A pH neutre des liaisons électrostatiques lient les molécules de façon non spécifique et un ratio très élevé de LAH4 est requis pour la saturation et la condensation de l'ADN. A plus faible pH des interactions électrostatiques et des contributions hydrophobes stabilisent le complexe peptide/ADN, et le ratio de saturation est réduit de presque moitié. Les données concordent à l'élaboration d'un modèle d'action du peptide LAH4 pendant les premières étapes de la transfection. En parallèle, nous avons développé une stratégie d'expression du LAH4 chez *E.coli* afin de le marquer ^{13}C uniformément pour son étude par RMN.

Des études par RMN du solide ont été entreprises sur le domaine T de la toxine diphtérique afin de comprendre la topologie dans des vésicules membranaires. Des échantillons de domaine T uniformément marqués en ^{15}N ont été préparés en reconstituant les conditions présentes dans l'endosome de façon très simplifiée. Les résultats montrent un rôle important joué autant par le lipide anionique POPG que par le pH dans l'insertion du peptide dans la membrane et dans l'interruption de celle-ci.

Mots-clés :

Spectroscopie RMN du solide, calorimétrie ITC, spectroscopie CD, mécanisme de transfection, peptide α -hélicale amphipathique, interactions macromoléculaires.

ABSTRACT:

Membrane associated proteins and peptides constitute a privileged medical target. Some of them also present also an important potential in therapeutics. This work has permitted the investigation of two peptides, the synthetic peptide LAH4 and the diphtherias toxin T domain in interaction with other macromolecules.

The LAH4 peptide designed and synthesized in our laboratory, presents all the general properties of amphipathic peptides and also binds strongly to the DNA allowing its transfer into the cells. In order to better understand the activity of the LAH4 peptide during transfection, I have examined its biophysical properties by ITC (Isothermal Titration Calorimetry), CD (Circular Dichroism) and solid-state NMR. The results show that the α -helical structure of the peptide is maintained after DNA complexation. At neutral pH, the molecules are bound in an electrostatic non-specific manner and a high ratio of LAH4 is required for DNA saturation and condensation. At low pH electrostatic interactions and hydrophobic contributions stabilize the complex and the saturation ratio is reduced. The data lead to the elaboration of a model of action for the LAH4 peptide during the first steps of transfection. In parallel, we have developed a strategy of expression of the LAH4 peptide in *E.coli* in order to uniformly label the peptide ^{13}C for its study by NMR.

Solid state NMR studies have been undertaken on the diphtheria toxin domain T in order to investigate its topology inside membrane vesicles. The samples of ^{15}N uniformly labeled T domain were prepared in a simplified system mimicking endosomal conditions. The data show an important role of the pH and of the anionic lipid POPG in the peptides membrane insertion and interruption.

Key-words:

Solid state NMR spectroscopy, ITC Calorimetry, CD spectroscopy, transfection mechanism, α -helical amphipathic peptide; macromolecular interactions.